RAIN ATTENUATION MODELLING FOR SOUTHERN AFRICA

CHRISPIN TSHIKOMBA MULANGU

2008

Submitted in fulfillment of the academic requirements for the degree of MSc Engineering
in the School of Electrical, Electronic and Computer Engineering,
University of KwaZulu-Natal, Durban, South Africa.

Abstract

In order to address rain attenuation scattering of millimetric waves and microwave sin Botswana, we have employed a comparison technique to determine the $R_{0.01}$ at fourteen diverse locations in Botswana. In addition we have identified two rain climatic zones for Botswana. We note that Mätzler employs Mie Scattering technique to determine the specific attenuation due to rain in Central Europe. Both Mätzler and Olsen use the exponential distribution of N(D) to calculate γ. In this dissertation we use the Mie scattering approach, but assume several distributions, including the log-normal distribution of N(D) as expounded by Ajayi et *al.*, to determine γ for tropical and subtropical regions of Africa. The results show that the extinction coefficients depend more strongly on temperature at lower frequencies than at higher frequencies for lognormal distribution: at selected frequencies, we record high attenuation values at rising SHF bands: at 300 GHz, tropical showers take on values of 12, 12.5, 11.9 and 14 dB/km for Gaborone, Francistown, Kasane and Selebi-Phikwe, respectively. The absorption coefficient is significant but decreases exponentially with rain temperature at lower microwave frequencies. The application of the proposed model (Continental Thunderstorm is shown using practical results from Durban) is corroborated using practical results from Durban.

Further, based on attenuation measurements, it is found that the lognormal distribution is suitable for Durban at rain rates greater than or equal to 21 mm/h. At rain rates below this, the Joss-Thunderstorm is the better fit. Finally in this dissertation the results show that for rainfall intensity below about 10 mm/h for Marshall-Palmer (MP), Joss-Drizzle (JD), Joss-Thunderstorm (JT) and Law-Parson (LP) distributions, and below about 4 mm/h for Continental-Showers (CS), Tropical Showers (TS), Continental Thunderstorms (CT) and Tropical Thunderstorm (TT) distributions, the specific rain backscattering follows Rayleigh scattering law where the rain drops are small with respect to the wavelength when the frequency is 19.5 GHz. At rain rates above 10 mm/h for exponential distribution, and above 4 mm/h for lognormal distribution, the specific

backscattering follows Mie scattering law. When the received echo power from rain becomes significant, it contributes to the rise in the noise floor and the radar receiver can lose its target. In addition, the result shows that Mie backscattering efficiency is highest at a raindrop diameter of 4.7mm.

Preface

The research work in this thesis was performed by Chrispin Tshikomba Mulangu, under the supervision of Professor Thomas Afullo in the school of Electrical, Electronic and Computer Engineering at the University of KwaZulu-Natal, Durban, South Africa. This work has been partially sponsored by Alcatel-Lucent and Telkom South Africa as part of the Centre of Excellence in Radio Access and Rural Technologies at the University of KwaZulu-Natal.

The work performed in this thesis has been published by the author at various fora: the SATNAC 2007 conference in Mauritius; the URSI General Assembly 2008 in Chicago, USA, (where the author received the Certificate of Young Scientist Award); and the SATNAC 2008 conference at Wild coast Sun, South Africa. A Portion of the research work has been published in Radio Science, a journal of the American Geophysical Union (AGU).

The author certifies that this thesis represents his own original and unaided work except where specifically indicated in the text and has not been submitted to any other university for degree purposes.

Acknowledgments

I wish to express my sincere gratitude to:

My supervisor Professor Dr. Eng. Thomas J. Afullo, for attention guidance over the last two years;

To the head of school of Electrical, Electronic and Computer Engineering, Professor Dr. Eng. Stanley Mneney for encouraging me to complete this MSc;

Those who have reviewed this thesis and suggested substantial improvements;

To my family, and those who love and care for me; finally, to almighty God who gave me strength.

Contents

List of Acronyms

CDF	Cumulative Distribution Function
CS	Continental Shower
CT	Continental Thunderstorm
DSD	Drop-size Distribution
FM	Fade margin
FSL	Free space Loss
ITU	International Telecommunications Union
JD	Joss-Drizzle
JT	Joss-Thunderstorm
LOS	Line-of-sight
LP	Laws-Parsons
MP	Marshall Palmer
RMS	Root mean square
TS	Tropical Shower
TT	Tropical Thunderstorm
WB	Weibull
UKZN	University of KwaZulu-Natal

List of Symbols

Symbols	Concept
θ	half-power beamwidth
γ	Attenuation coefficient
γ_{sca}	Scattering coefficient
γ_{ext}	Extinction coefficient
γ_{abs}	Absorption coefficient
γ_b	Backscattering coefficient
k	Wave number in free space
f	Frequency
ε_c	Complex dielectric constant of water
ε_r	Relative permittivity
ε'	Real part of dielectric constant of water
ε''	Imaginary of part dielectric constant of water
λ	Wavelength
a	Raindrop radius
σ	Cross-section
v	Terminal velocity of raindrops
$\rho < \sigma >$	Average cross-sections per unit volume
ξ	Aperture efficiency
ζ	Absorption coefficient
m	Refractive index
η	Intrinsic impedance
ϖ	Viscosity
$A_{0.01}$	Attenuation exceeded for 0.01% of the time
A_s	Specific Attenuation

D	Raindrop Diameter
d	Path length
d_{eff}	Effective path length,
$\hat{e}_x$	Unit vector in the x-direction
$\hat{e}_y$	Unit vector in the y-direction
$\hat{e}_z$	Unit vector in the z-direction
$\hat{e}_k$	Unit vector in the k-direction
E	Electric field
H	Magnetic field
F_1	First Fresnel radius
F_2	Second Fresnel radius
Π	Power flux density
F_V	Volume fraction of rain water in air
G_a	Amplifier gain
G_t	Transmitter antenna gain
h	Earth buldge,
k_B	Boltzmann's constant
N_T	Total number of raindrops
N_v	Volumetric-based drop-size distribution
N_o	Receiver noise power
$N(D)$	Raindrop-size distribution
P	Atmospheric pressure
P_0	Standard atmospheric pressure at sea level
P_r	Received Power
P_t	Transmitted Power
Q_{sca}	Scattering Efficiency
Q_{ext}	Extinction Efficiency
Q_{abs}	Absorption Efficiency

Q_b	Backscattering Efficiency
R	Rain rate
$R_{0.01}$	Rain rate exceeded for 0.01% of the time
R_N	Rain rate integral equation
Norm	Normalizing function
Re (~)	Real component
S/N_o	Signal-to-Noise ratio
S	Scattering amplitude
T_X	Transmitter
R_X	Receiver
$f(j_s, k_s)$	Forward scattering amplitude
T	Atmospheric temperature
T_0	Standard atmospheric temperature at sea level
x	Size parameter

List of Tables

List of Figures

Chapter 1

Introduction

1.1 How Precipitation Affects Radio Wave Propagation

It has been pointed out that the employment of microwave links for applications such as radar, remote and communication systems, requires a reliable performance at all weather conditions. Here are some of the factors that must be taken into consideration in adverse weather conditions.

Hydrometeors are essentially particles of water within the atmosphere, which take the form of liquid water as in rain, mist and fog or ice as in clouds, hail and snow. Plane electromagnetic waves traveling through air containing precipitation are scattered and absorbed by the particles of ice, snow or water. Water, with its larger dielectric constant (87.9 at 0°C, 78.4 at 25°C, 55.6 at 100°C, [Murrell, 1994]) scatters electromagnetic wave more strongly than ice, [Joseph Nemarich et al. (1988), Manabe et al. (1987) and M. M. Z. Kharadly (1989)]. In addition, it has a much larger dielectric loss and the attenuation due to thermal dissipation is therefore much greater for water particles than for ice particles [Akira Ishimaru (1978) and Jonathan H et al. (2004)]. This makes rain degrade the performance of millimeter wave and microwave signals more than ice. Radiowave propagating through a rain zone will be scattered, depolarized, absorbed and delayed in time. All these effects of rain on the wave propagation are related to the frequency at which the signal is transmitted, and polarization of the wave as well as to the rain rate, which influences the form of the raindrop size distribution.

Primarily, attenuation is caused by the absorption of microwave energy by tropospheric gases (water vapour and molecular oxygen) where the maximum absorption occurs when the frequency coincides with one of the molecular resonances of water or oxygen. Thus atmospheric attenuation has distinct peaks at these frequencies [Pozar, 2005]. Transmission of microwave signals above 10 GHz is vulnerable to precipitation, as has been shown by many researchers over several decades, [Fedi, 1981; Mätzler, 2002]. Consider a radio path where the Fresnel zone is partially filled with rain droplets. As seen in Figure 1-1, each particular raindrop will contribute to the attenuation of the wanted signal. The actual amount of attenuation is dependent on the frequency of the signal and the size of the raindrop. The two main causes of attenuation are scattering and absorption. When the wavelength is fairy large relative to the size of raindrop, scattering is predominant. Conversely, when the wavelength is small compared to the raindrop size, attenuation due to absorption is dominant [Ivanovs et *al.*, 2006].

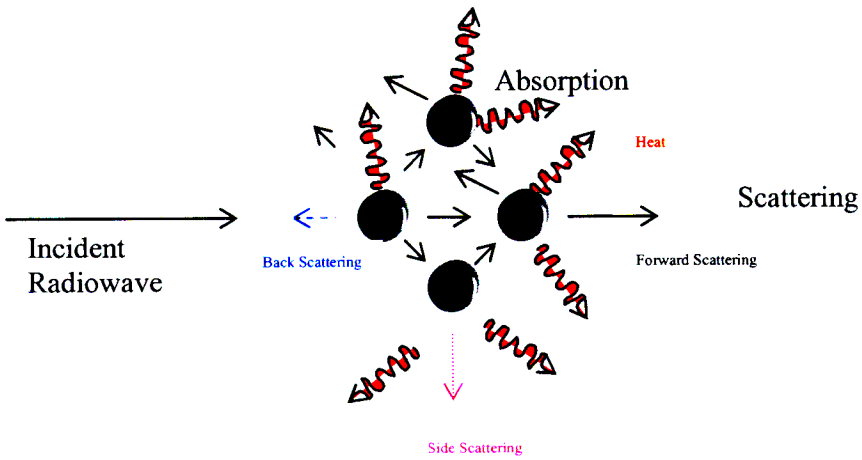

Figure 1-1: Radio wave incident in rainy medium

Since the radio waves are a time varying electromagnetic field, the incident field will induce a dipole moment in the raindrop. The raindrop dipole will have the same time variation as the radio waves and will therefore act as an antenna and re-radiate the energy or scatter it, as shown in Figure 1-1. A raindrop is thus an antenna with low directivity: some energy will be reradiated in arbitrary directions giving a net loss of energy in the direction towards the receiver. Also, when the wavelength becomes small relative to the

drop, more and heating of the raindrop absorbs more energy, as shown in Figure 1-1. The radio waves will thus vary in field strength over the raindrop to induce a dipole effect.

1.2 Raindrop Size Distributions

Drop size distribution and extinction coefficient are two parameters required for establishing the specific rain attenuation model. The latter will be explained in detail in Chapter 3. Raindrops are randomly distributed in space with a special drop size distribution that depends on the rainfall rate or rain intensity, R [Hassen (2006)].

1.2.1 Terminal Fall Velocity of Raindrop

The raindrop terminal fall speed in still air $v(D)$ and the equivalent spherical raindrop diameter D represents the functional relationship between the raindrop terminal fall speed in still air v (in meters per second) and the equivalent spherical raindrop diameter D (in millimeters).
Atlas and Ulbrich (1977) provide a close fit to the data of Gunn and Kinzer (1949) in the range $0.5 \le D \le 5.0mm$ (the diameter interval contributing most to rain rate).

$$v(D) = 3.78D^{0.67} \tag{1.1}$$

Although more sophisticated relationships have been proposed in the literature (e.g., Best (1950); Atlas et al. (1973); Beard (1976)) the power-law relationship of Sekhon and Srivastava (1971) is given by:

$$v(D) = 14.20(0.1D)^{0.5} \tag{1.2}$$

Mook (2002) come up with an analytic formula for an accurate fit of the Gunn and Kinzer (1949) measurement given by:

$$v(D) = 9.40(1 - e^{-1.57 \cdot 10^3 (0.001D)^{1.15}}) \tag{1.3}$$

Similarly, Atlas et al. (1973) suggested a more accurate fit given by

$$v(D) = 9.65 - 10.30e^{-0.6D} \tag{1.4}$$

Mätzler (2002) proposed a solution to the negative value in equation (1.4) when $D < 0.1\ mm$, written as:

$$v(D) = \begin{cases} 0 & D < 0.03mm \\ 4.233(D - 0.03) & 0.03mm < D < 0.6mm \\ 9.65 - 10.30e^{-0.6D} & D > 0.6mm \end{cases} \tag{1.5}$$

Also, Mätzler (2002) determined that the terminal velocity for arbitrary atmospheric conditions can be seen as adjustment to equation (1.5) under atmospheric pressure, given by:

$$v(D,P) = v(D)\left(\frac{P_0}{P}\right)^{0.291+0.0256D} \tag{1.6}$$

where D is the drop diameter in mm, P is the atmospheric pressure in mbar and P_0 is the standard atmospheric pressure of 1013 mbar.

1.2.2 Drop size Distribution and Exponential Distribution

The drop size distribution (DSD) is the number of raindrops of a given diameter range per unit volume of air. Then two definitions of DSD arise, namely: a volumetric-based $N_V(D,R)$ and a flux-based $N_A(D,R)$. The former is the mean number of raindrops of diameter D arriving at a horizontal surface of unit area, per unit time per increment in drop diameter dD and has the units m^{-3} mm^{-1}; the later is the mean number of raindrops of diameter D arriving at a horizontal surface of unit volume of air per increment in drop

diameter dD, and has the units m^{-2} $mm^{-1}s^{-1}$ as suggested by Uijlenhoet, (2001). Those two distributions can be converted by:

$$N_A(D,R) = v(D)\,N_V(D,R) \tag{1.7}$$

where $v(D)$ is the terminal fall velocity. The number N_T of drops per unit volume and the volume fraction F_V of rain-water in air are given by the moments in D of $N_V(D,R)$ of order zero and three, respectively, [Mätzler (2002)]:

$$N_T = \int_0^\infty N_V(D,R)dD; \qquad F_V = \frac{\pi}{6}\int_0^\infty D^3 N_V(D,R)dD \tag{1.8}$$

Similarly for rain-water, F_A arriving at a horizontal surface of unit area per unit time, are given by the moments in D of $N_A(D,R)$ of three. Then F_A can be expressed in terms of N_V as

$$F_A = \frac{\pi}{6}\int_0^\infty D^3 N_V(D,R)V(D,P)dD \tag{1.9}$$

F_A is the download flux density of rain-water volume, has units m s^{-1}. The rain rate is obtained as integral equation of F_A, and can be express in mm/h as

$$R_N(R) = 6\pi\times 10^4 \int_0^\infty D^3 N_V(D,R)V(D,P)dD \tag{1.10}$$

If $N_V(D,R)$ is self-consistent, $R_N = R$ and the rain-rate integral equation (1.10) will be satisfied. Similar if equality does not exist, then $N_V(D,R)$ has to be normalized, as:

$$Norm(R,P) = \frac{R}{R_N(R,P)}, \tag{1.11}$$

To transform $N_V(D,R)$ to the normalized distribution function $N_N(D,R,P)$ as suggested by Mätzler (2002a) we have:

$$N_N(D,R,P) = Norm(R,P_0)\, N_V(D,R) \tag{1.12}$$

where *Norm*(R) = aX^2+bX+c with X= ln(R), where R is mm/hr. These are tabulated in Table 1.1.

Table 1-1-1: The normalized exponential distributions, Mätzler (2002a).

Distribution	$N_0(R)$ [mm^4]	*Norm*(R,P_0)	$\Lambda(R)$ [mm^{-1}]
LP	$1.98\ 10^{-5}\ R^{-0.384}$ *Norm*	$1.047-0.0436X+0.00734X^2$	$5.38R^{-0.188}$
MP	$0.80\ 10^{-5}$ *Norm*	$0.842-0.00915X+0.0072X^2$	$4.1R^{-0.21}$
JD	$3.00\ 10^{-5}$ *Norm*	$1.1194-0.0367X+0.0079X^2$	$5.7R^{-0.21}$
JT	$0.14\ 10^{-5}$ *Norm*	$1.0945-0.0052X+0.0124X^2$	$3.0R^{-0.21}$

1.2.3 Lognormal Distribution

The lognormal model for drop size distribution was found to give a better fit to the data obtained at the tropical stations than L-P laws and provides a better fit for widespread, shower and thunderstorm rains in the both the continental and tropical regions, Ajayi (1990). The numerical values are given in Tables 1-2 and 1-3.

Fang and Chen (1982) discussed the following log-normal distribution for the case of showers and thunderstorms rain. These values are given in Table 1-2.

$$N(D) = \frac{N_T}{D\sqrt{2\pi}\ln\sigma} e^{-[\ln(D/D_M)/2\ln\sigma]^2}. \tag{1.13}$$

where D_M is the mean drop size diameter, and N_T is the total number of raindrops per cubic meter per mm and σ is the standard deviation.

Table 1-1-2: Coefficients for Shower and Thunderstorm Rain Lognormal Models, Fang and Chen (1982).

Shower ($R \leq 50\ mm\ /\ h$)	**Thunderstorms** ($R \leq 50\ mm\ /\ h$)	**Thunderstorms** ($R > 50 mm/h$)
$40R^{0.64}$	$46R^{0.55}$	8.8R
$D_M = 0.306+0.059\ln R$	$D_M = 0.222+0.397\ln R$	$D_M = 1.76+7.33\ 10^{-4}\ \ln R$
$s = e^{0.29-0.001}$	$s = e^{0.5-0.0035R}$	$s = 1.37$
$Norm(R) = 1.167-0.2314X+0.04632X^2$	$Norm(R) = 5.508-2.798X+0.4253X^2$	$Norm(R) = 0.9952-1.446\ 10^{-3}\ X+1.379\ 10^{-6}\ X^2$

Table 1-1-3: Ajayi (1996) Coefficients for Shower and Thunderstorm Lognormal Models.

Type of Rain		N_T	μ_g	s^2_g
Continental	***Showers***	$127R^{-0.477}$	**-0.476+0.221lnR**	**0.269-0.043lnR**
	Thunderstorms	$70R^{-0.564}$	**-0.378+0.224lnR**	**0.306-0.059lnR**
Tropical	***Showers***	$137R^{-0.37}$	**-0.414+0.234lnR**	**0.223-0.034lnR**
	Thunderstorms	$63R^{-0.491}$	**-0.178+0.195lnR**	**0.209-0.030lnR**

Ajayi and Olsen (1985) have shown that the L-P and M-P overestimate the number of drops in the small and large diameter regions. It was shown by Ajayi and Olsen that a lognormal model gives better fit to the measured drop size data at Ile-Ife, Nigeria. Making use of the attenuation at a number of frequencies, Moupfouma and Tiffon (1982), using an inversion method to obtain the rain drop size distribution, have also confirmed that the L-P and M-P distributions overestimate the number of drops in the small diameter regions. Similar conclusions have been made by Massambani and Morales (1988) and Massambani and Rodriguez (1990), making use of the data obtained in Brazil, as shown in Figure 1-2.

In his approach, Mätzler computed the coefficients γ_j, $\{\ j = ext, abs, sca, b\ \}$, from the corresponding Mie efficiencies Q_j and the drop size distribution using Marshall Palmer, (MP), Joss -Thunderstorm, (JT), Joss-Drizzle, (JD) and Laws and Parson, (LP) distributions.

$$\gamma_j = 0.25\pi \int_0^\infty D^2 Q_j N(D) dD;\ j = ext, abs, sca, b \tag{1.14}$$

In this dissertation we determine propagation coefficients (γ_j) due to rain in Botswana for fourteen stations from the corresponding Mie efficiencies Q_j and the drop size distribution based on lognormal distribution for tropical and subtropical countries, [Ajayi et al (1996), Ajayi (1990)].

$$N(D) = \frac{N_t}{\sigma_g D\sqrt{2\pi}} \exp\left(\frac{-[\ln(D) - \mu_g]^2}{2\sigma^2}\right) \tag{1.15}$$

where, μ_g is the mean of $\ln(D)$, σ_g is the standard deviation, N_t is the total number of the drops per cubic meter per mm.

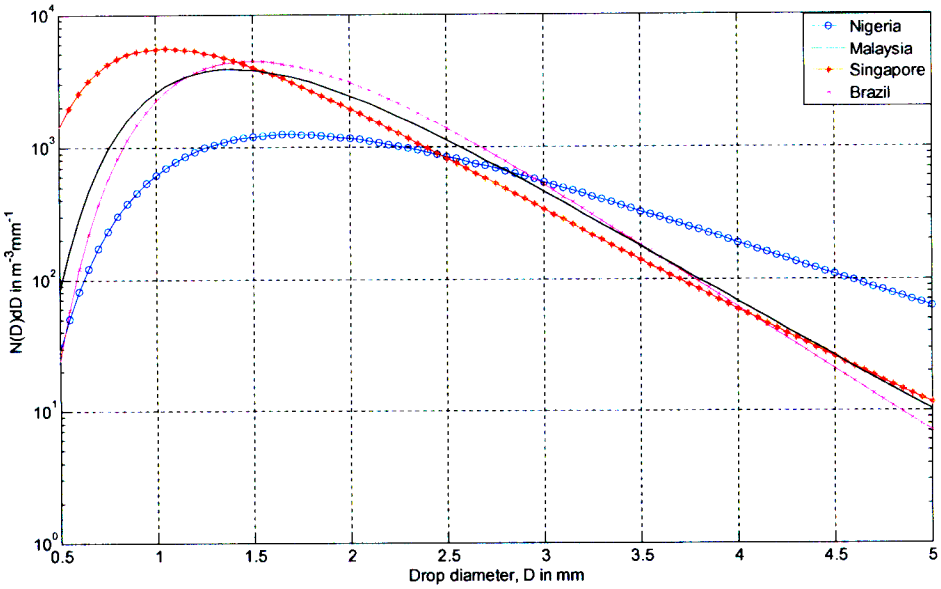

Figure 1-2: Comparison models of the raindrop size distribution for tropical zones: Malaysia, Singapore, Nigeria and Brazil.

Table 1-1-4: Normalization Functions for Ajayi (1996) Coefficients for Shower and Thunderstorm Lognormal Models.

Type of Rain		Norm(R) with X=ln(R)
Continental	*Showers*	$0.9936-4.721\ 10^{-3}X+6.587\ 10^{-4}\ X^2$
	Thunderstorms	$1.019-7.353\ 10^{-3}\ X+1.100\ 10^{-3}\ X^2$
Tropical	*Showers*	$0.9894-6.257\ 10^{-3}X+1.851\ 10^{-3}\ X^2$
	Thunderstorms	$1.000-5.032\ 10^{-3}\ X+1.088\ 10^{-3}\ X^2$

1.2.4 Weibull Distributions

Sekine (1979) proposed the Weibull raindrop size distribution , given by:

$$N(D,R) = N_0 \frac{c}{b}\left(\frac{D}{b}\right)^{c-1} \exp\left[-\left(\frac{D}{b}\right)^{c}\right] \qquad (1.16)$$

where D is the diameter in mm, N_0 =1000 m^{-3} (mm^{-1}), c=0.95$R^{0.14}$ and b=0.26$R^{0.44}$ with the precipitation rate R in mm/hr. This distribution is retained for microwave applications for drizzle, widespread rain, and shower rain cases. Figure 1-3 shows the Weibull Drop Size Distribution.

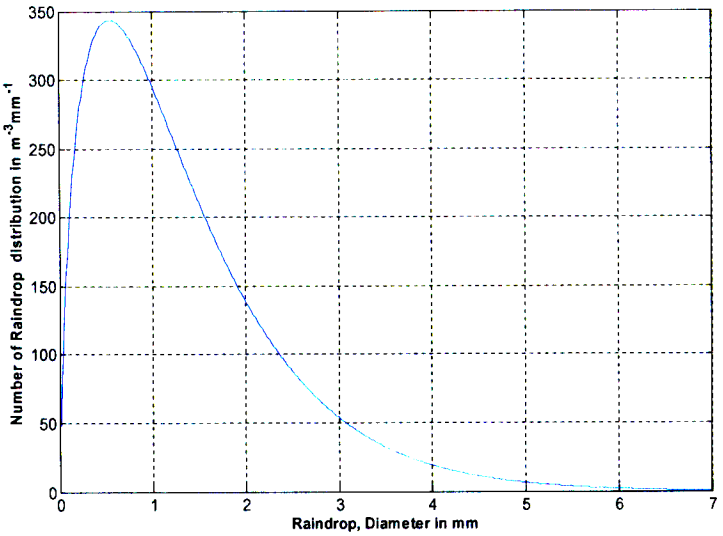

Figure 1-3: Weibull distribution.

The normalization function is given by

$$Norm(R) = 1.184 - 0.03466X - 0.02591X^2 \tag{1.17}$$

1.2.5 Gamma Drop-Size Distribution

Ulbrich (1983) proposed the modified gamma distribution as:

$$N_V(D,R) = N_0 D^{\mu} e^{-\Lambda D}, \tag{1.18}$$

where $\Lambda = \alpha R^{-\beta}$, $N_0 = C_N e^{3.2\mu}$ ($m^{-3}\, mm^{-1-\mu}$), μ is a real number and C_N is a constant. The gamma DSD with three parameters (N_0, μ and Λ) is able to describe a wider range of raindrop size distributions than an exponential distribution, which is a special case of

the gamma distribution with $\mu = 0$ [Ulbrich (1983); Chandrasekar and Bringi (1987); Kozu (1991); Haddad et al. (1997)].

De Wolf (2001) suggested a more accurate fit of the Laws and Parsons (1943) measurement given by:

$$N_0 = 1.98 \times 10^4 \ (m^{-3} mm^{-1-\mu}), \tag{1.19}$$

$$\mu = 2.93 \text{ and } \Lambda = 5.38 R^{-0.186} \quad (mm^{-1})$$

The normalization can be split into two for accuracy:

$$Norm_1 = 1.274 - 0.0866X + 0.01287X^2 \qquad \text{for } R \le 25 mm\,h^{-1}$$

$$Norm_2 = 1.0484 - 0.0416X + 0.006404X^2 \text{ for } R > 25 mm\,h^{-1} \tag{1.20}$$

Figure 1-4 shows gamma distribution suggested by de Wolf (2001) along Marshall and Palmer (1948) (MP),

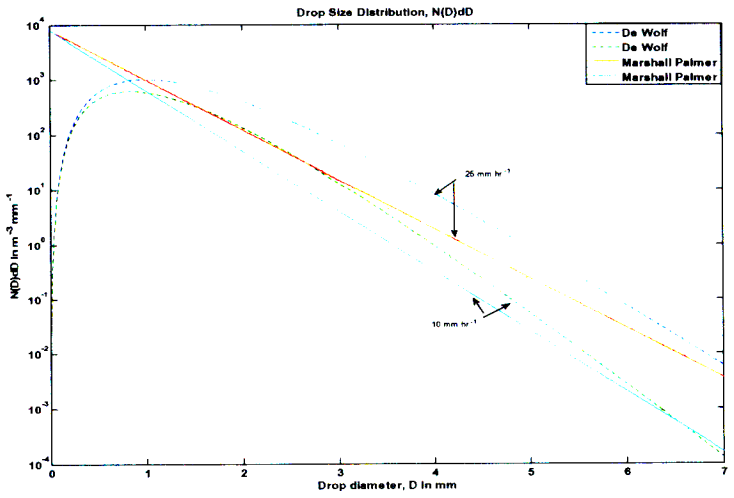

Figure 1-4: Gamma distribution by de Wolf (2001).

1.3 Problem formulation

Daily rainfall accumulations are universally recorded and hourly data are also fairly widely available by national bureaus. In Nigeria, Ajayi and Ofoche determined that the use of one-minute rain rates gives the best agreement with the ITU-R stipulations for the design of microwave radio links. Therefore, there is a need to convert the available one-hour rain rates measured by most national weather bureaus to one-minute data. ITU-R Recommendation P-837 classifies the Southern Africa region into seven climatic regions, namely: C, D, E, J, K, L and N. Out of these, Botswana has three zones, namely, J, L and N. Fashuyi and Owolawi used the same approach to classify the South Africa rain zones. This was then used to estimate the signal outages at 0.01% of the time on radio communication links, since it defines the rainfall rate recommended by ITU-R to evaluate the availability of terrestrial and satellite radio links.

In this study, we use daily and hourly rainfall data for Botswana (1995-2004) to model the rain climatic zones for that part of southern Africa. In particular, we perform the following tasks:

1) Identify types of rain, and determine expressions for terminal velocity of raindrop, optimum raindrop size, and shape of the drop size.
2) Study the raindrop size distributions: Laws-Parsons, Marshal and Palmer, and the Log-normal model of Ajayi & Olsen. Indicate their significance in radio wave propagation.
3) Using meteorological ground measurements over 10 years, determine
   Botswana Rain Zones compared with those of ITU- R Rec. 837
4) Estimate the cumulative distribution of rainfall rate for 24 hours and 1-minute (Compare with those of ITU-R Rec. 837)
5) Relate the 1-minute and 24 hours rainfall rates to determine the constants a and b.
6) Determine $R_{0.01}$ for the determined Botswana rain zones.
7) Determine the scattering coefficients for the Botswana rain zones.
8) Determine these scattering coefficients for Durban, and compare the estimated rain attenuation with measurements.

1.4 Climate Characteristic in Botswana

Botswana lies around latitude $18^0 - 22^0 S$ and longitude $20^0 - 24^0 E$ with an area of 582000 squared kilometers. It is landlocked and very nearly in the centre of the Southern Africa subcontinent. As shown in Figure 1-5, it has an average elevation of 1000 m but lower than that of the plateaus of Zambia to the North, Zimbabwe in North East, South Africa in the South East, and South Namibia to the West. Also, Botswana is in between two Oceans, about 675 km inland to the Indian and 1025 km to the Atlantic. According to the Department of Meteorological Services of Botswana (DMSB), the country enjoys a warm and dry tropical climate with semi-arid lands. In the winter season (dry Season) of May to August, there is almost no rain anywhere in the country. In the spring season August to September, temperatures rise rapidly. During the hot, dry period of September, there is a slight rainfall. In the summer season of November to March, rainfall is more moderate, with most rain being in April.

Also, according to the Department of Meteorological Services Botswana (DMSB), from 1922 to 1985 mean annual rainfall accumulation varies from a maximum of 680 mm in Kasane to a minimum of less than 290 mm in the Kgalagadi (Tshabong).

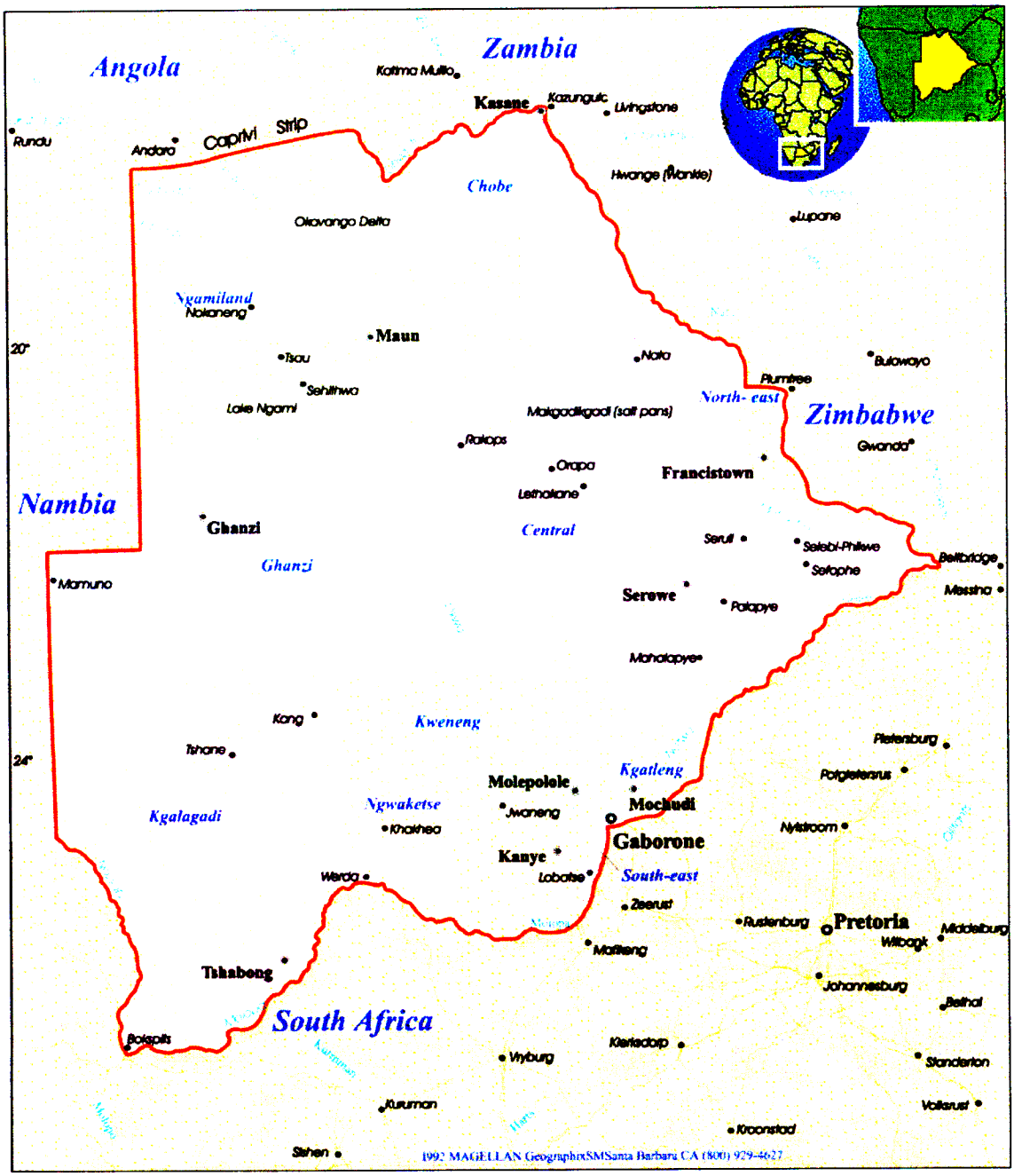

Figure 1-5: The geographic location of Botswana.

Since Botswana has a large desert area known as Kgalagadi, the diurnal (daily) variation of temperature is large with hot day temperature and cooler nights, from maximum of 43.9 °C in Gaborone to a minimum of -15.0 °C in Tshabong, as seen in Table 1-5.

Table 1-1-5: Annual Rainfall for Selected Locations in Botswana.

Mean, Maximum & Minimum Annual Rainfall - selected Stations				
Station	**Period**	**Mean (mm)**	**Max (mm)**	**Min (mm)**
Gaborone	1922-86	531.1	925.3	243.2
Francistown	1921-85	462.5	897.9	114.4
Kanye	1925-85	516.6	970.6	104.7
Kasane	1922-85	676.9	1405.6	298.7
Molepolole	1924-85	495.1	914.0	100.2
Maun	1922-85	463.4	1183.9	193.0
Lobatse	1921-85	555.7	1070.4	262.1
Shakawe	1945-85	531.1	1091.4	221.8
Mochudi	1925-85	490.9	888.8	72.9
Ghanzi	1922-85	432.1	698.2	122.2
Mahalapye	1912-85	464.9	891.3	143.9
Tshane	1958-85	347.5	756.7	145.2
Serowe	1921-85	455.5	978.7	194.5
Tsabong	1939-85	290.4	706.0	134.0

1.5 Motivation and Objectives

Today mobile and wireless communications networks require high data transmission rates to meet modern technology services such as video conference, Voice over IP, Video streaming, E-commerce, etc. The C band (4-8 GHz) and X band (8-12 GHz) alone are not able to meet this increasing demand of broadband communication; the solution incorporates the use of higher radio frequencies in microwave and millimeter bands, Ulaby et al (1981).

With this high data transmission rate, wireless communication applications such as satellite-to-earth link, mobile communication technology, and terrestrial point-to-point broadband communication, are very sensitive and can not stand much interference from the environment, especially rain. Therefore the study of the rain effects on radio propagation is important. To this end, for Botswana, ten-year rain measurement has been made in fourteen sites all over the country, namely Francistown, Selebi-Phikwe, Maun, Tshabong, Kasane, Tshane, Lethakane, Mahalapye, Gaborone, Shakawe, Jwaneng, Sua-Pan, Ghanzi and Pandamatenga. In the study we shall establish specific rain attenuation

models for the fourteen sites in Botswana at microwave and millimetric frequencies up to 1 THz.

Also, based on attenuation measurements realized by Naicker in the South Africa coastal city of Durban, we will establish a path attenuation model for Durban. We will establish a model of the effects of rain on microwave remote sensing systems and ground-based radars use in Durban.

1.6 Outline of the thesis

In this thesis the contents will be organized in the order listed here: Chapter 1 includes how precipitation affects radio wave propagation, raindrop size distributions, problem formation, climate characteristics in Botswana, motives, objectives, and the outline of the thesis. Chapter 2 gives an essential summary regarding radio wave propagation in lossless and lossy media or materials. This will involve the application of Maxwell equations, Snell' law of reflection, Snell law of refraction and Fermat principle; as well as dielectric properties of water drops at microwave frequencies and the scattering problems of electromagnetic waves in general. In Chapter 3 a simple approach is used to determine the rain rate conversion factors for the Botswana sites which lack one-minute exceedence; the rainfall CDF identity is employed to find the conversion factor for Botswana which has daily rainfall data. Botswana's daily cumulative distributions are compared with South African daily cumulative distributions. South Africa is chosen because daily, hourly, five-minute and one-minute rainfall results are available. Also, ITU-R Recommendations P-837-1 and P-837-4 classifies the Southern Africa region into seven climatic rain zones by using the median cumulative distribution of rain rate for the rain climatic region. The same method is employed in this thesis to classify the Botswana regions into their classes of rain zones. However, these ITU-R designations are not necessarily adequate, as they need further refinement; thus there is need to redefine the ITU-R regional climatic zones based on the actual local data. From the local data measured by Botswana Weather Services for the fourteen locations, appropriate climatic

rain zones are thus determined for Botswana based on the analysis of the fourteen locations. We also study a practical case of the performance of the link in Gaborone by determining the fade margin at 99.99% of exceedence under extreme weather conditions. In Chapter 4, we begin our study of propagation coefficients due to rain in Botswana. Specifically, we focus on propagation coefficient analysis, an understanding of which is particularly essential for forward attenuation, while being of general importance, and also extend the discussion to compare our model to rain attenuation measurements realized in Durban by Naicker (2006) and processed by Fashuyi (2007). In Chapter 5 we investigate the impact of rain on sensor systems at microwave frequencies in Durban. As there is no measurement on radar, we have used the rain attenuation measurement for the path profile for the 6.73km terrestrial line-of-sight from the Westville campus to Howard College campus [Naicker et *al.*, 2006 and Fashuyi et *al.*, 2007], since the hydrometeors act in the same way for both links. We investigate the specific backscattering for that link which could be applied to radar systems in Durban and can be used as an indicator of the degree of possible degradation of radar system performance. Chapter 6 gives the conclusions and recommendations for future work.

Chapter 2

Fundamental Theory

2.1 Introduction

In Chapter 1 we studied how precipitation affects radio wave propagation, various raindrop size distributions, and climate characteristics in Botswana. In this chapter, we focus on the essentials of propagation of waves through rain at microwave or millimeter-wave frequency bands.

The atmosphere is not a homogeneous medium. The transmission characteristics of air change with height and time due to changes in temperature, pressure and humidity.
Line of sight (LOS) radio systems transmit their energy through the dersiest part of the atmosphere and are significantly affected by variations in the index of refraction along the path. The refractive index is the ratio of the velocity of light in a vacuum to the local velocity in the medium of concern.

The space variations of the electric and magnetic field components are related to the time variations of magnetic and electric field components, through Maxwell's equations. This interdependence gives rise to the phenomenon of electromagnetic wave propagation. In the general case, electromagnetic wave propagation involves electric and magnetic fields having more than one component, each dependent on all three coordinates, in addition to time. In particular case, electromagnetic waves involves electric and magnetic fields that are perpendicular to each other and to the direction of propagation and are uniform in planes perpendicular to the direction of propagation. These directional properties characterize a transverse electromagnetic (TEM). These waves are known as uniform plane waves. By orienting the coordinate axes such that the

electric field is in the x-direction, the magnetic field is in the y-direction, and the direction of propagation is in the z-direction, as shown in Figure 2.1, we have

$$\vec{E} = \vec{E}_0 e^{-jkz}. \tag{2.1}$$

The electric field is perpendicular to magnetic field and then the magnetic field can be written as

$$\vec{H} = \pm\sqrt{\varepsilon/\mu}\,\hat{a}_k \times \vec{E} = \vec{H}_0\, e^{jkz}, \tag{2.2}$$

where $\vec{E}_0 = E_x\,\hat{e}_x + E_y\,\hat{e}_y + E_z\,\hat{e}_z$ (2.3)

and $\hat{k} = k\,\hat{e}_k$.

The next problem is due to fact that rain drops are created by a material which can be considered as a lossy dielectric. Therefore, plane waves in different media will be studied and both the reflected and transmitted wave will be analyzed in this chapter.

2.2 Radiowave Propagation

2.2.1 Plane Wave in Lossless media

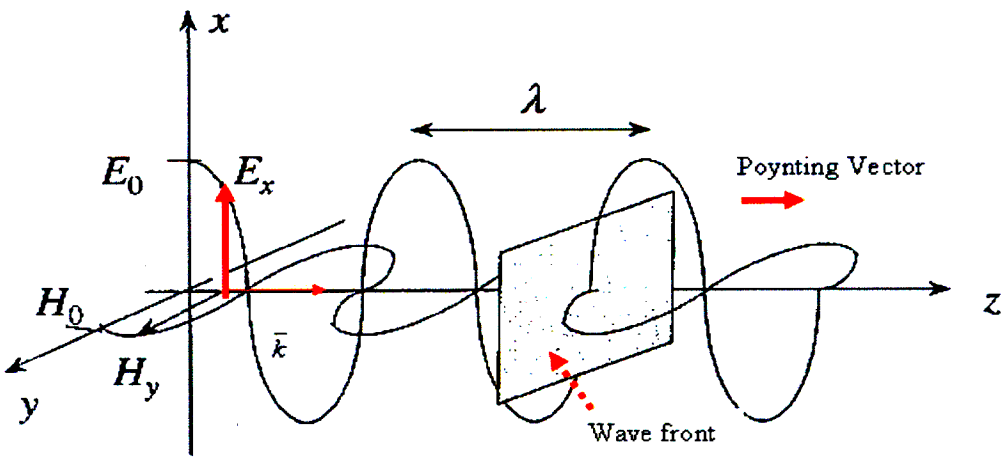

Figure 2-1: The alignment of the electric field vector of a plane wave.

A medium is said to be lossless if it does not attenuate the amplitude of the wave travelling within it or on its surface. Since we are interested in propagation in the z direction, we assume the field components to be:

$$\vec{E}(z,t) = E_0 \exp[j(\omega - k\,z)]\hat{e}_x \tag{2.4}$$

$$\vec{H}(z,t) = H_0 \exp[j(\omega - k\,z)]\hat{e}_y \tag{2.5}$$

$$\vec{E} = E_x(z,\,t)\hat{e}_x \tag{2.6}$$

$$\vec{H} = H_y(z,\,t)\hat{e}_y \tag{2.7}$$

While early rain attenuation studies relied on the Ray empirical model for the complex refractive index of water, (e.g. Olsen et al. 1978; Oguchi 1981, 1983), recently the more accurate model of Liebe (1991, 1993) has been employed.

In a medium with conductivity σ, the current density $\vec{J}$ is related to $\vec{E}$ by $\vec{J} = \sigma\vec{E}$. From Maxwell's equation, we obtain:

$$\begin{aligned}\left(\nabla \times \vec{H}\right) &= \vec{J} + j\omega\varepsilon\vec{E} \\ &= (\sigma + j\,\omega\varepsilon)\vec{E} = j\,\omega\left(\varepsilon - j\frac{\sigma}{\omega}\right)\vec{E}\end{aligned} \tag{2.8}$$

By introducing the complex permittivity ε_c defined as

$$\varepsilon_c = \varepsilon - j\frac{\sigma}{\omega} \tag{2.9}$$

equation (2.8) can be rewritten as:

$$\left(\nabla \times \vec{H}\right) = j\omega \varepsilon_c \vec{E} \tag{2.10}$$

The complex permittivity ε_c given by equation (2.10) is often written in terms of a real part ε' and imaginary part ε'',

$$\varepsilon_c = \varepsilon - j\frac{\sigma}{\omega} = \varepsilon' + j\varepsilon'', \tag{2.11}$$

where $\varepsilon' = \varepsilon$ and $\varepsilon'' = -\sigma/\omega.$ (2.12)

For a lossless medium with $\sigma = 0$, it follows that $\varepsilon'' = 0$ and $\varepsilon_c = \varepsilon' = \varepsilon$.

In the absence of charges and currents, the electric and magnetic fields are solutions of the Helmholtz equation

$$(\nabla^2 - \gamma^2)\vec{E} = 0, \tag{2.13}$$

$$(\nabla^2 - \gamma^2)\vec{H} = 0\ , \tag{2.14}$$

where $\gamma^2 = -\omega^2 \varepsilon \mu$.

When the medium is lossless, it is customary to introduce the wave number k defined by

$$k = \omega\sqrt{\mu\varepsilon}\ . \tag{2.15}$$

Equation (2.13) in view of equation (2.14) and (2.15), can then be written a

$$(\nabla^2 + k^2)\vec{E} = 0. \tag{2.16}$$

The wave impedance or intrinsic impedance η and the phase velocity v are given by:

$$\frac{|\vec{E}|}{|\vec{H}|} = \frac{E_0}{H_0} = \sqrt{\frac{\mu}{\varepsilon}} = \eta\ , \tag{2.17}$$

$$\upsilon = \frac{\omega}{k} = \frac{1}{\sqrt{\varepsilon\,\mu}}. \tag{2.18}$$

In free space, $\varepsilon = \varepsilon_0$ and $\mu = \mu_0$, in which case the intrinsic impedance η and the phase velocity v are given by

$$\eta = \eta_0 = \sqrt{\frac{\mu_0}{\varepsilon_0}} = 120\pi = 377\,\Omega, \tag{2.19}$$

$$\upsilon = c = \frac{1}{\sqrt{\varepsilon_0\,\mu_0}} = 3\times 10^8 \qquad \text{(m/s)}, \tag{2.20}$$

where c is the velocity of light and η_0 is called the intrinsic impedance of free space.

2.2.2 Plane wave in Lossy medium (conductor or lossy dielectric)

Losses are due to the presence of an imaginary part in the dielectric permittivity (even in the absence of conductivity). In the general characterization of lossy dielectrics, the relative permittivity ε_r is defined as:

$$\varepsilon = \varepsilon_r\varepsilon_o = \varepsilon_o(\varepsilon' - j\varepsilon'') = \varepsilon_o\varepsilon'(1 - j\varepsilon''/\varepsilon') = \varepsilon_o\varepsilon'(1 - j\tan\delta) \tag{2.21}$$

where ε_r is the ability of the material to be polarized by the external electric field, and ε'' and $\tan\delta$ are the loss factor and loss tangent, respectively. The loss tangent quantifies the efficiency with which the electromagnetic energy is converted to heat.

Consider a forward-traveling wave in a lossy material having material constants, ε, μ and σ; to examine wave propagation in a conducting medium, we return to the wave equation given by equation (2.13),

$$\left(\nabla^2 - \gamma^2\right)\vec{E} = \vec{0} \tag{2.22}$$

with $\gamma^2 = -\omega^2 \mu\varepsilon = -\omega^2 \mu(\varepsilon' - j\varepsilon'')$

where $\varepsilon' = \varepsilon$ and $\varepsilon'' = \sigma/\omega$. Since γ is complex, we express it as:

$$\gamma = \alpha + j\beta \tag{2.23}$$

where, α is the attenuation constant [Np/m] and β is the phase constant [rad/m]. By replacing γ with $(\alpha + j\beta)$ in equation (2.25), the solution of this wave equation leads to electric and magnetic fields which can be written as

$$\vec{E} = E_0 \exp[j(\omega t - \beta z) - \alpha z]\hat{e}_x, \tag{2.24}$$

$$\vec{H} = H_0 \exp[j(\omega t - \beta z) - \alpha z]\hat{e}_y, \tag{2.25}$$

and, E_0 and H_0 are the magnitudes of the electric and magnetic field, respectively. As the wave travels through the material, its amplitude will be attenuated by a factor $e^{-\alpha z}$. Define

$$\delta = \frac{1}{\alpha}. \tag{2.26}$$

This quantity δ is termed the skin depth or depth of penetration.
From Maxwell's equation:

$$\nabla \times \vec{E} = -j\omega\mu\vec{H}, \tag{2.27}$$

$$\nabla \times \vec{H} = (\sigma + j\omega\varepsilon)\vec{E} = j\omega\varepsilon\left(1 - j\frac{\sigma}{\omega\varepsilon}\right)\vec{E}. \tag{2.28}$$

Thus in equation (2.13), γ becomes

$$\gamma = \sqrt{j\omega\mu(\sigma + j\omega\varepsilon)}\,. \tag{2.29}$$

For a good dielectric, we have:

$$\left(\frac{\sigma}{\omega\varepsilon}\right) << 1. \tag{2.30}$$

Then equation (2.29) for a good dielectric can be written as

$$\gamma = j\omega\sqrt{\mu\varepsilon}\sqrt{1 - j\frac{\sigma}{\omega\varepsilon}}\,. \tag{2.31}$$

Using binomial expansion, the propagation constant can be written as:

$$\gamma = j\omega\sqrt{\mu\varepsilon}\left(1 - j\frac{\sigma}{2\omega\varepsilon} + \frac{\sigma^2}{8\omega^2\varepsilon^2}\right). \tag{2.32}$$

The attenuation constant after simplifying the expression for a good dielectric and taking the real part, becomes:

$$\alpha \approx \frac{\sigma}{2}\sqrt{\frac{\mu}{\varepsilon}}\,. \tag{2.33}$$

The wave number for a good dielectric (taking the imaginary part of 2.32) is given by

$$k \approx \omega\sqrt{\mu\varepsilon}\left(1 + \frac{\sigma^2}{8\omega^2\varepsilon^2}\right). \tag{2.34}$$

The expression of the wave impedance is:

$$\eta = \sqrt{\frac{j\omega\mu}{\sigma + j\omega\varepsilon}} = \sqrt{\frac{\mu}{\varepsilon}}\left(1 - j\frac{\sigma}{\omega\varepsilon}\right)^{-1/2}. \tag{2.35}$$

Again, using the binomial expansion, η becomes:

$$\eta \approx \sqrt{\frac{\mu}{\varepsilon}}\left(1 + j\frac{\sigma}{\omega\varepsilon} - \frac{1}{8}\frac{\sigma^2}{\omega^2\varepsilon^2}\right) \tag{2.36}$$

Equation (2.36) can be simplified as ($\sigma / \omega\varepsilon << 1$):

$$\eta \approx \sqrt{\frac{\mu}{\varepsilon}}. \tag{2.37}$$

After simplifying equation (2.12), the phase velocity equation becomes

$$\upsilon = \frac{\omega}{k} = \frac{\omega}{\omega\sqrt{\varepsilon\mu}\left(1 + \frac{\sigma}{8\omega^2\varepsilon^2}\right)} \approx \frac{1}{\sqrt{\varepsilon\mu}}. \tag{2.38}$$

For a good conductor,

$$\left(\frac{\sigma}{\omega\varepsilon}\right) >> 1. \tag{2.39}$$

Equation (2.29) can be written

$$\gamma = \sqrt{j\omega\mu\sigma\left(1 + j\frac{\omega\varepsilon}{\sigma}\right)} \approx \sqrt{j\omega\mu\sigma} = \sqrt{\frac{\omega\mu\sigma}{2}}(1 + j). \tag{2.40}$$

The attenuation constant, after taking the real part the equation for a good conductor can be written as

$$\alpha \approx \sqrt{\frac{\omega\mu\sigma}{2}} \tag{2.41}$$

The wave number for a good conductor (taking the imaginary part) is given by

$$k \approx \sqrt{\frac{\omega\mu\sigma}{2}}. \tag{2.42}$$

Equation (2.35) can be written as:

$$\eta = \sqrt{\frac{j\omega\mu}{\sigma}} = \sqrt{\frac{\omega\mu}{2\sigma}}(1+j). \tag{2.43}$$

Again simplifying equation (2.38), the phase velocity becomes

$$\upsilon = \frac{\omega}{\beta} = \frac{\omega}{\sqrt{\frac{\omega\mu\sigma}{2}}} \approx \sqrt{\frac{2\omega}{\mu\sigma}}. \tag{2.44}$$

2.2.3 Polarization

Figure 2-1 and Figure 2-2 show the alignment of the electric field vector of a plane wave relative to the direction of propagation. This defines the polarisation of the wave.

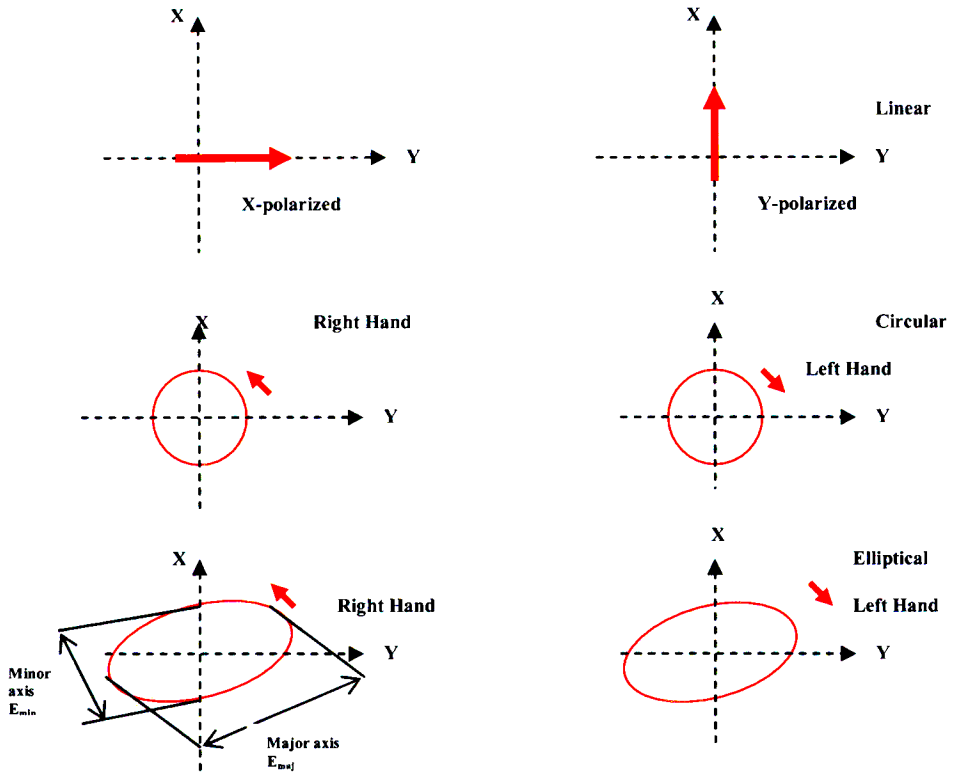

Figure 2-2: Wave polarization.

Consider the field electric expression given by

$$\vec{E} = E_x \hat{e}_x + E_y \hat{e}_y \tag{2.45}$$

Then the mathematical representation of the polarisation (phasors) can be summarised in Table 2-1.

Table 2-1: Polarization of the plane wave.

Polarization state	E_x	E_y
Vertical	$E_0 / \sqrt{2}$	0
Horizontal	0	$E_0 / \sqrt{2}$
RH circular	$-E_0 / \sqrt{2}$	$jE_0 / \sqrt{2}$
LH circular	$E_0 / \sqrt{2}$	$jE_0 / \sqrt{2}$
RH elliptical	$-aE_0 / \sqrt{2}$	$jE_0 / \sqrt{2}$
LH elliptical	$aE_0 / \sqrt{2}$	$jE_0 / \sqrt{2}$

2.2.4 Impact of the Environment on the Propagation of Radio waves

In the lossless media the angle of the reflected wave is related to the angle of incidence accoding to Snell' law of reflection:

$$\theta_i = \theta_r \tag{2.46}$$

This law is also a consequence of the Fermat principle:
Every path represents an extremum (usually a minimum) of the total electrical length of the ray.

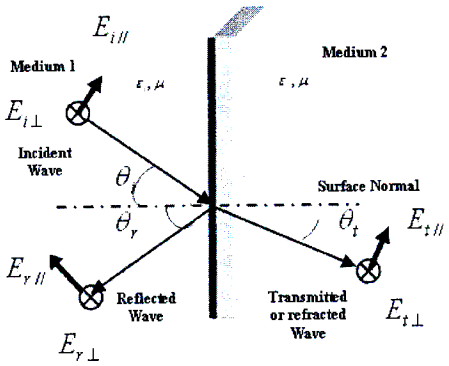

Figure 2-3: Uniform plane wave in lossless media.

In Figure 2-3 shows the reflection of plane wave onto a plane boundary for lossless media, and all quantities associated with the incident field will be denoted by the subscript i and those associated with the reflected and transmitted field by the subscript r and t, respectively. Thus $\vec{E}_i$, $\vec{E}_r$ and $\vec{E}_t$ denote the electric vectors of the incident, reflected and transmitted waves.

Similarly, $\vec{H}_i$, $\vec{H}_r$ and $\vec{H}_t$ denote the magnetic vectors of the incident, reflected and transmitted waves. ε_1 and μ_1 are the electric permittivity and magnetic permeability of

the first medium. Similarly ε_2 and μ_2 are the electric permittivity and magnetic permeability of the second medium.

When an incident plane wave hits a boundary between two homogeneous media of different dielectric properties, it is divided into two waves; a transmitted wave proceeding into the second medium and a reflected wave propagated back into the first medium, both at the same frequency as the incident wave, and both having their Poynting vectors in the incident plane.

Any arbitrarily polarized plane wave may be split into two waves, namely perpendicular ($E_{\perp}$) and parallel ($E_{//}$) components to the plane of incidence plane in Figure 2-4. These wave components are also known as Transversal Electric Wave (denoted by TE-Wave) and Transversal Magnetic Wave (denoted by TM-Wave), respectively. The angle of the refracted wave is related to the angle of incidence, as follows (Snell law of refraction):

$$\frac{\sin\theta_i}{\sin\theta_t} = \sqrt{\frac{\varepsilon_2\,\mu_2}{\varepsilon_1\,\mu_1}}. \tag{2.47}$$

The phase velocity of the wave in the medium with higher permittivity and permeability is reduced, causing the transmitted wave to bend toward the surface normal. The Fermat principle is also applicable.

The refractive index is defined as the ratio of the free space velocity to the phase velocity in the medium, and can be written as:

$$m = \frac{c}{\upsilon} = \sqrt{\frac{\varepsilon\,\mu}{\varepsilon_0\,\mu_0}}. \tag{2.48}$$

Then Snell's law becomes:

$$\frac{\sin\theta_i}{\sin\theta_t} = \frac{m_2}{m_1} \tag{2.49}$$

where m_1 and m_2 are refractive index of the first and second medium, respectively. The refractive index by layers depends on the pressure and the temperature of the gases. Based on Figure 2-3 the Fresnel reflection and transmission coefficients can be written as

$$\eta_1 = \sqrt{\frac{\mu_1}{\varepsilon_1}} \text{ and } \eta_2 = \sqrt{\frac{\mu_2}{\varepsilon_2}} \tag{2.52}$$

$$R_{//} = \frac{E_{r//}}{E_{i//}} = \frac{\eta_2\cos\theta_t - \eta_1\cos\theta_i}{\eta_2\cos\theta_t + \eta_1\cos\theta_i} \tag{2.53}$$

$$R_{\perp} = \frac{E_{r\perp}}{E_{i\perp}} = \frac{\eta_2\cos\theta_i - \eta_1\cos\theta_t}{\eta_2\cos\theta_t + \eta_1\cos\theta_t} \tag{2.54}$$

$$T_{//} = \frac{E_{t//}}{E_{i//}} = \frac{2\eta_2\cos\theta_t}{\eta_2\cos\theta_t + \eta_1\cos\theta_i} \tag{2.55}$$

$$T_{\perp} = \frac{E_{t\perp}}{E_{i\perp}} = \frac{2\eta_2\cos\theta_i}{\eta_2\cos\theta_i + \eta_1\cos\theta_t} \tag{2.56}$$

where η_1 and η_2 are the wave impedances for medium 1 and 2, respectively, which are characterized by the constitutive parameters of ε_1, μ_1 and ε_2, μ_2 and // means parallel to the scattering plane and $\perp$ means perpendicular to the scattering plane. The total reflected field and transmitted field are given by

$$\vec{E}_r = E_{r//}\hat{e}_{//} + E_{r\perp}\hat{e}_{\perp} = E_{i//}R_{//}\,\hat{e}_{//} + E_{i\perp}R_{\perp}\hat{e}_{\perp} \tag{2.57}$$

$$\vec{E}_t = E_{t\perp}\hat{e}_{\perp} + E_{t//}\hat{e}_{//} = E_{t//}T_{//}\,\hat{e}_{//} + E_{t\perp}T_{\perp}\hat{e}_{\perp} \tag{2.58}$$

The parallel and perpendicular reflected field and parallel and perpendicular transmitted field can be expressed in matrix as

$$\begin{bmatrix} \vec{E}_{r//} \\ \vec{E}_{r\perp} \end{bmatrix} = \begin{bmatrix} R_{//} & 0 \\ 0 & R_{\perp} \end{bmatrix} \begin{bmatrix} \vec{E}_{i//} \\ \vec{E}_{i\perp} \end{bmatrix} \tag{2.59}$$

$$\begin{bmatrix} \vec{E}_{t//} \\ \vec{E}_{t\perp} \end{bmatrix} = \begin{bmatrix} T_{//} & 0 \\ 0 & T_{\perp} \end{bmatrix} \begin{bmatrix} \vec{E}_{i//} \\ \vec{E}_{i\perp} \end{bmatrix} \tag{2.60}$$

2.2.5 Huygen's principle and Fresnel zone problem

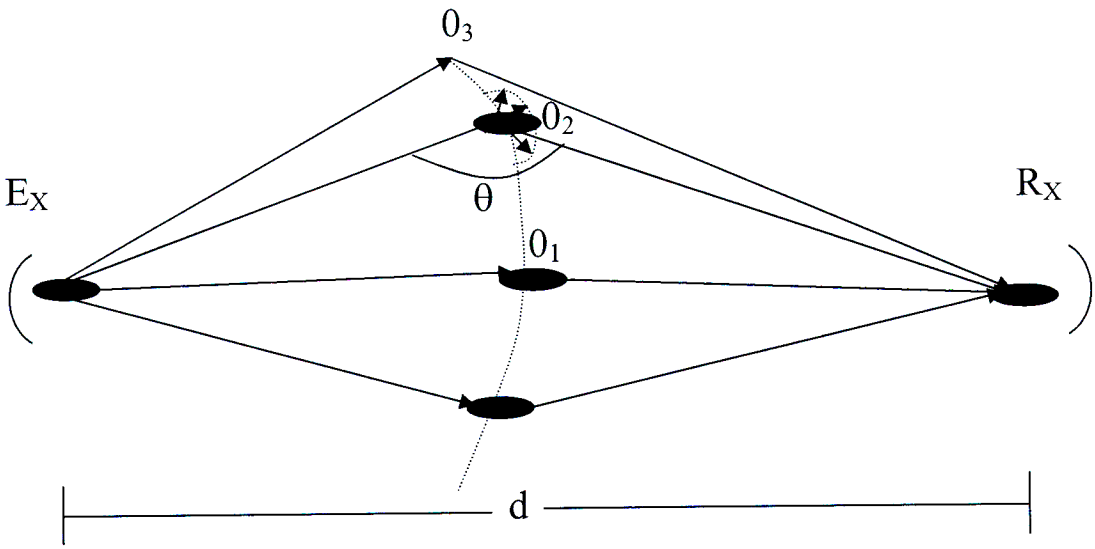

Figure 2-4: Huygen's principle.

A radio transmitter at E_X emits energy which travels outwards from the source in an expanding wave front. Huygen's principle states that each element of the primary wave front acts as a new source of radiation sending out a secondary wave front, such as at 0_2. The secondary wave radiations from all the elements of the original wave add up to form a new wave front.

The field strength at any point R is a vector sum of an infinite number of wavelets set up by the transmitting antenna. Only part of the new wave front from 0_2 will reach R depending on the distance of 0_2 from the transmitting antenna and the angle θ. If the path

difference between the direct path and the indirect path is λ/2, the phase difference between the two wave fronts will be 180 ^{0}C and the two wave fronts will add destructively. Similarly if the path difference is λ, the two wave fronts will add constructively.

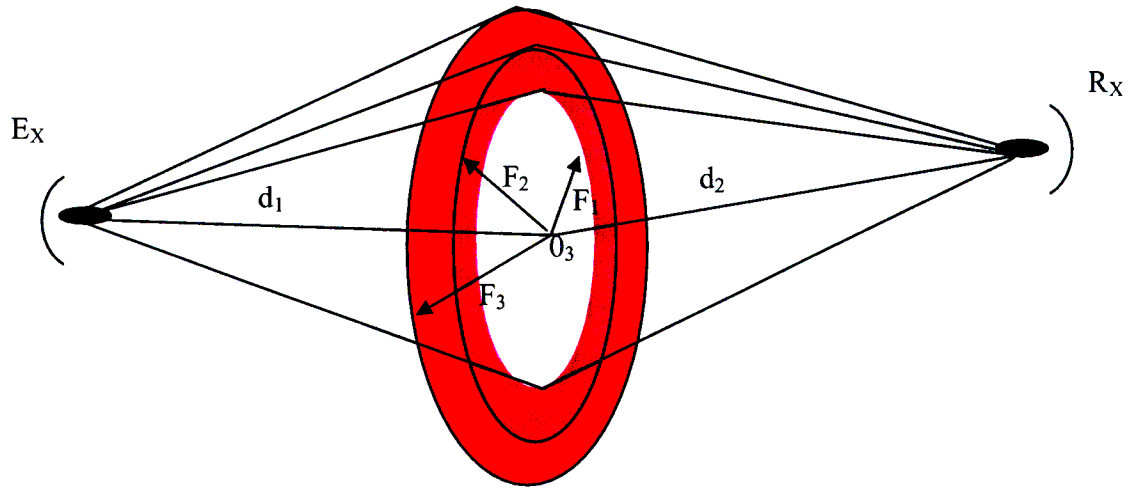

Figure 2-5: The Fresnel radius

In Figure 2-5 d_1 and d_2 are the distances in km to the near and far ends of the path respectively ($d = d_1 + d_2$ is the path length in km), and f is the frequency (MHz). The figure shows a cross-section of the area perpendicular to the direction of transmission. The shaded area with a radius F_1 shows the area in which the wave fronts add constructively. The area between F_1 and F_2 shows the area where the wave fronts add destructively while the area between F_2 and F_3 shows the area where the wave fronts add constructively. The area bounded by of the circle whose radius is F_1 is called the First Fresnel Zone, and F_1 is the first Fresnel radius. Similarly F_2 is the second Fresnel radius. These are defined mathematically by:

$$F_1 = 17.3\sqrt{\frac{d_1 d_2}{fd}} \tag{2.61}$$

$$F_2 = \sqrt{2}F_1, \qquad F_3 = \sqrt{2}F_2$$

About half of the signal energy reaching the receiving antenna passes through F_1. Therefore any terrain features that intrude into the first Fresnel Zone will lead to further reduction in the signal energy reaching the receiver. This is the basis of the clearance criteria which will be discussed later in Chapter 4.

2.2.6 Dielectric Properties of Water drops at Microwave Frequencies

Mie approximation needs the complex refractive index of spheres of which hydrometeors are examples such as rain (water drops), hail and snow. Most published studies usually relied on old dielectric data, such as Ray (1972), which are inaccurate at frequencies above 10 GHz.

The complex refractive index $m(f,T)$ depends on temperature T and frequency f, and is related to the dielectric permittivity $\varepsilon(f,T)$ by

$$m(f,T) = \sqrt{\varepsilon(f,T)} \tag{2.62}$$

In Cole and Cole (1941, cited Ray 1972), the complex permittivity of water was represented using the Debye relaxation. The Debye approximation was shown to be valid for frequencies up to 200 GHz and Ray (1972) extends this up to 300 GHz.

The knowledge of the dielectric properties of lossy materials, as explained above, of which water is an example, is important in the study of microwave propagation. The observation of dielectric properties of water at different temperatures is interesting, since water in these states generally occurs in rain, ice and clouds from which microwave signal may be attenuated.

Debye, in his original theory, supposed that the molecular dipoles could be visualized as tiny spheres, the rotation of which was opposed by forces related by Stokes's law to the macroscopic viscosity ϖ of the surrounding medium, and he deduced that

$$\tau = \frac{4\pi\varpi a^3}{k_B T} \tag{2.63}$$

where a is the molecular radius, k_B is the Boltzmann's constant, T is the absolute temperature and τ is the relaxation time, which is a measure of the time required for the dipole to rotate. Also, the relaxation time τ can be considered as the delay for the dipole to respond to the field change, or for reversion after disorientation. Further approaches to the problem of dipole relaxation have been studied by Frohlich (1949) and Eyring (1941).

The complex relative dielectric constant ε_r of a medium is related to the refractive index m and absorption coefficient ζ as follows:

$$\varepsilon_r = \varepsilon' - j\varepsilon'' = (m - j\zeta)^2 \tag{2.64}$$

The refractive index m and absorption coefficient k of water (rain) can be determined after getting both ε' and ε'' according to (2.63), τ depends on temperature in a way which can be written from the well-known Debye expression for the dielectric constant of a polar medium in a time-dependent fields.

$$\varepsilon' = \varepsilon_\infty + \frac{\varepsilon_s - \varepsilon_\infty}{1 + (\omega\tau)^2}, \tag{2.65}$$

$$\varepsilon'' = \frac{(\varepsilon_s - \varepsilon_\infty)\omega\tau}{1 + (\omega\tau)^2}. \tag{2.66}$$

Here, ε_∞ is the permittivity of water at infinity frequency. In his measurement of dielectric properties of pure polar liquids (water, methyl and ethyl alcohols) at different wavelengths within the temperature range of -8 to 50 °C, Lane and Saxton (I, 1952), observed the attenuation in transmission through wave guides of differing cross-section dimensions containing the liquid. Lane and Saxton (I, 1952) proposed:

The variations of the refractive index and absorption coefficient of water over the temperature range -8 to 50 °C, and for the three wave-lengths 6.2 mm, 124 cm and 3.21 cm, are shown in Table 2.2. The values of m have been calculated from the equation

$$(m - jk)^2 = \varepsilon_\infty + \frac{\varepsilon_s - \varepsilon_\infty}{1 + j\omega\tau}, \tag{2.67}$$

the corresponding values of k being known. In equation (2.67) ε_s is the static dielectric constant, ε_∞ is that part of the dielectric constant due to the electronic and atomic polarizations, reduced to 4.9, $\omega = 2\pi f$, where f is the frequency, and τ is a relaxation time (Debye 1929). Measurements of ε_s at temperatures below 0 °C do not exist, and it has been assumed here that a linear extrapolation between 0 and - 10 °C is sufficiently accurate. ε_∞ may be taken to be independent of temperature; τ varies with temperature in a manner which can be obtained from equation (2.67) when k is known.

This temperature range also covers the Southern Africa region. Thus the expressions in equations (2.65) and (2.66) follow from this, and are plotted in Figure 2-6.

Based on the value τ and measured data of ε_s (see Table 2.3), the components of the complex relative permittivity of pure water and its corresponding loss tangent have been calculated for microwave and millimeter waves range using equations (2.64), (2.65) and (2.66).

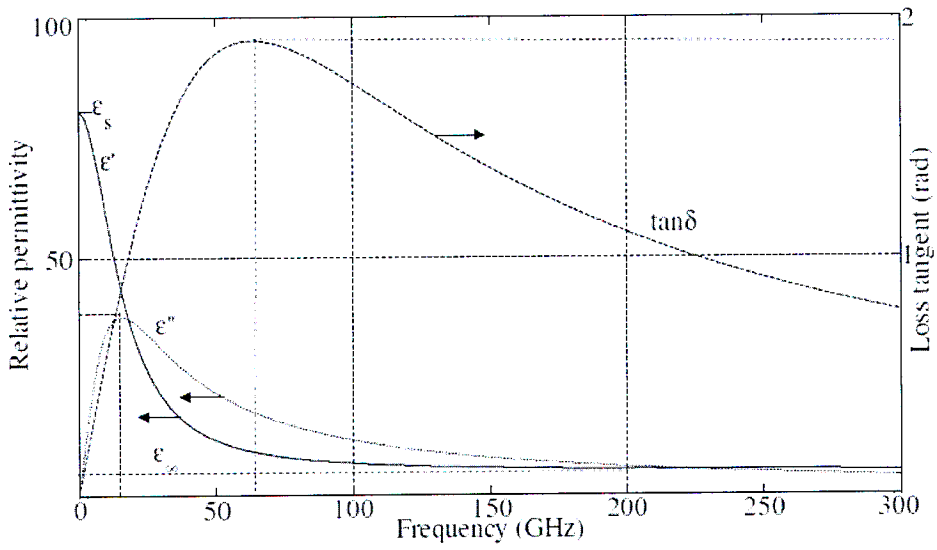

Figure 2-6: The complex dielectric properties of water at 20^0 C versus frequency at microwave and millimeter waves: [Hassen (Ch.2, 2006)].

Table 2-2: Dielectric properties of water: [Lane and Saxton (I, 1952)].

Temperature	$\lambda = 6.2mm$		$\lambda = 1.24mm$			$\lambda = 3.21mm$	
°C	k(meas.)	n(calc.)	k(meas.)	m(calc.)	m(calc.)	k(meas.)	m(calc.)
-10	1.77	3.10	2.55	-	4.15	-	6.48
0	2.04	3.45	2.77	4.75	4.70	2.89	7.14
10	2.37	3.94	2.90	5.45	5.42	2.44	7.80
20	2.59	4.44	2.86	6.15	6.10	2.00	8.14
30	2.70	4.90	2.67	6.70	6.62	1.60	8.24
40	2.70	5.35	2.41	7.10	7.02	1.29	8.22
50	2.63	5.73	2.13	7.30	7.20	1.08	8.13

The permittivity at infinite frequency ε_∞ is, [Liebe et al., 1991] [Liebe et al., 1993]

$$\varepsilon_\infty = \begin{cases} 3.52 + 7.52\theta \\ 3.512 \end{cases}, \tag{2.68}$$

Where $\theta = 1 - 300/T$ and T is the temperature in Kelvin. Thus at frequencies near or below 30 GHz the difference between the two models is negligible. It can be seen in Mätzler (2002) that the difference increases with increasing frequency and with temperature decreasing from 300^0K. In this dissertation the presently assumed standard dielectric model of water will be applied, as in Liebe et al (1991).

Table 2-3: Relaxation time (τ) in water (ε_∞ = 4.9).

Temperature °C	ε_s	τ (ps)
-10	92.3(extrap.)	27.5 (extrap.)
0	88.2	18.7
10	84.2	13.6
20	80.4	10.1
30	76.7	7.5
40	73.1	5.9
50	69.8	4.7

2.3 Conclusion

In this chapter we have presented the differential forms of Maxwell's equations. Materials and media which are conductors, semi-conductors and dielectrics contain charged particles that react to applied electric and magnetic fields to produce secondary fields. We learned that there are three basic phenomena resulting from the interaction of the charged particles with the electric and magnetic fields (semi-conduction, conduction and polarization). We studied problems involving two different media and the boundary conditions, which are a set of conditions for the fields to satisfy at the boundaries between the different media. We used the boundary conditions to study the reflection and transmission of uniform plane waves at plane boundaries. Finally, we then studied the dielectric properties of water at different temperatures versus frequency based on Ray, Debye and Liebe approaches.

Chapter 3

Rainfall Rate Distribution Models and Rain Zones Proposed

3.1 Introduction

In Appendix A we study the Rayleigh and Mie scattering theories applied to rain. In the study of rain attenuation, two vital factors are rain rate and rain drop size distribution (DSD). Any rain rate can correspond to different DSDs, that is different DSD may have the same rain rate. It also means that rain rate itself does not constitute enough data in the model to be the only parameter to estimate or predict rain attenuation. Actual raindrop size distribution in the real world is controlled by many factors such as rainfall intensity, circulation system, type of precipitation, etc.

As a result of the rapidly varying nature of rainfall at a given point, the cumulative rainfall rate distribution measured is dependent on the sampling time of the rain gauge. There is need to convert the available one-hour rain rates measured by most national weather bureaus to one-minute data. In this chapter, a simple approach is used to determine the conversion factors for the Botswana sites which lack one-minute exceedence; the cumulative identity is employed to find the conversion factor for regions in Botswana which have daily rainfall data. Botswana's daily cumulative distributions are compared with South African daily cumulative distributions. South Africa is chosen because both daily, hourly, five-minute and one-minute rainfall results are available. Also, ITU-R Recommendation P-837-1 and P-837-4 [ITU-R, 2001] classify the Southern Africa region into seven climatic rain zones by using the median cumulative distribution of rain rate for the rain climatic region. The same method is employed in this thesis to classify the Botswana regions into their classes of rain zones. However, these ITU-R

designations are not necessarily adequate, as they need further refinement; thus there is need to redefine the ITU-R regional climatic zones based on the actual local data. From the local data measured by Botswana Meteorological Service for fourteen locations, two climatic rain zones are determined for Botswana based on the analysis of the fourteen locations, namely, M and Q. Also, we study a practical case of the performance of an existing radio link in Gaborone by determining the fade margin at 99.99% of exceedence under extreme weather conditions.

3.2 Rainfall Rate Modeling

In Southern Africa, especially in South Africa, the work on rain rate and raindrop size distribution models for line-of-sight millimetric or satellite systems, has been carried out [Owolawi, 2006; Naicker, 2006; Fashuyi, 2006 and Fashuyi et al., 2006]. Typical values of rain intensity R are 0.25 mm/h (drizzle), 1 mm/h (light rain), 4 mm/h (moderate rain), 16 mm/h (heavy rain), and 100 mm/h (extremely heavy rain) [Hassen, 2006]. Based on Laws and Parsons' theory, Alfred and Bogush (1989) determined that a very big fraction of raindrops are larger than $D \geq 1$ mm at rainfall intensities $R \geq 2.5$ mm/h. According to Akira Ishimaru (1991, Chapter 3), these raindrops may have large extinction (σ_{ext}) and absorption (σ_{abs}) cross sections as described in Section A.4.

The relationship between one-minute rain rate and daily rain rate has been found by regression fit to match the power law relationship to some known theoretical power laws by Segal (1986) and Ajayi et al (1983). Using the RMS criterion to test the regression fit, a good relationship is obtained between rain rate and DSD. The root mean square (RMS) and Chi-square test are given in equations (3.1) and (3.2).

$$RMS = \sqrt{\frac{1}{n}\sum_{i=1}^{n}(x_i - x_n^{'})^2} \tag{3.1}$$

$$Chi-square\ \chi^2 = \sum_{i=1}^{n}\frac{(x_i - x_i')^2}{x_i'} \tag{3.2}$$

where $\{x_1, x_2, x_3, ..., x_n\}$ is experiment data set; $\{x_1', x_2', x_3', ..., x_n'\}$ is theoretical model data set.

Table 3-1 shows cumulative distribution identities which are optimized by RMS criterion in order to determine, for a location in Botswana, the closest rain rate distribution for several sites in South Africa. In the case of Gaborone, the closest Cumulative distribution functions (CDF) in South Africa are Nongoma, Langgewacht, Middelwater and Victoria. In this case, the CDF which gives the lowest RMS value is determined to be Middelwater; we thus conclude that for Gaborone, the closest CDF is that of Middelwater. The other thirteen Botswana sites, namely, Gaborone, Francistown, Kasane, Selebi-Phikwe, Mahalapye, Tshabong, Shakawe, Tshane, Sua Pan, Maun, Lethlakane, Gansi, Jwaneng and Pandamatenga have least RMS values of 6.301, 5.379, 2.580, 6.174, 2.584, 4.782, 4.766, 7.188, 4.782, 5.499, 5.554, 4.153, 4.865, and 7.096 respectively, corresponding to South African sites of Langgewacht, Victoria, Stanger, Victoria, Victoria, Victoria, Victoria, Victoria, Victoria, Victoria, Victoria, Victoria and Middelwater respectively. Table 3-1 summarizes the model results.

3.3 Model Parameters Fitting

As a result of the rapidly varying nature of rainfall at a given point, the cumulative rainfall rate distribution measured is dependent on the sampling time of the rain gauge. There are several existing methods to convert 1-minute rainfall rate distribution from various time rainfalls. They include: the Canadian model suggested by Segal (1986); the French model by Moupfouma (1995), and the Japanese model by Karasawa (1990). Since in radio wave prediction techniques, an integration time of one minute has been adopted by the ITU-R as the most desirable compromise for attenuation prediction [Segal, 1986], Segal has defined a conversion factor, $\rho_\tau(P)$ for converting data obtained with a gauge having an integration time of τ minutes to the equivalent one-minute statistics, as follows [Segal, 1986]:

$$\rho_\tau(P) = R_1(P)/R_\tau(P) \tag{3.2}$$

where R_1 and R_τ are the rainfall rate exceeded, with equal probability P, for the two integration times (referred to as equiprobable rain rates) R_1 and R_τ [Segal,1986 and Ajayi et al 1983]. The factor $\rho_\tau(P)$ is also given by the power law [Rice et al 1973]:

$$\rho_\tau(P) = a.P^b \tag{3.3}$$

over the range $0.001\% \leq P \leq 0.03\%$, with a and b being constants that depend on the climatic zone. It has also been found that a power law relationship exists between the equiprobable rain rates of two integration times. The power law relationship is given by [Watson et al 1981]:

$$R_\tau = aR_T^b \tag{3.4}$$

where R is the rain rate, τ is the integration time at which the rain rate is required, and T is the integration time at which the rain rate is available.

Next, the Segal and Ajayi approaches are used to determine the conversion factor to convert from daily integration time to an effective one-minute integration time [Ajayi et al., 1983 and Segal, 1986]. Note that only the South African data is used to effect this conversion due to the fact that 1-minute data was only available for South Africa for the 5 years, but was not available for the other fourteen sites in Botswana. This results in a linear scatter plot of data points, in which a simple power law fits, as shown in Figure 3-1:

$$R_{1\min} = \alpha R_{Daily}^{\beta} \tag{3.5}$$

Thus, the corresponding coefficients of α and β in equation (3.5) are used to convert daily rain rate data from locations in Botswana to an effective 1-minute integration time. Figures 3-2 shows conversion factors graphs with their coefficients shown in Table 3-2. R^2 is the correlation coefficient, which should be close to one.

Table 3-1: Summary of the model testing results.

Sites in Botswana		Sites in SA			
		Victoria	Langgewacht	Middelwater	Nongoma
Gaborone	RMS error	7.340	7.002	6.301	19.189
		Langgewacht	Middelwater	Victoria	Port Nolloth
Jwaneng	RMS error	6.409	8.799	4.865	5.625
		Langgewacht	Middelwater	Victoria	Nongoma
Mahalapye	RMS error	3.405	4.513	2.584	8.619
		Nongoma	Middelwater	Victoria	Laggewacht
Ghanzi	RMS error	11.137	6.861	4.153	5.683
		Nongoma	Middelwater	Laggewacht	Victoria
Lethalakane	RMS error	21.208	6.088	7.094	5.554
		Nongoma	Langgewacht	Middelwater	Victoria
Shakawe	RMS error	12.209	6.140	7.411	4.766
		Nongoma	Langgewacht	Middelwater	Victoria
Tshabong	RMS error	25.839	6.431	8.556	4.782
		Nongoma	Langgewacht	Middelwater	Victoria
Tshane	RMS error	15.046	8.573	9.749	7.188
		Nongoma	Langgewacht	Middelwater	Victoria
Sua Pan	RMS error	11.369	5.442	9.749	4.782
		Nongoma	Langgewacht	Middelwater	Victoria
Francistown	RMS error	15.863	7.184	5.379	8.147
		Nongoma	Osisweni	Middelwater	Stanger
Selebi-Phikwe	RMS error	6.881	8.003	10.868	6.174
		Langgewacht	Victoria	Middelwater	Nongoma
Kasane	RMS error	3.360	2.580	4.347	8.156
		Langgewacht	Victoria	Middelwater	Port No
Maun	RMS error	6.708	5.499	8.465	17.329
		Langgewacht	Nongoma	Middelwater	Victoria
Pandamatenga	RMS error	9.493	13.874	7.096	17.765

Table 3-2: Coefficients for R = 1 Min and T= 24 hrs

Station	α	β	R^2
Gaborone	4.9592	0.5028	0.9442
Francistown	3.2882	0.5877	0.9822
Kasane	3.01	0.6117	0.9776
Selebi-Phikwe	0.4508	1.1159	0.9817
Mahalapye	3.241	0.5958	0.9619
Shakawe	4.0693	0.5538	0.9572
Tshane	3.7964	0.614	0.9663
Sua Pan	4.1418	0.5436	0.9401
Maun	3.7913	0.5999	0.9748
Lethakane	3.7494	0.5701	0.9527
Ganzi	2.4546	0.7684	0.885
Pandamatenga	3.2049	0.5965	0.9783
Tshabong	3.1736	0.6433	0.9324
Jwaneng	3.46	0.6132	0.977

Note that this conversion procedure has been used in (Mulangu et al., 2007), and found to be reliable.

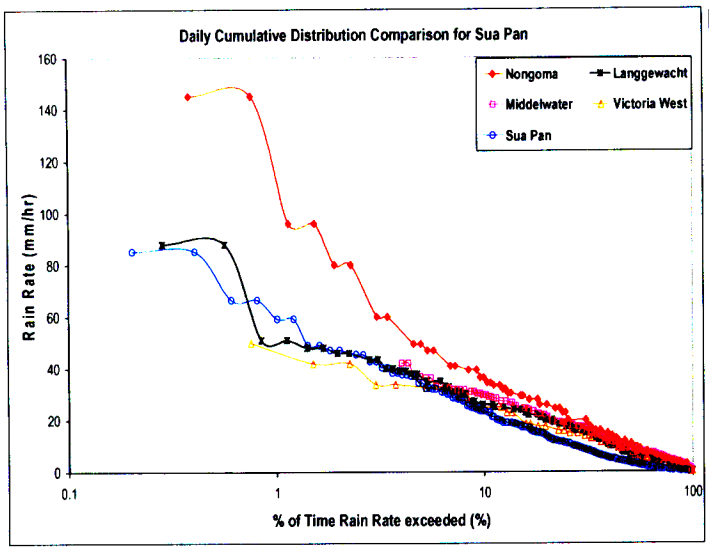
Daily Cumulative Distribution Comparison for Sua Pan
Nongoma
Langgewacht
Middelwater
Victoria West
Sua Pan
Rain Rate (mm/hr)
% of Time Rain Rate exceeded (%)

(a)

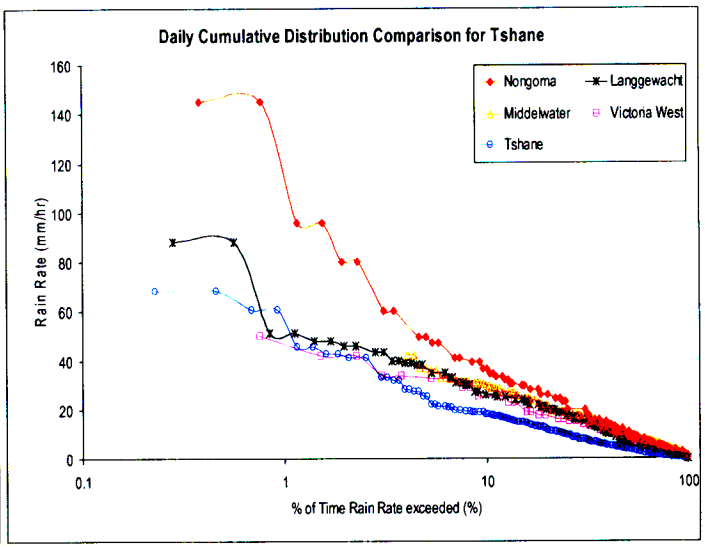
Daily Cumulative Distribution Comparison for Tshane
Nongoma
Langgewacht
Middelwater
Victoria West
Tshane
Rain Rate (mm/hr)
% of Time Rain Rate exceeded (%)

(b)

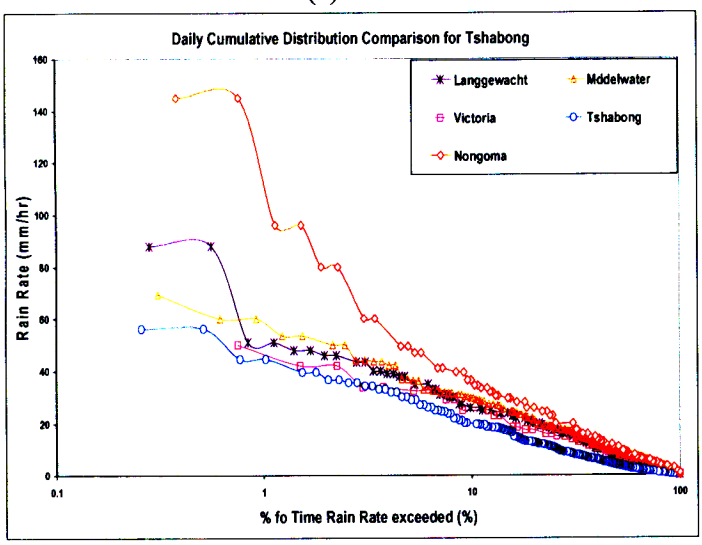
Daily Cumulative Distribution Comparison for Tshabong
Langgewacht
Middelwater
Victoria
Tshabong
Nongoma
Rain Rate (mm/hr)
% fo Time Rain Rate exceeded (%)

(c)

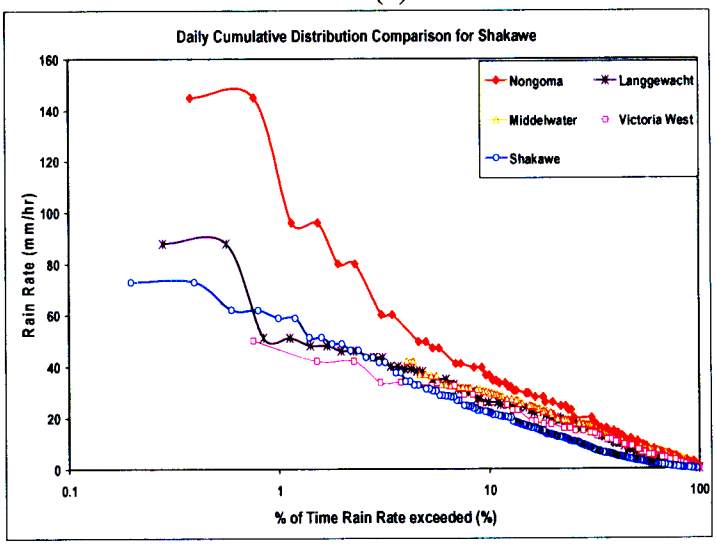
Daily Cumulative Distribution Comparison for Shakawe
Nongoma
Langgewacht
Middelwater
Victoria West
Shakawe
Rain Rate (mm/hr)
% of Time Rain Rate exceeded (%)

(d)

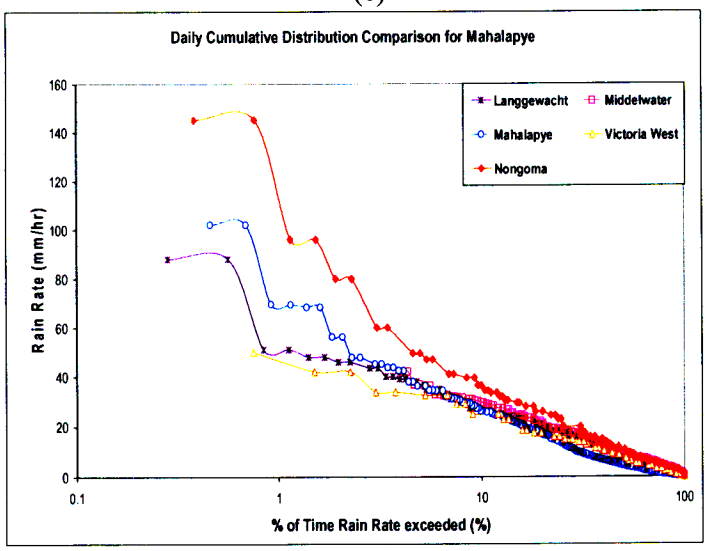
Daily Cumulative Distribution Comparison for Mahalapye
Langgewacht
Middelwater
Mahalapye
Victoria West
Nongoma
Rain Rate (mm/hr)
% of Time Rain Rate exceeded (%)

(e)

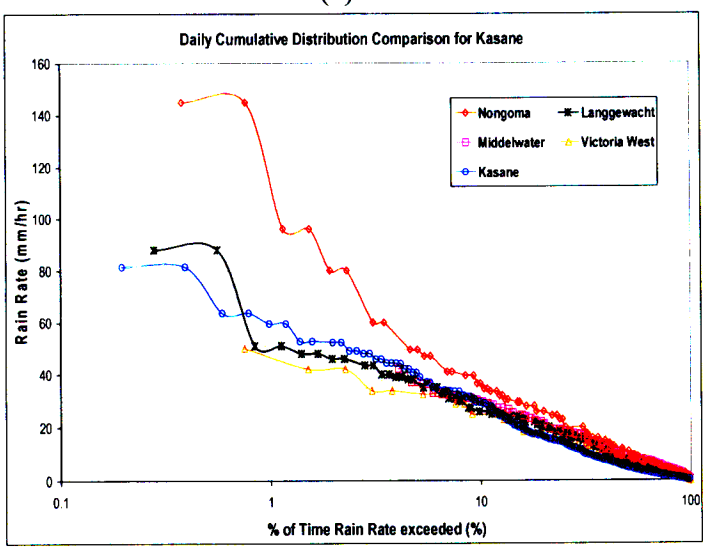
Daily Cumulative Distribution Comparison for Kasane
Nongoma
Langgewacht
Middelwater
Victoria West
Kasane
Rain Rate (mm/hr)
% of Time Rain Rate exceeded (%)

(f)

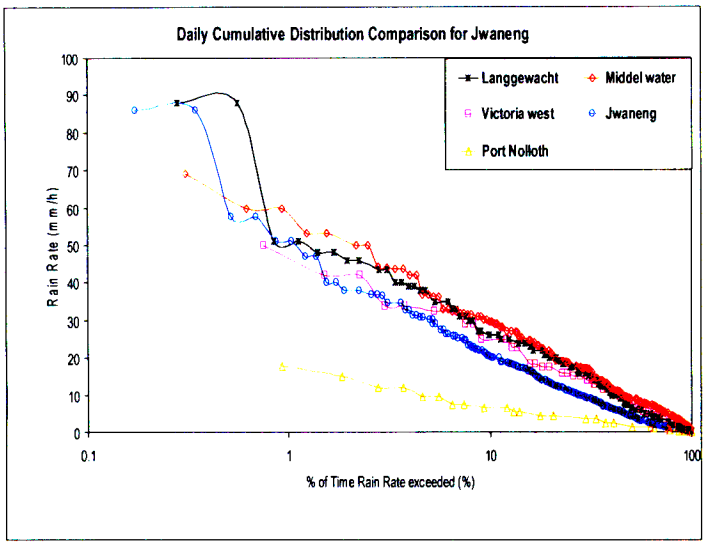
Daily Cumulative Distribution Comparison for Jwaneng
Langgewacht
Middel water
Victoria west
Jwaneng
Port Nolloth
Rain Rate (mm/h)
% of Time Rain Rate exceeded (%)

(g)

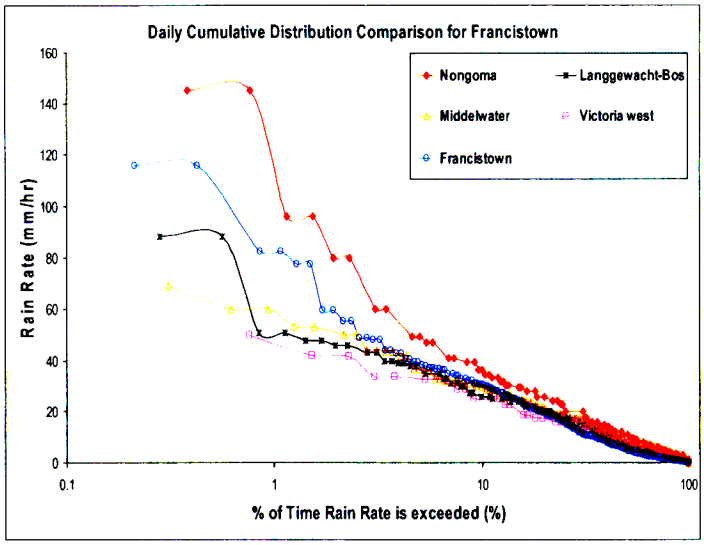
Daily Cumulative Distribution Comparison for Francistown
Nongoma
Langgewacht-Bos
Middelwater
Victoria west
Francistown
Rain Rate (mm/hr)
% of Time Rain Rate is exceeded (%)

(h)

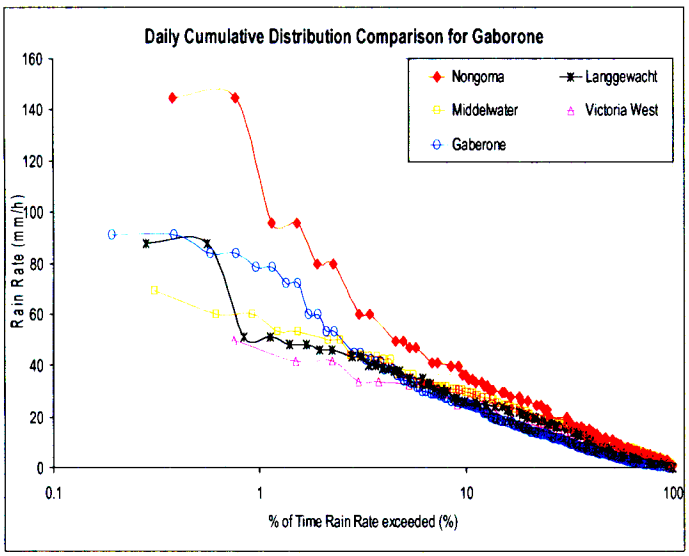
Daily Cumulative Distribution Comparison for Gaborone
Nongoma
Langgewacht
Middelwater
Victoria West
Gaberone
Rain Rate (mm/h)
% of Time Rain Rate exceeded (%)

(i)

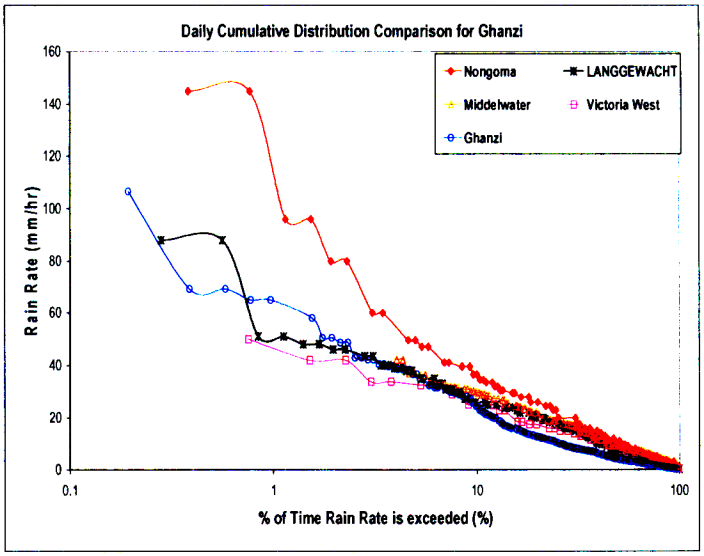
Daily Cumulative Distribution Comparison for Ghanzi
Nongoma
LANGGEWACHT
Middelwater
Victoria West
Ghanzi
Rain Rate (mm/hr)
% of Time Rain Rate is exceeded (%)

(j)

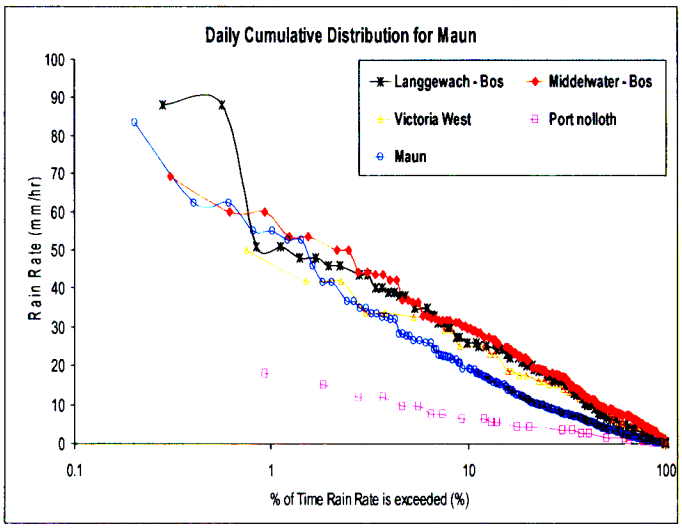
Daily Cumulative Distribution for Maun
Langgewach - Bos
Middelwater - Bos
Victoria West
Port nolloth
Maun
Rain Rate (mm/hr)
% of Time Rain Rate is exceeded (%)

(k)

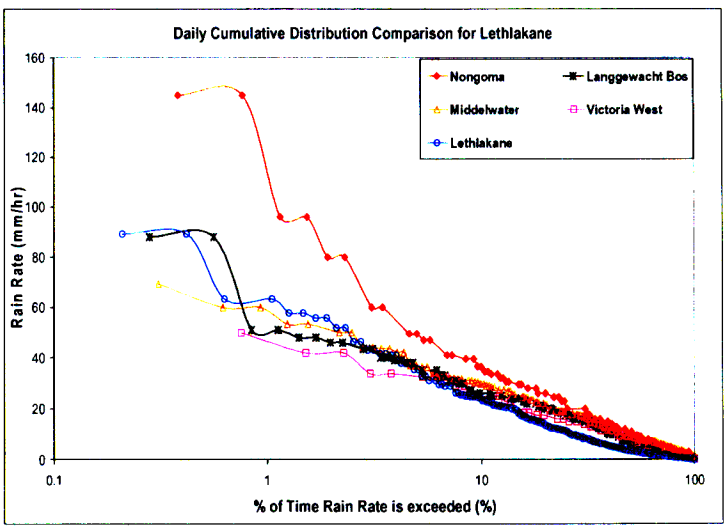
Daily Cumulative Distribution Comparison for Lethlakane
Nongoma
Langgewacht Bos
Middelwater
Victoria West
Lethlakane
Rain Rate (mm/hr)
% of Time Rain Rate is exceeded (%)

(l)

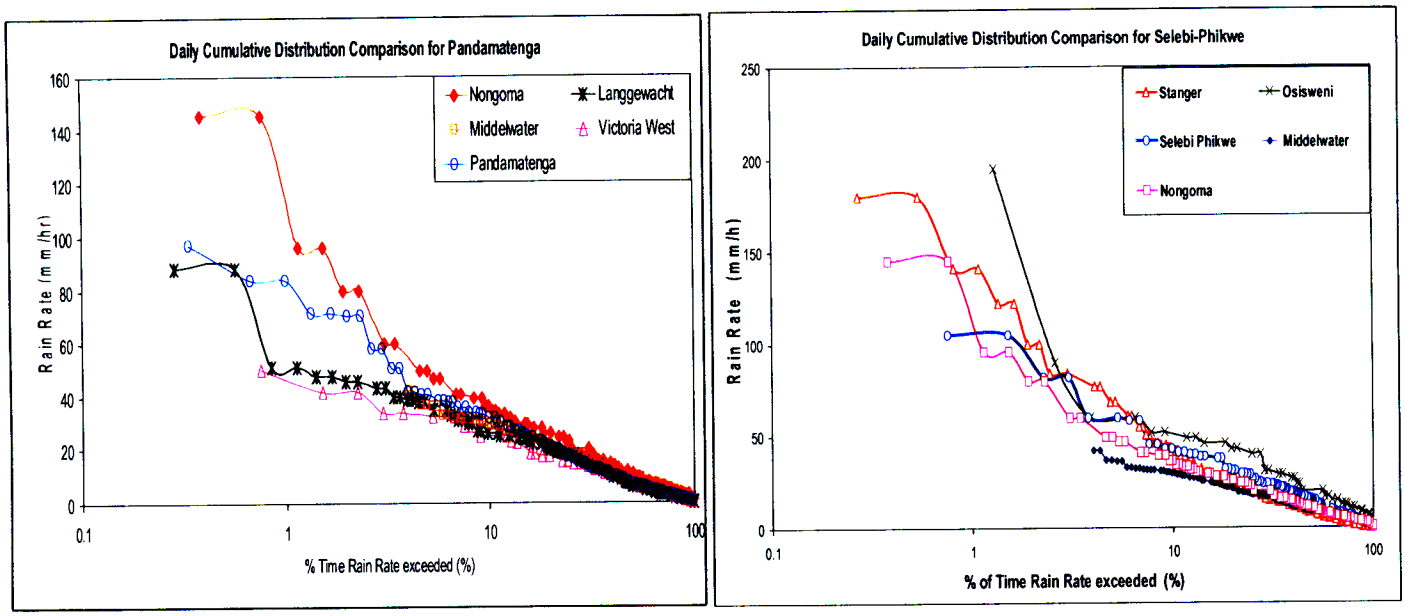

(m) (n)

Figure 3-1a, b and up to n: Cumulative Distribution of Rain Rate intensity for Botswana.

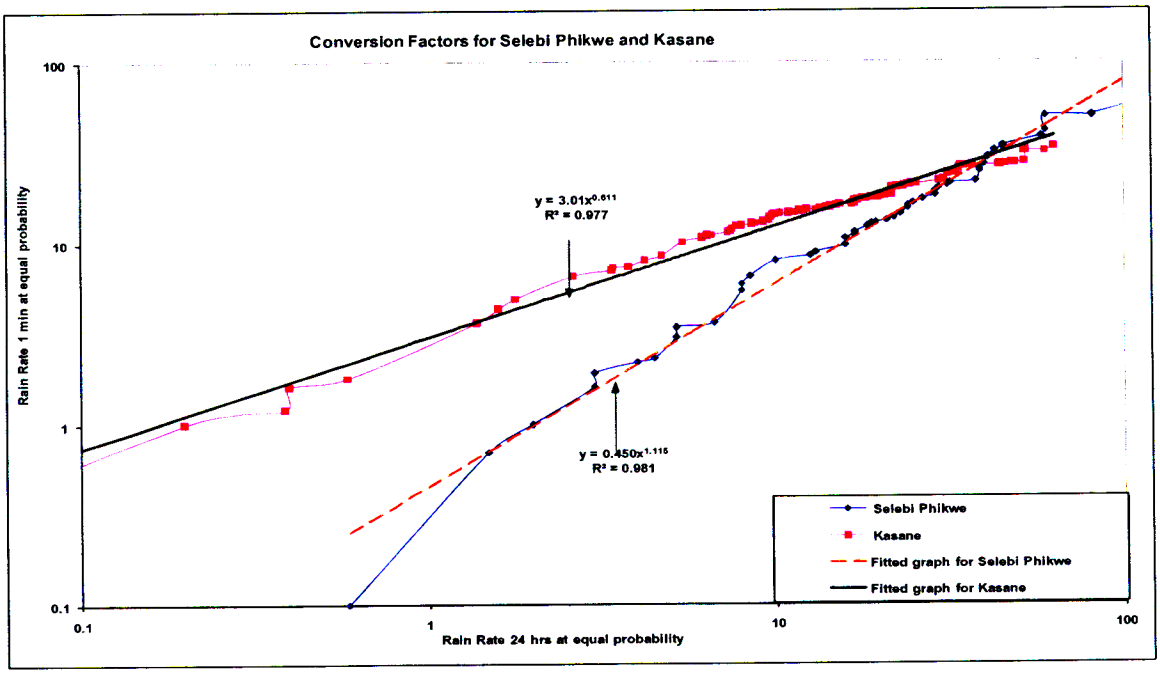

(a)

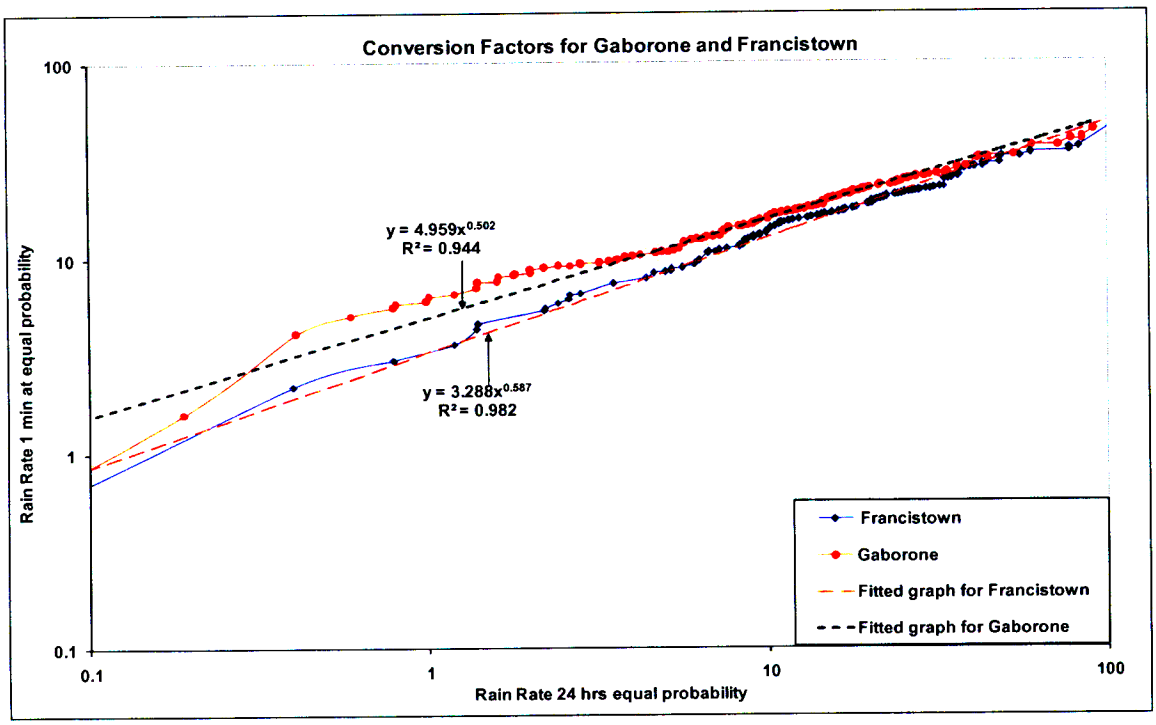
Conversion Factors for Gaborone and Francistown
Rain Rate 1 min at equal probability
Rain Rate 24 hrs equal probability
y = 4.959x^0.502
R² = 0.944
y = 3.288x^0.587
R² = 0.982
Francistown
Gaborone
Fitted graph for Francistown
Fitted graph for Gaborone
100
10
1
0.1
0.1
1
10
100

(b)

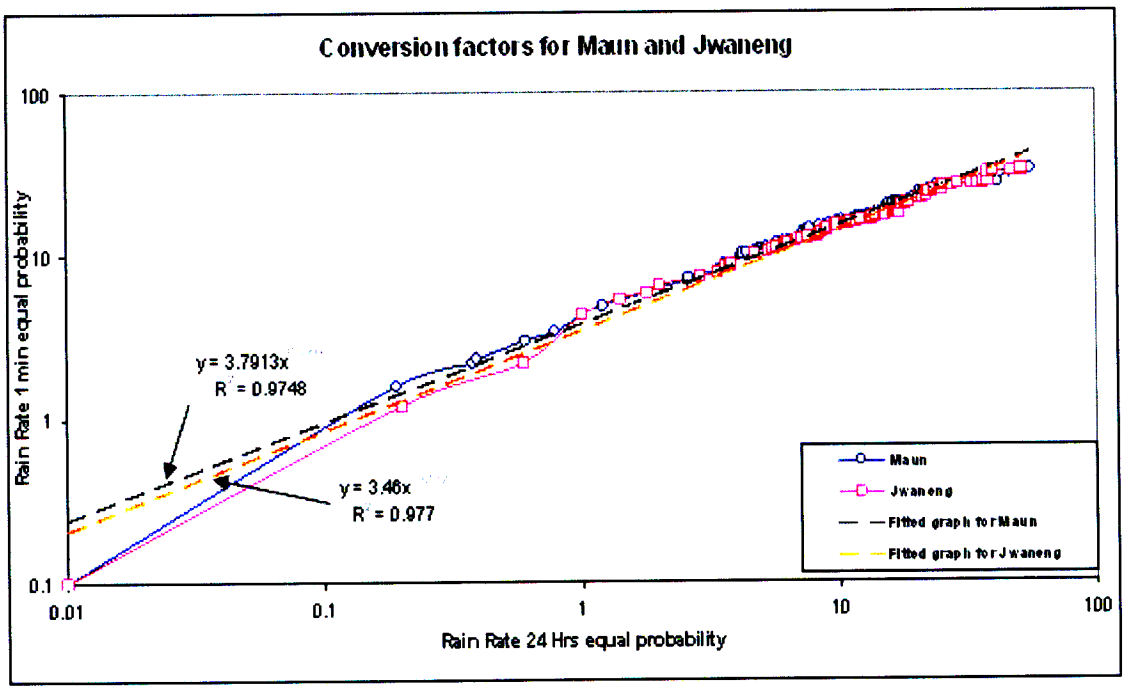
Conversion factors for Maun and Jwaneng
Rain Rate 1 min equal probability
Rain Rate 24 Hrs equal probability
y = 3.7913x
R² = 0.9748
y = 3.46x
R² = 0.977
Maun
Jwaneng
Fitted graph for Maun
Fitted graph for Jwaneng
100
10
1
0.1
0.01
0.1
1
10
100

(c)

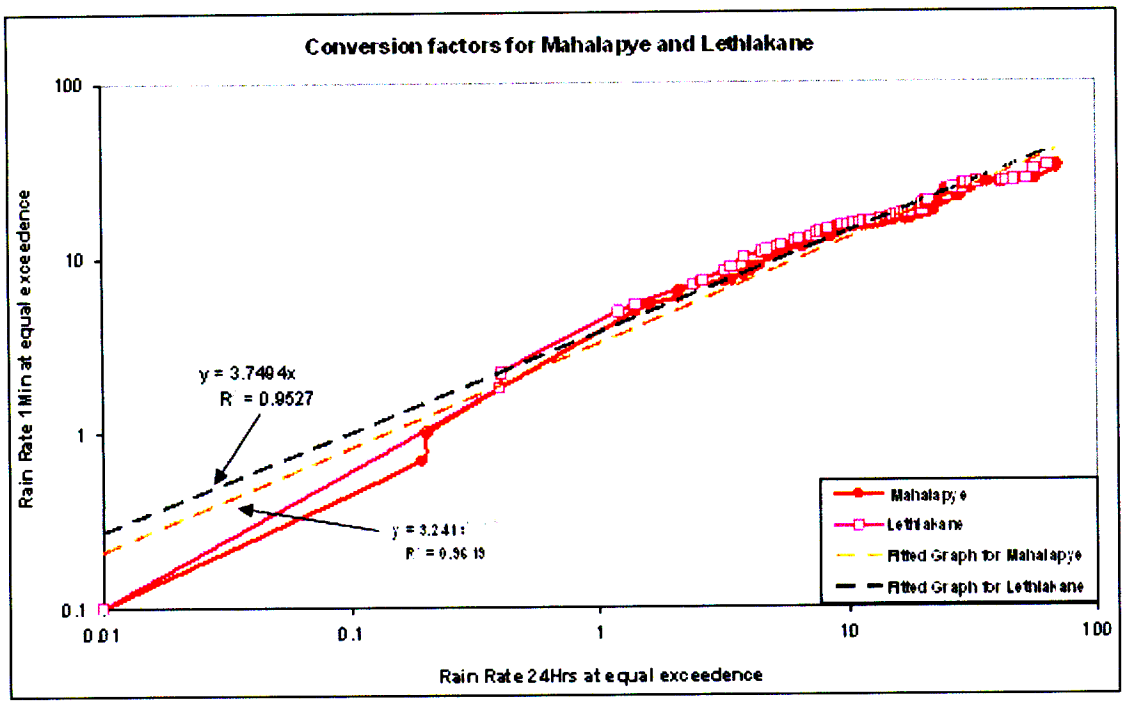
Conversion factors for Mahalapye and Lethlakane
Rain Rate 1Min at equal exceedence
Rain Rate 24Hrs at equal exceedence
100
10
1
0.1
0.01
0.1
1
10
100
y = 3.7494x
R = 0.9527
Mahalapye
Lethlakane
Fitted Graph for Mahalapye
Fitted Graph for Lethlakane

(d)

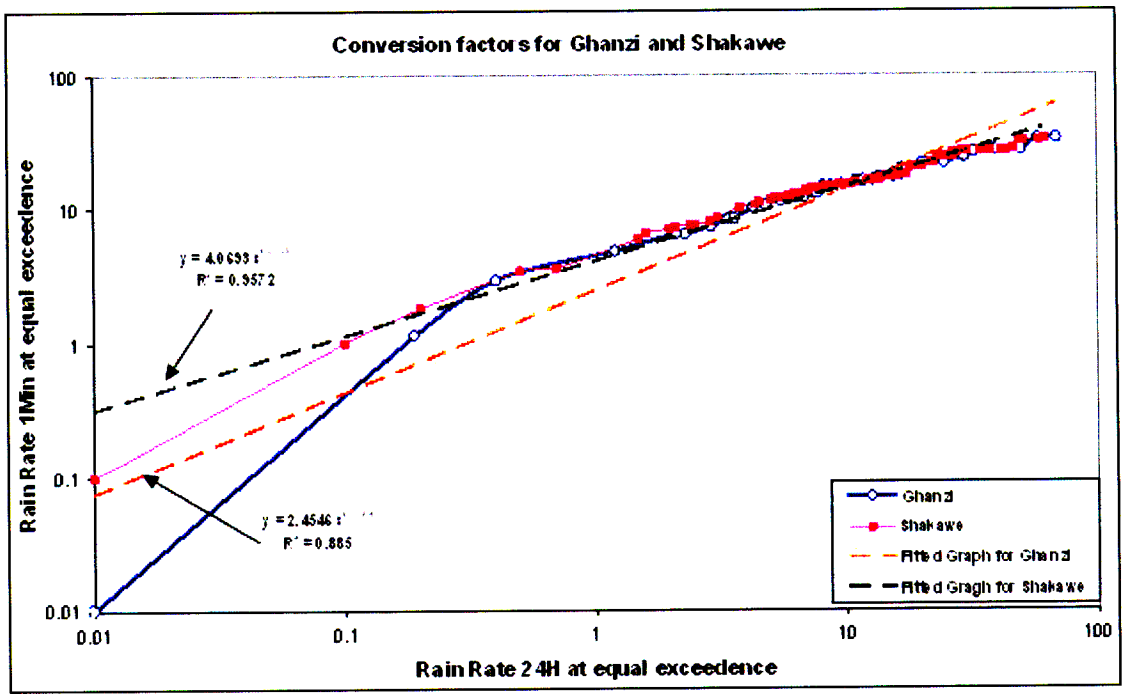
Conversion factors for Ghanzi and Shakawe
Rain Rate 1Min at equal exceedence
Rain Rate 24H at equal exceedence
100
10
1
0.1
0.01
0.01
0.1
1
10
100
Ghanzi
Shakawe
Fitted Graph for Ghanzi
Fitted Gragh for Shakawe

(e)

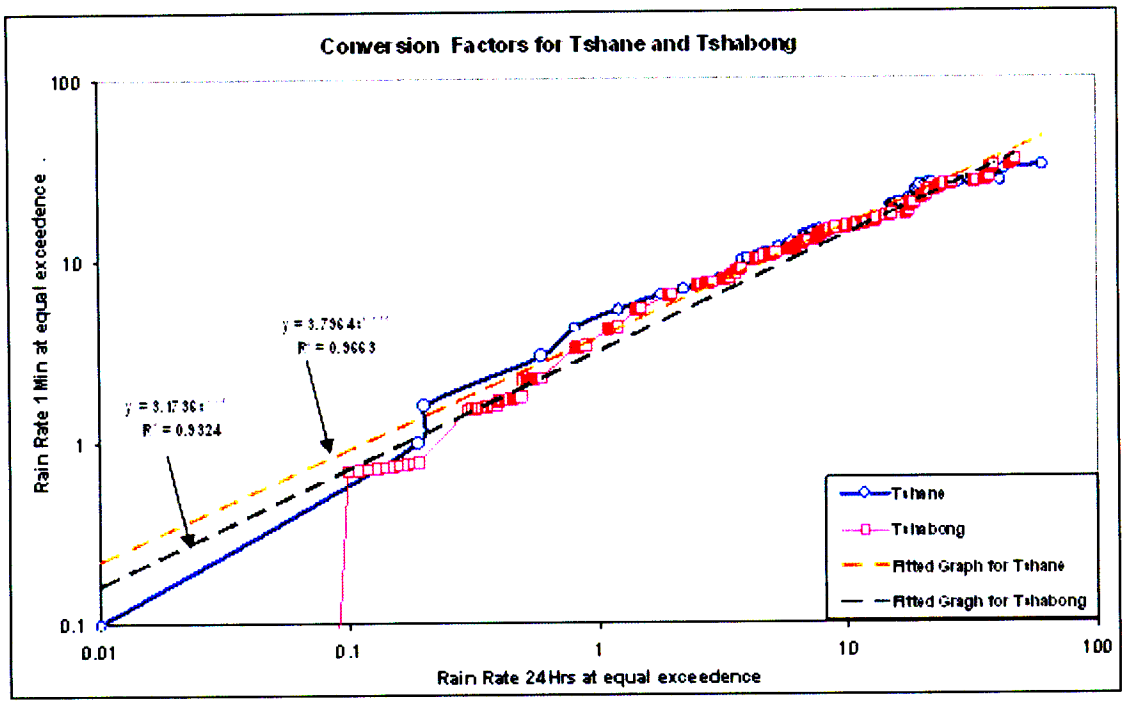

(f)

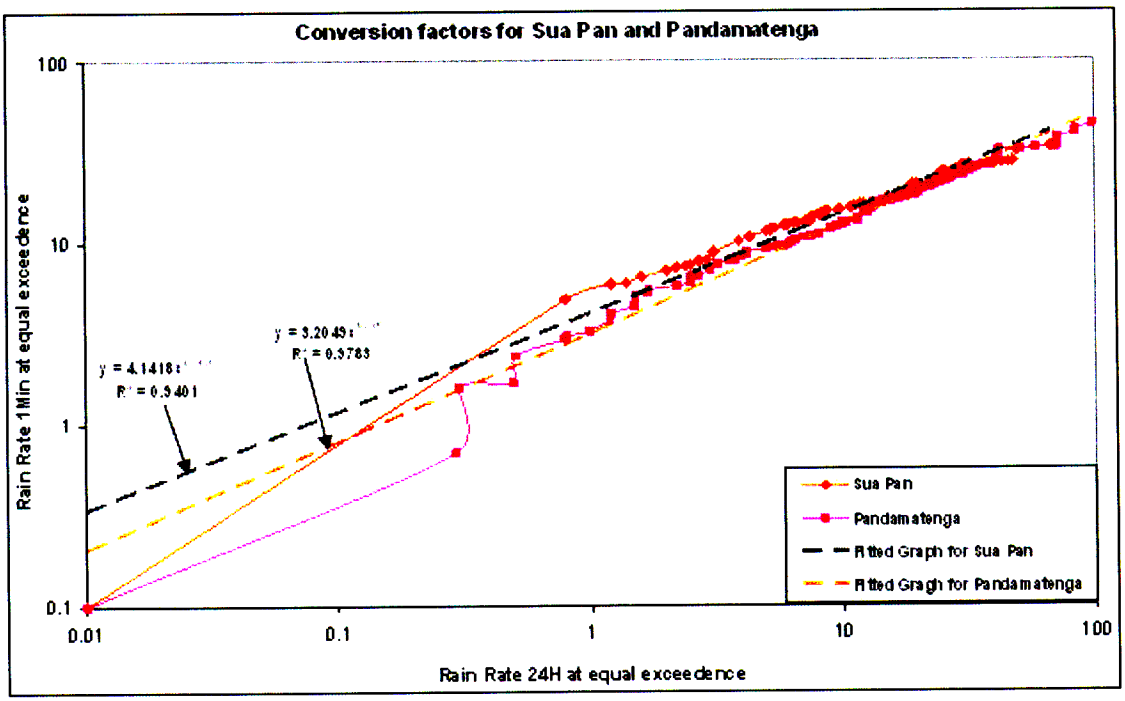

(g)

Figure 3-2 a, b and up to g: Conversion factors for Botswana locations

3.4 Estimated Cumulative Distribution of Rain Rate for Botswana

Cumulative distributions (CD's) of ten-year 1-minute rain intensities for fourteen regions in Botswana are plotted in Figure 3-3. The cumulative distribution is based on rain intensities and percentages of time: the higher the rain intensity the lower the corresponding percentage of time recorded, while the lower the rain intensity the higher the percentage of time for it to occur. For Gaborone, at 0.1% of time percentage, the rain intensity is 52.64 mm/h, while at the lower time percentage of 0.01%, the rain intensity is 68.9 mm/h. This results in a rain rate difference between 0.1% and 0.01% of 16.26 mm/h. In the case of Kasane, the distribution shows that at 0.1% the rain intensity is 48.95 mm/h, while at 0.01% the intensity is 64.4 mm/h. The rain rate difference between 0.1% and 0.01% of the time is thus 15.45 mm/h. Table 3-3 summarizes rain rates for fourteen locations in Botswana.

Table 3-3: Rain rate for fourteen locations in Botswana.

Location	Rain rate (mm/h)		
	$R_{0.01}$	$R_{0.1}$	difference
Gaborone	68.9	52.64	16.26
Francistown	85.97	65.3	20.94
Kasane	64.4	48.95	15.45
Selebi-Phikwe	137.06	100.83	36.23
Mahalapye	87.70	66.15	18.28
Shakawe	78.14	59.86	18.28
Tshane	79.77	60.2	19.57
Sua Pan	67.89	51.49	16.40
Maun	78.44	59.43	19.01
Lethlakane	72.31	54.77	17.54
Ghanzi	114.37	86.16	28.21
Pandamatenga	73.64	56.09	17.55
Tshabong	64.20	48.71	15.49
Jwaneng	75.74	57.46	18.28

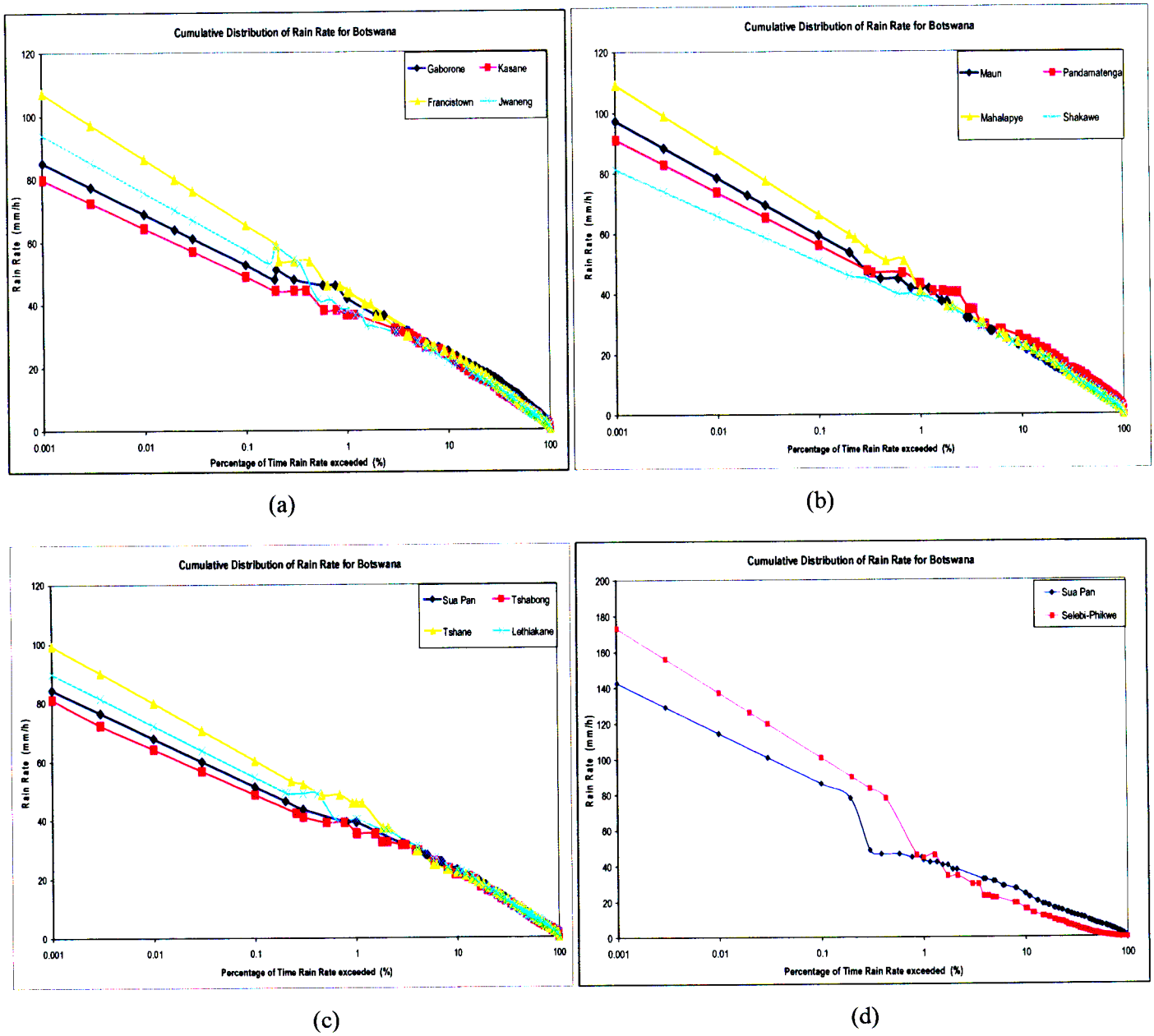

Figure 3-3 a, b c, d: Average Cumulative Distribution of Rain Rate for Botswana of 10 years.

From Figure 3-4 and 3-5, rainfall accumulation in Botswana is different from year-to-year, month-to-month and day-to-day for all locations. In Figure 3-4 it can be seen that Tshane and Tshabong which are located in a desert environment area in Botswana are seen to record the lowest annual rainfall accumulation in all years; 1996, 2000 and 2004 compared to other locations.

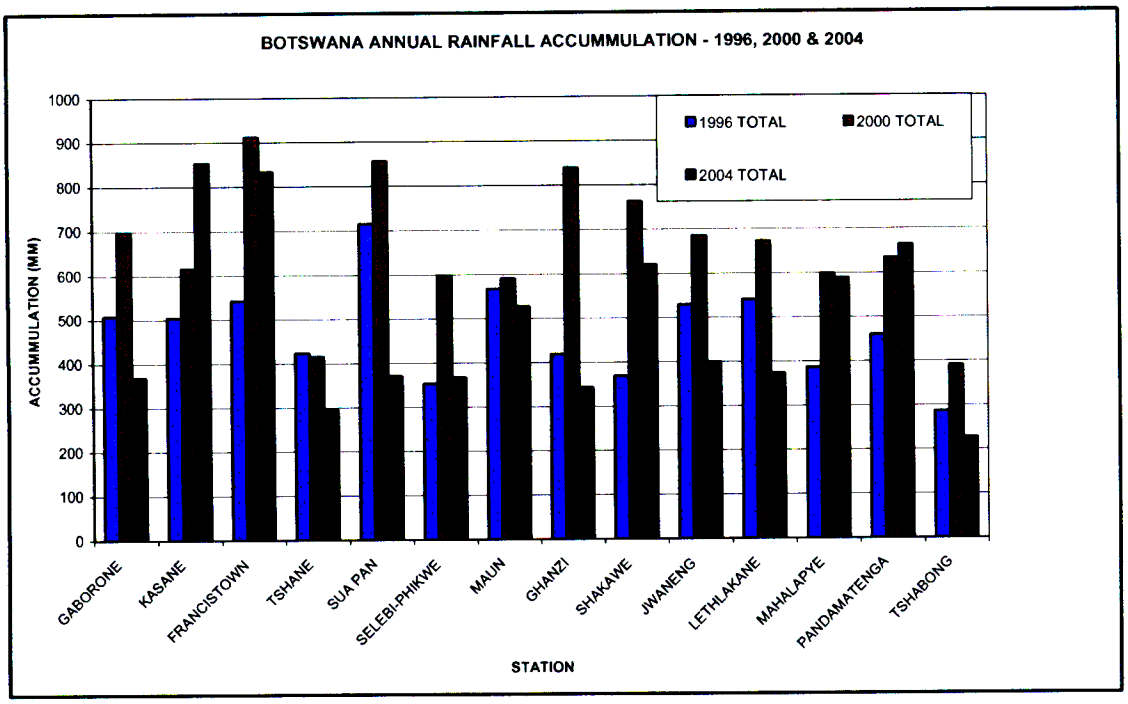

Figure 3-4: Botswana annual rainfall accumulation

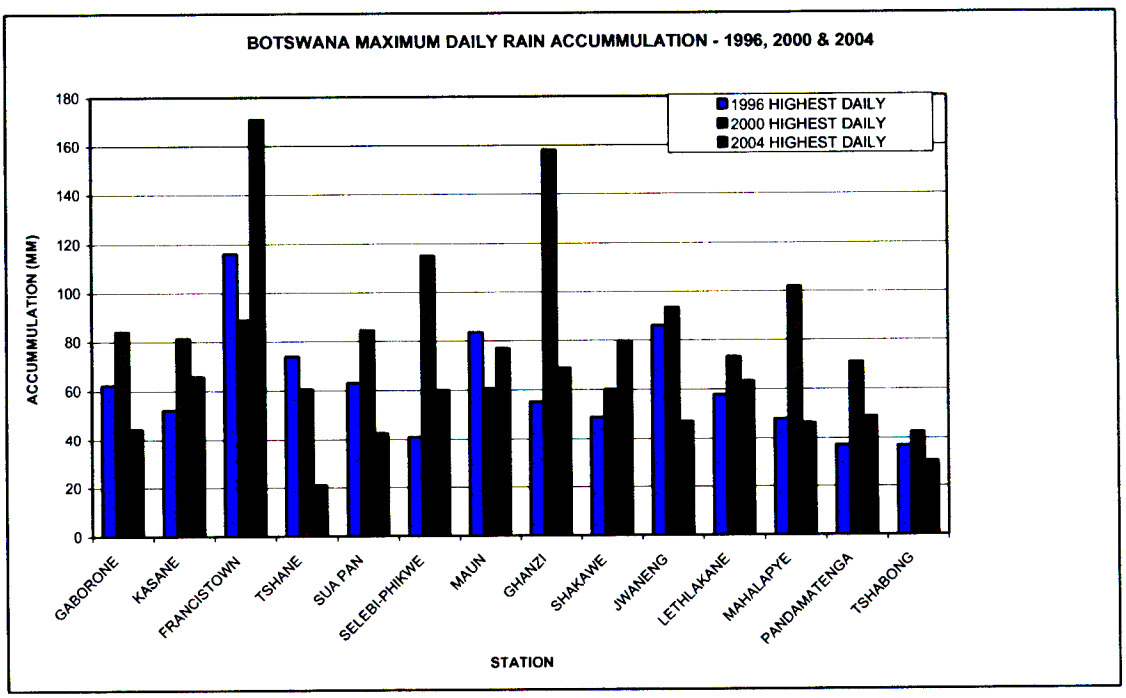

Figure 3-5: Botswana maximum daily rain accumulation

Tshane has a rain accumulation of 423, 415 and 295 mm in 1996, 2000 and 2004, respectively, and Tshabong has 286, 390 and 228 mm in 1996, 2000 and 2004,

respectively. Also, Ghanzi which is located in desert environment is seen to record one of the highest annual rainfall accumulations in 2000 (840 mm).

In Figure 3-5 it can be seen that Francistown and Ghanzi are seen to record the highest daily rainfall accumulation in all years; 1996, 2000 and 2004 compared to other locations. Also observe the figure, Pandamatenga, Tshane and Tshabong are seen to record the lowest daily accumulation in all the years.
Tshane has a daily rain accumulation of 74, 61 and 21 mm in 1996, 2000 and 2004, respectively, Tshabong has 37, 43 and 30 mm in 1996, 2000 and 2004, respectively and Pandamatenga has 37 in 1996.

3.5 Determination of Botswana Rain zones

The ITU-R climatic map for the world divides the whole globe into 15 climatic zones. This map shows the rain intensities for the various climatic zones [ITU-R 837-4]. According to the ITU-R 837-1 as shown in Table 3.5, and ITU-R 837-4 classifications, Southern Africa has seven rain zones, namely: C, D, E, J, K, L and N. Out of these, Botswana has three zones, namely, J, L and N. However, these ITU-R designations are not necessarily adequate, as they need further refinement; thus there is need to redefine the ITU-R regional climatic zones based on the actual local data. Owolawi et al. (2007) proposed new rain zones for South Africa. From the 10-year actual rain data for fourteen different geographical locations in Botswana (which are converted into one-minute integration time based on cumulative frequency identity with one-minute South Africa data), the resulting rainfall rate distributions at 1.0%, 0.3%, 0.1%, 0.03% and 0.01% probability level (percentage of time ordinate exceeded) are shown in Figure 3-3. The rain intensity exceeded for each of the fourteen geographical locations in Botswana are compared with the ITU-R rain climatic zone table. The errors obtained by comparing each location against different ITU-R climatic zones are determined; and the ITU-R zone that gives the least recorded RMS error value for each geographical location is chosen as the location's rain climatic zone. The resulting climatic rain zones are shown in Table 3-5.

Table 3-4: Botswana rain climatic zones (ITU-R 837-1)

Percentage of time (%)	A	B	C	D	E	F	G	H	J	K	L	M	N	P	Q
1.0	<0.1	0.5	0.7	2.1	0.6	1.7	3	2	8	1.5	2	4	5	12	24
0.3	0.8	2	2.8	4.5	2.4	4.5	7	4	13	4.2	7	11	15	34	49
0.1	2	3	5	8	6	8	12	10	20	12	15	22	35	65	72
0.03	5	6	9	13	12	15	20	18	28	23	33	40	65	105	96
0.01	8	12	15	19	22	28	30	32	35	42	60	63	95	145	115
0.003	14	21	26	29	41	54	45	55	45	70	105	95	140	200	142
0.001	22	32	42	42	70	78	65	83	55	100	150	120	180	250	170

Table 3-5: Botswana rain climatic zones

LOCATION	ITU-R P.837-1	ITU-R P.837-4	SUGGESTED RAIN ZONE
SELEBI-PHIKWE	J	N	Q
FRANCISTOWN	J	L	M
MAUN	E	N	M
GABORONE	J	L	M
GHANSI	E	N	Q
PANDAMATENGA	J	N	M
KASANE	J	N	M
JWANENG	E	L	M
SUA PAN	E	N	M
LETHLAKANE	E	N	M
SHAKAWE	E	N	M
TSHABONG	C	J	M
TSHANE	E	L	M
MAHALAPYE	E	L	Q

3.6 LOS Link Budget Calculations for Gaborone

Consider a 44-km analogue FDM/FM link between Gaborone and Molepolole, as shown in Figure 3-6, IF bandwidth of 108 MHz and receiver noise figure of 14 dB. Due to the desert condition in Botswana, we assume a tree height of 5 m. There exists a tower height of 56 m at Gaborone terminal, a transmit power of 15 mW, and a 1.2 m paraboloidal

reflector antenna with 84% efficiency at each terminal, and a feeder loss of 2.6 dB at Gaborone and 3 dB at Molepolole.

As pointed out earlier, in adverse weather conditions, rain is one of the most important considerations in the propagation path of microwave links. In Gaborone the rain rate is 68.9 mm/h for 0.01% of time and it is 52.64 mm/h for 0.1% of time (see Table 3-3). With horizontal polarization, we determine the effective path length, d_{eff}, of the link of path length d. Use is made of a reduction factor r, given by ITU Recommendation 530-12 [ITU-R, 2007], see details in the following chapter. In the case of the actual path in Gaborone, r is 0.22 and d_{eff} is 9.7051. Thus the estimated path attenuation exceeded 0.01% of the time is:

$$A_{0.01} = \gamma_R d_{eff} = \gamma_R dr \ \text{(dB)} \qquad (3.6)$$
$$= 1.48 \times 9.7051$$
$$\approx 14.4 dB$$

where the specific attenuation γ_R (dB/km) is obtained from the rain rate $R_{0.01}$ (mm/h) using the power-law relationship:

$$\gamma_R = kR^{\alpha} \qquad (3.7)$$

The earth buldge, h at any point d and for any value of k is given by:

$$h = \frac{4}{51} \cdot \frac{d_1 d_2}{k} \qquad (3.8)$$

where d_1 and d_2 are the distances in km to the near and far ends of the path respectively ($d = d_1 + d_2$ is the path length in km). Thus the path profiles for k= 4/3, k=1.1, and k=0.6 are shown in Figure 3-6, [Odedina et *al.* (2006)].

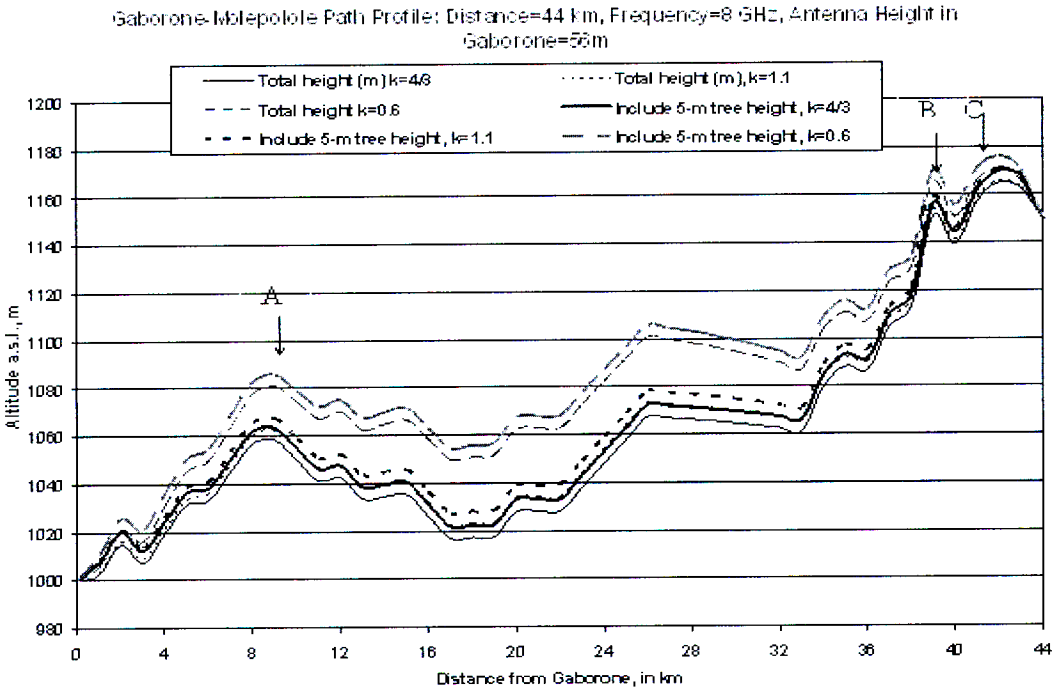

Figure 3-6: Gaborone-Molepolole Path Profile.

The minimum tower height at Molepolole is determined by clearances at points A, B and C placed at 8 km, 38 km and 42 km from Gaborone. Thus we calculate Fresnel ellipsoid radius F_1 (in m), in these points for 8 GHz using the formula,

$$F_1 = 17.3\sqrt{\frac{d_1 d_2}{fd}} \tag{3.9}$$

and we get 14 m, 11 m and 4 m respectively. Thus the minimum tower height equals 14 m at Molepolole.

The Free space Loss (FSL), is given by:

$$FSL(dB) = 20\log_{10}\left(\frac{4\pi d}{\lambda}\right) \tag{3.10}$$

$$= 20\log_{10}\left(\frac{4\pi \times 44 \times 10^3}{3\times 10^8 / 8\times 10^9}\right) = 143.37\,dB$$

The effective aperture for an antenna with gain G is given by:

$$A_e = \frac{G\lambda^2}{4\pi} \qquad \Rightarrow \qquad G = \frac{4\pi A_e}{\lambda^2} \tag{3.11}$$

But the effective aperture, A_a, through the antenna efficiency ξ,

$$\xi \,.\, A_e = \xi\, A_a = \xi \frac{\pi D^2}{4}, \tag{3.12}$$

where D is antenna diameter.

To determine if a link is feasible, one compares the received signal level (P_r) with the receiver sensitivity (FM_T). The link is theoretically feasible if

$$P_r(dBm) \geq FM_T \tag{3.13}$$

$$P_r(dBm) = P_t(dBm) - FSL(dB) + G_t(dB) + G_r(dB) - FeederLoss \tag{3.14}$$

$$G = \frac{4\pi}{\lambda^2}\xi\frac{\pi D^2}{4} = \xi\left(\frac{\pi D}{\lambda}\right)^2 = 0.84\left(\frac{\pi 1.2}{3\times 10^8/8\times 10^9}\right)^2 = 8489.43$$

(3.14)

$$G = 39.2dB$$

$$P_r(dBm) = (11.76 - 143.37 + 39.2 + 39.2 - 2.6 - 3)$$

$$= \text{-}58.81 \text{ dBm.}$$

where P_t is 11.76 dBm; G_t is the transmitted antenna gain and G_r is the received antenna gain.

If the received signal level is responded to that condition then the link may be feasible since the signal should be strong enough to be successfully by the receiver. In our case the receiver threshold FM_T is 10 dB above P_n, the thermal noise power:

$$FM_T(dBm) = P_n(dBm) + 10dB \tag{3.15}$$

$$\begin{aligned} P_n(dBm) &= -174dBm + 10\log(B_{IF}) + NF(dB) \\ &= -174dBm + 10\log(108\times10^6) + 14(dB) \\ &= -79.67dBm \end{aligned} \tag{3.16}$$

Thus

$$FM_T = -69.67dBm$$

where P_n is the total thermal noise for an intermediate frequency (IF) bandwidth B_{IF} an NF is the receiver noise figure. The fade margin equals 10.86 dB which is extremely low, with an availability of 99.95%. The received signal-to-noise ratio is:

$$SNR(dB) = P_r(dBm) - P_n(dBm) = 20.86dB \tag{3.17}$$

Fade margin FM, by definition is the difference between the received signal level and the received sensitivity threshold. The fade margin must have sufficient value to guarantee against unpredicted system outages. It is known that fade margin is directly related to link availability, which is the percentage of time that the link is functional. The percentage of time that the link is available increases as the fade margin increases. With a greater fade margin a link will experience fewer system outages. Also if a link with little or no fade margin may experience periodic outages due to path fading phenomena.

It is found that the appropriate reception is not achieved. In order to have a link margin of at least 64.4 dB, the transmit power needs to be at least 200 mW. However to cater for diffraction and multipath fading, the power can be increased to 300 mW, leaving a margin of 23.87 dB.

To optimize this link reliability or availability the radio engineer designer or network planner will need either to increase the system transmit power P_t or the gain of the antenna by increasing the diameter of the antenna, or again by inserting a repeater between two terminals. Some may ask why we did not increase frequency to solve the problem. This is simply because it is the only one channel that the regulation authority allocates to the client.

3.7 Conclusion

The ten-year rainfall data measured by the Botswana Meteorological department for fourteen different locations have been utilized to study the effect of integration time on the cumulative distribution of rain rate for Botswana. The cumulative distribution identities of different regions in South Africa with daily data are compared with Botswana daily data. The closest cumulative distributions of both countries are compared using root-mean-square (RMS) values, and thus the CDF giving the least RMS value in South Africa is taken as the comparable site with a corresponding Botswana site. Values of equiprobable rain rate for 1-minute and 24-hour integration times for probabilities of 0.1% or less have been employed to confirm the power law relationship between the rain rates at 1-minute and 24-hour integration times. Selebi-Phikwe which lies in the border of South Africa and Zimbabwe has the highest rain intensity $R_{0.01}$ of 137.06 mm/h, and Kasane which is found in the border region of Zambia has the lowest rain intensity of 64.4 mm/h. The cumulative distributions of 1-minute rain intensities for a period of 10 years are obtained for each location that lies in the same climatic region. Based on the available 24-hour rain data converted to 1-minute integration time, two climatic rain zones M and Q are determined for Botswana, as against the ITU-R classification of J, L

and N based on the examined fourteen sites.

As it is pointed out early, in adverse weather conditions, during the microwave line design planning we have considered unavailability which can happen during the rain events. In order to meet client requirements better we have to have local statistic about rain intensities and apply them to link budget calculations. The required fade margin is 14 dB at 99.99% for 44 km Gaborone-Molepolole microwave link.

Chapter 4

Propagation Coefficients Due to Rain and Application

4.1 Introduction

In Chapter 3, we alluded to rainfall rate modeling and proposed rain zones for Botswana. In this chapter, we begin our study of propagation coefficients due to rain in Botswana. Specifically, we focus on propagation coefficient analysis, an understanding of which is particularly essential for forward attenuation, while being of general importance, and also extend the discussion to compare our model to rain attenuation measurements realized in Durban by [Naicker, 2006] and processed by [Fashuyi, 2007].

[Rogers and Olsen, 1976] employed Mie scattering theory and Laws and Parsons (LP) drop-size distribution to obtain plots of specific attenuation γ (dB/km) against frequency (from 1 to 1000 GHz) for rain rate, varying from 0.25 mm/h to 150 mm/h. For each of the nine values of rain rate, the effect of rain temperature on specific attenuation was also shown at two temperatures, namely 273°K and 293°K. [Ajayi and Ofoche, 1983] determined that the use of one-minute rain rates gives the best agreement with the ITU-R stipulations for the design of microwave radio links. This was then used to estimate the signal outages at 0.01 % of the time on radio communication links, since it defines the rainfall rate recommended by ITU-R to evaluate the availability of terrestrial and satellite radio links.

Ajayi and Olsen [1985] have shown that the LP and MP (Marshal and Palmer) distributions overestimate the number of raindrops in the small and large diameter regions; and that the lognormal model gives a better fit to the measured drop size data at Ile-Ife, Nigeria (a tropical climate). [Moupfouma and Tiffon, 1982] used measurement

data over a 33.5-km 7 GHz terrestrial radio link in the Congo (equatorial region of Africa) to propose a new rain drop-size distribution, and also confirmed that the MP distribution overestimates the number of small drops while it underestimates the larger ones for this region. Similar conclusions have been made by Massambani and Morales [1988] and [Massambani and Rodriguez, 1990], making use of the rain data obtained in Brazil.

To determine specific attenuation due to rain using Mie computations, [Olsen *et al,* 1978] employed the Ray method to determine the refractive index for water at various temperatures and frequencies. However, the Ray data are regarded as inaccurate especially at frequencies above 10 GHz [Mätzler, 2002a]. On the other hand Mätzler developed MATLAB functions based on the formulation of Bohren and Huffman [1978]: he used the more accurate dielectric model of Liebe to determine the refractive index of water for computation of Mie parameters [Mätzler, 2002a]. The parameters required were the interaction cross-sections by rain per unit volume of a rainy atmosphere, i.e. the propagation coefficients for rain extinction, γ_{ext}, scattering, γ_{sca}, absorption, γ_{abs}, backscattering, γ_b, and the asymmetry parameter $<\cos\theta>$ [see Mätzler (2002a), Mätzler (2002b), and Mätzler (2002c)]. Here, $<\cos\theta>(D)$ is the effective cosine of the scattering angle, and is a function of D, the rain drop size. In his approach, Mätzler computed the coefficients γ_j, $\{j = ext, abs, sca, b\}$ from the corresponding Mie efficiencies Q_j and the drop size distributions using Marshall and Palmer (M-P), Joss-Thunderstorm (JT), Joss-Drizzle (JD) and Laws and Parsons (LP) distributions of N(D), from the equations [see Mätzler (2002b)]:

$$\gamma_j = 0.25\pi \int_0^\infty D^2 Q_j N(D) dD;\ j = ext, abs, sca, b. \tag{4.1}$$

$$\gamma_{sca} <\cos\theta> = 0.25\pi \int_0^\infty D^2 <\cos\theta>(D) \cdot Q_{sca} N(D) dD. \tag{4.2}$$

These coefficients are used in radiative transfer theory, as in, for example, Chandrasekhar (1960), and [Meador and Weaver, 1980]. In this presentation we determine propagation coefficients, γ_j, due to rain in Botswana for fourteen stations from the corresponding Mie efficiencies Q_j and the drop size distribution based on lognormal distribution for tropical and subtropical countries, as presented in [Ajayi, 1996]:

$$N(D) = \frac{N_t}{\sigma D\sqrt{2\pi}} \exp\left(\frac{-[\ln(D) - \mu]^2}{2\sigma^2}\right). \tag{4.3}$$

Here μ is the mean of $\ln(D)$, σ is the standard deviation, N_t is the total number of the drops per cubic meter per mm. We use $R_{0.01}$=68.9 mm/h for Gaborone, $R_{0.01}$=137.06 mm/h for Selebi-Phikwe, $R_{0.01}$=86.87 mm/h for Francistown and $R_{0.01}$=64.4 mm/h for Kasane, for Botswana, in Southern Africa, as determined by [Mulangu et *al*, 2007]. We also discuss the variability of the propagation coefficients due to rain with temperature for Gaborone, Selebi-Phikwe, Kasane and Francistown, comparing the same with the results of [Olsen and Rogers1976], [Ajayi and Adimula1996], and [Moupfouma and Tiffon, 1982]. Since our work is based on the procedures presented by the various works of Mätzler, the brief theoretical basis that follows is based purely on Mätzler (2002a, b).

4.2 Rain Attenuation Variability

The two main causes of rain attenuation are scattering and absorption. When the wavelength is fairy large relative to the size of raindrop, scattering is predominant. Conversely, when the wavelength is small compared to the raindrop size, attenuation due to absorption is dominating. An empirical procedure based on the approximate relation between γ and rain rate R is given as [Olsen et al., 1978]:

$$\gamma = kR^{\alpha}, \tag{4.4}$$

where k and α are power law parameters, which depend on frequency, raindrop size distribution, rain temperature, and polarization. The coefficients γ_j, $j = ext, abs, sca, b$, can be obtained from the rain drop-size information. Mie approximation also needs the complex refractive index of water drops. The complex refractive index $m(f,T)$, being a function of frequency f and temperature T, is related to the complex relative dielectric permittivity $\varepsilon(f,T)$ by:

$$m(f,T) = \sqrt{\varepsilon(f,T)} = \frac{k}{k_0} \tag{4.5}$$

Here k_0 is the wave number in free space and k is the wave number in water. The permittivity at infinite frequency is given by [Liebe et al., 1991]:

$$\varepsilon_\infty = 3.52 + 7.52\theta \tag{4.6}$$

where $\theta = 1 - 300/T$ and T is the temperature in $^\circ K$.

The efficiencies Q_i for the interaction of the radiation with a sphere of radius a are cross sections σ_i normalized to the geometrical particle cross section, $\sigma_g = \pi a^2$, where i stands for extinction $(i = ext)$, absorption $(i = abs)$, scattering $(i = sca)$, and backscattering. Energy conservation requires that [see Mätzler (2002b)]:

$$Q_{ext} = Q_{sca} + Q_{abs}, \text{ or } \sigma_{ext} = \sigma_{sca} + \sigma_{abs} \tag{4.7}$$

$$\begin{aligned} Q_{sca} &= \frac{2}{x^2}\sum_{n=1}^{\infty}(2n+1)(|a_n|^2 + |b_n|^2); \quad Q_{ext} = \frac{2}{x^2}\sum_{n=1}^{\infty}(2n+1)\,\mathrm{Re}(a_n + b_n) \\ Q_{sca} &< \cos\theta >= \frac{4}{x^2}\left[\sum_n \frac{n(n+2)}{n+1}\mathrm{Re}\{a_n a_{n+1}^* + b_n b_{n+1}^*\} + \sum_n \frac{2n+1}{n(n+1)}\mathrm{Re}\{a_n b_n^*\}\right] \end{aligned} \tag{4.8}$$

The key parameters for Mie calculations are the Mie Coefficients a_n and b_n to compute the amplitudes of the scattered field. The index n runs from $1\ to\ \infty$, but the infinite series occurring in Mie formulas can be truncated at a maximum n_{max}, given by Bohren and Huffman [1978]:

$$n_{max} = x + 4x^{1/3} + 2. \tag{4.9}$$

This value is used in this computation. The size parameter is given by $x = ka$, a is the radius of the sphere and $k = 2\pi/\lambda$ is the wave number, λ the wavelength in the ambient medium.

4.3 Analytical Results from Rain Data

Table 4-1 shows the coefficients of log-normal distributions for tropical and continental showers and thunderstorms, as per Ajayi and Ofoche [1983]. Tables 4-2 and 4-3 summarise the variability of propagation coefficients due to temperature for the four sites in Botswana.

Table 4-4-1: Coefficients for tropical and continental shower and thunderstorm for lognormal models [Ajayi and Ofoche, 1990]

Type of Rain		N_T	μ_g	s^2_g
Continental	*Showers*	$127R^{-0.477}$	-0.476+0.221lnR	0.269-0.043lnR
	Thunderstorms	$70R^{-0.564}$	-0.378+0.224lnR	0.306-0.059lnR
Tropical	*Showers*	$137R^{-0.37}$	-0.414+0.234lnR	0.223-0.034lnR
	Thunderstorms	$63R^{-0.491}$	-0.178+0.195lnR	0.209-0.030lnR

where, μ_g is the mean of $\ln(D)$, σ_g is the standard deviation, N_t is the total number of the drops per cubic meter per mm and R is the rain rate.

Table 4-4-2: Summary of the variability of propagation coefficients with rain type with temperatures of 270°K and 318°K at 1 GHz

Sites	Propagation Coefficients dB/Km	Tropical Thunderstorms		Tropical Showers		Continental Showers		Continental Thunderstorms	
		318°K	270°K	318°K	270°K	318°K	270°K	318°K	270°K
Gaborone	γ_{ext}	0.0052	0.0017	0.024	0.0075	0.012	0.0036	0.004	0.00145
	γ_{abs}	0.005	0.0013	0.023	0.006	0.018	0.0028	0.0037	0.001
	γ_{sca}	0.023	0.006	0.002	0.002	0.0009	0.0009	0.00025	0.00025
	γ_b	0.0005	0.0005	0.003	0.003	0.001	0.001	0.0008	0.0008
	$\gamma_{sca} <\cos\theta>$	0	0	0	0	0	0	0	0
Kasane	γ_{ext}	0.005	0.0016	0.02	0.0065	0.009	0.0031	0.0049	0.00125
	γ_{abs}	0.005	0.0013	0.018	0.006	0.0091	0.0025	0.0037	0.001
	γ_{sca}	0.0003	0.0003	0.002	0.002	0.0005	0.0005	0.00025	0.00025
	γ_b	0.0004	0.0004	0.0025	0.0025	0.0009	0.0009	0.00035	0.00035
	$\gamma_{sca} <\cos\theta>$	0	0	0	0	0	0	0	0
Selebi-Phikwe	γ_{ext}	0.0071	0.0022	3.05	3.05	0.0179	0.005	0.075	0.0019
	γ_{abs}	0.0067	0.0018	1.5	1.2	0.015	0.0039	0.0066	0.0015
	γ_{sca}	0.00025	0.00025	1.75	1.8	0.0017	0.0017	0.0002	0.0002
	γ_b	0.00045	0.00045	0.025	0.04	0.0019	0.0019	0.0003	0.0003
	$\gamma_{sca} <\cos\theta>$	0	0	1.5	1.5	0	0	0	0
Francistown	γ_{ext}	0.0057	0.0019	0.024	0.0055	0.0115	0.0039	0.0045	0.0016
	γ_{abs}	0.0054	0.0015	0.0225	0.0056	0.011	0.0035	0.0041	0.0011
	γ_{sca}	0.0004	0.0004	0.0015	0.0015	0.0018	0.0018	0.0005	0.0005
	γ_b	0.0005	0.0005	0.0025	0.0025	0.001	0.001	0.0005	0.0005
	$\gamma_{sca} <\cos\theta>$	0	0	0	0	0.001	0.001	0	0

A requirement of the model is that it should be able to predict attenuation from rain at a frequency range of 1-1000 GHz. To this extent, we have examined predictions based on the calculation by Olsen et al. [1978], using Marshal-Palmer (MP) drop size distributions at 263°K, 273°K and 293°K; and we have applied the work of Liebe [Liebe, 1991] to

obtain the frequency dependence of the complex permittivity ε of rain at the same temperatures. The plots of the specific attenuation, γ_{ext} (in dB/km) as a function of rain intensity R (in mm/h) for two frequencies of 5 and 1000 GHz, at temperature values of 293°K, 273°K and 263°K, are shown in Figures 4-2 and 4-3. These plots are compared to those in Figure 5 of [Rogers and Olsen 1976], shown in Figure 4-1, and Figure 3 of [Olsen et *al*, 1978]. It is seen that a very close agreement exists between the values of γ_{ext} for the plots of Olsen *et al* and our model, with a variation at any rain rate not exceeding about 2 dB/km at 5 GHz, reducing to about 1 dB/km at 1000 GHz. Thus as the operating frequency rises much above 5 GHz, the specific attenuation proposed by Olsen et al. tends to be more accurate for tropical application.

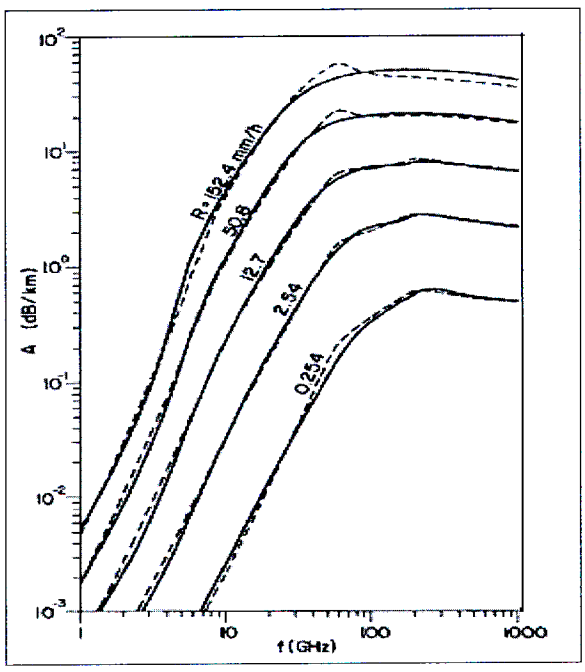

Figure 4-1: Comparison of Mie calculations and analytic approximation on an A versus f scale at several rain rates and a rain temperature of 0°C. —— Mie calculations; ------ analytic approximation. (Figure 5 in [Olsen et al. 1978]).

Table 4-4-3: Summary of the variability of propagation coefficients with rain type with temperatures of 270°K and 318°K at 300 GHz

Sites	Propagation Coefficients dB/Km	Tropical Thunderstorms		Tropical Showers		Continental Showers		Continental Thunderstorms	
		318^0K	270^0K	318^0K	270^0K	318^0K	270^0K	318^0K	270^0K
Gaborone	γ_{ext}	2.9	2.9	12	12	5.9	5.9	2.25	2.25
	γ_{abs}	1.3	1.1	5	3	2.2	2.1	1	0.85
	γ_{sca}	1.8	1.7	7.5	7	3.8	3.4	1.25	1.4
	γ_b	0.7	0.3	1.9	1	0.9	0.5	0.27	0.2
	γ_{sca} <cos θ>	1.5	1.5	5.9	5.9	2.9	2.9	1.1	1.1
Kasane	γ_{ext}	2.9	2.9	11.9	11.9	7.5	7.5	2.3	2.3
	γ_{abs}	1.2	1.1	5	4.5	2.45	2.2	0.99	0.8
	γ_{sca}	1.8	1.75	7	6.5	3.6	3.3	1.4	1.3
	γ_b	0.04	0.03	1.8	1	0.8	0.5	0.27	0.2
	γ_{sca} <cos θ>	1.45	1.45	5.5	5.5	2.8	2.8	1.1	1.1
Selebi-Phikwe	γ_{ext}	3.05	3.05	14	14	6.8	6.8	2.45	2.45
	γ_{abs}	1.5	1.2	6	5.5	2.9	2.7	1	0.9
	γ_{sca}	1.8	1.75	1.8	1.7	3.6	3.3	1.5	1.49
	γ_b	0.04	0.025	2	1	0.9	0.6	0.27	0.2
	γ_{sca} <cos θ>	1.5	1.5	7	7	3.1	3.1	1.2	1.2
Francistown	γ_{ext}	2.9	2.9	12.5	12.5	6.1	6.1	2.8	2.8
	γ_{abs}	1.3	1.2	5.5	5	2.6	2.2	1	0.9
	γ_{sca}	1.8	1.75	7.9	7.5	3.9	3.5	1.48	1.38
	γ_b	0.04	0.025	1.98	1.7	0.9	0.7	0.27	0.2
	γ_{sca} <cos θ>	1.4	1.4	6	6	3	3	1.2	1.2

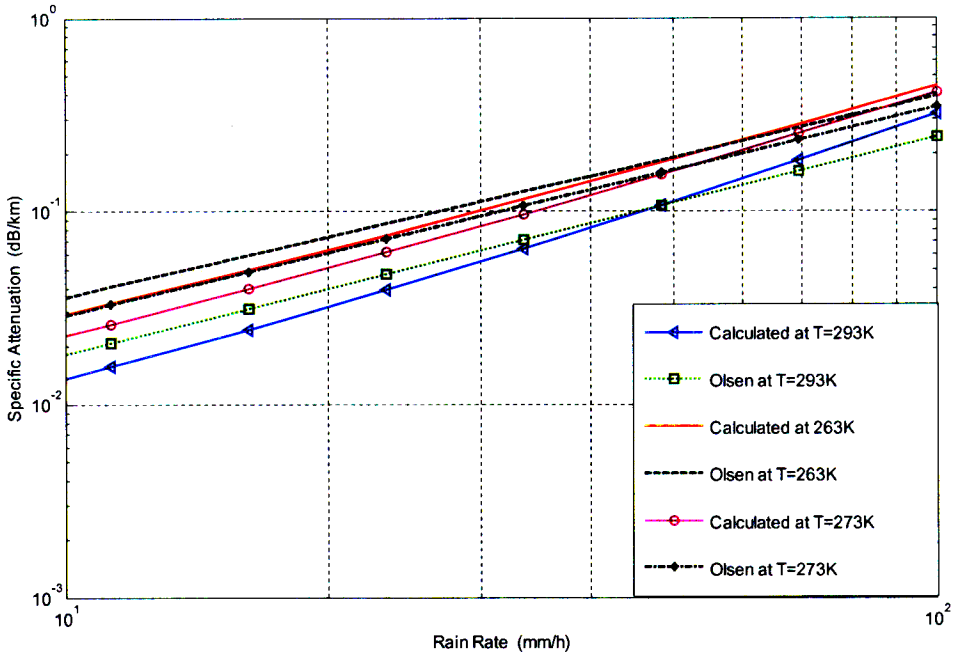

Figure 4-2: Specific attenuation as function of rain intensity R (mm/h), using the M-P drop size distribution at 263^0 K, 273^0 K and 293^0 K at 5 GHz.

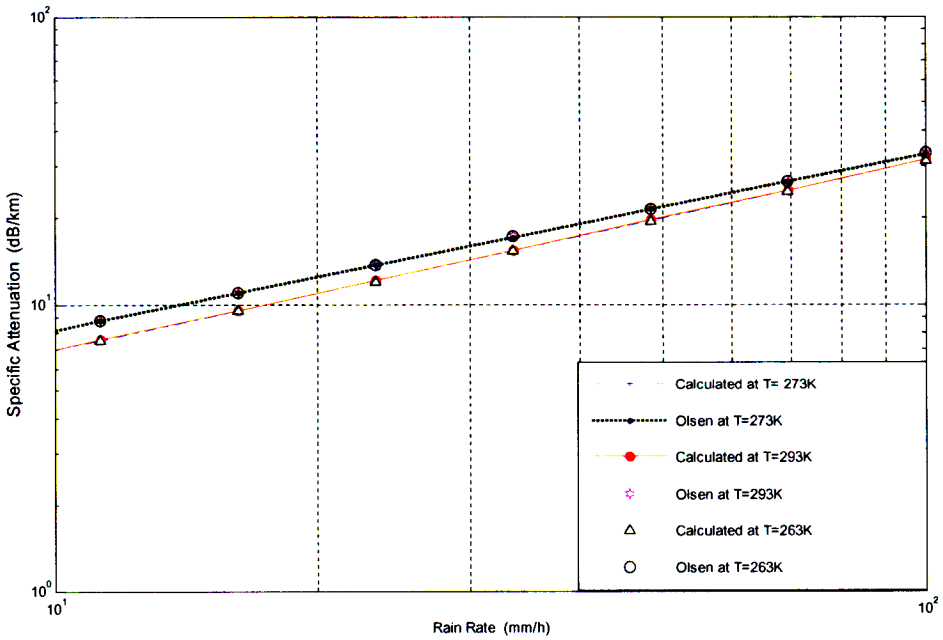

Figure 4-3: Specific attenuation as function of rain intensity R (mm/h), using the MP drop size distribution at 263^0 K, 273^0 K and 293^0 K at 1000 GHz.

In Figure 4-4, we show plots of the variability of the propagation coefficients with frequency and drop-size distribution for fourteen Botswana stations as seen in Chapter 3 at rain rates of $R_{0.01}$=86.87 mm/h, $R_{0.01}$=68.9 mm/h, $R_{0.01}$=64.4 mm/h, $R_{0.01}$=64.2 mm/h, $R_{0.01}$=67.89 mm/h, $R_{0.01}$=87.7 mm/h, $R_{0.01}$=72.31 mm/h, $R_{0.01}$=78.44 mm/h, $R_{0.01}$=79.77 mm/h, $R_{0.01}$=73.64 mm/h, $R_{0.01}$=75.74 mm/h, $R_{0.01}$=78.14 mm/h, $R_{0.01}$=114.37 mm/h and $R_{0.01}$=137.06 mm/h, respectively. The drop-size distributions assumed in calculating the Mie coefficients are four exponential DSD's (MP, JD, JT and LP) and four log-normal DSD's (CS, TS, CT and TT) and the Weibull (WB) distribution. In almost all the four stations, for frequencies below 15 GHz, the upper bound of γ is due to the Tropical Showers (TS) DSD, while the lower bound is due to the JD (Joss-Drizzle) distribution. The exception to this is Selebi-Phikwe, with a high $R_{0.01}$=137.06 mm/h. For the frequency range of 15 to 50 GHz, the upper bound of γ is due to the Weibull (WB) DSD, while the lower bound is due to the Continental Thunderstorm (CT) distribution. Finally, at frequencies between 50-1000 GHz, the upper bound of specific rain attenuation is due to JD (Joss-Drizzle) DSD, while the lower bound is still due to the CT DSD.

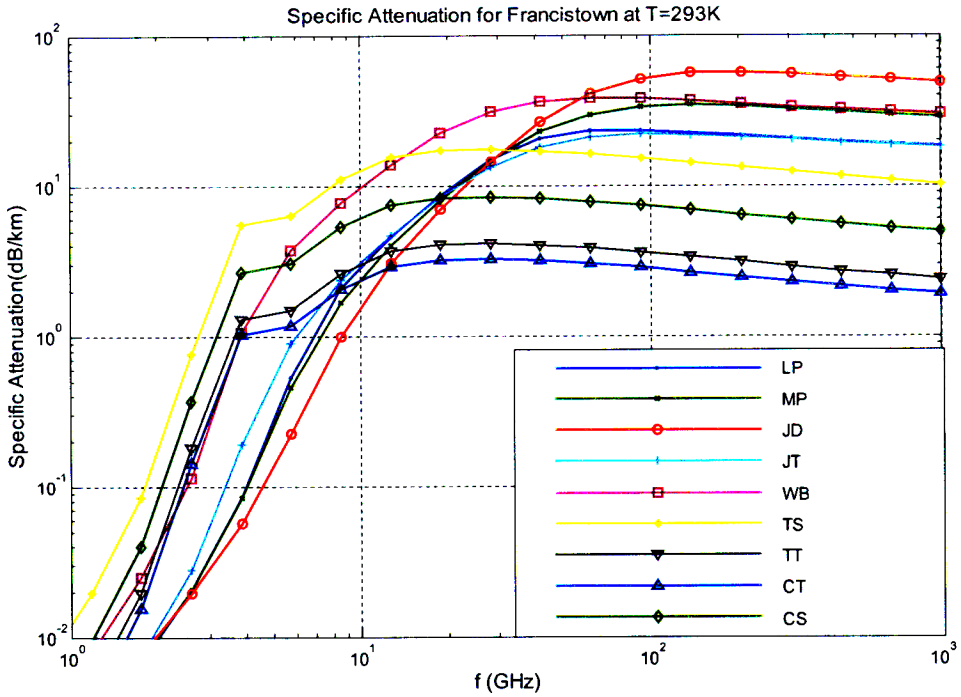

(a) $R_{0.01}$=86.87 mm/h

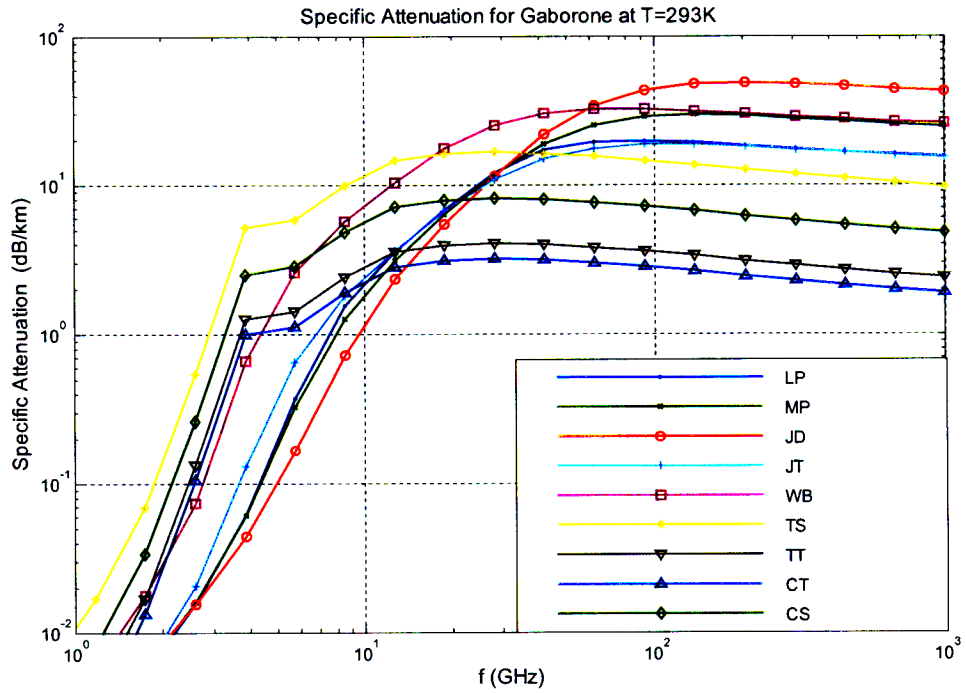

(b) $R_{0.01}$=68.9 mm/h

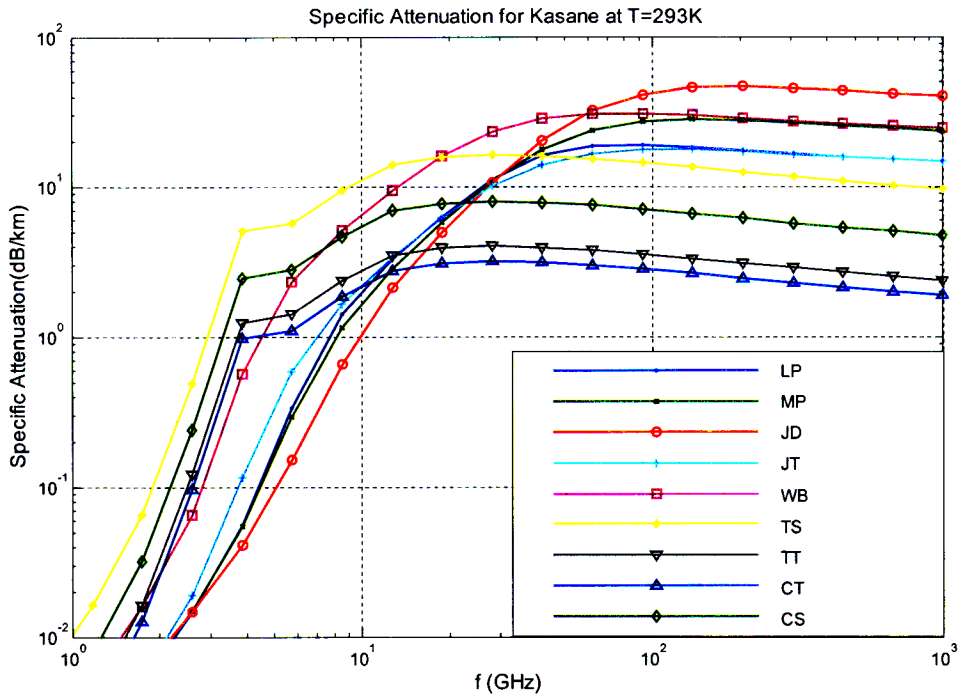

(c) $R_{0.01}$=64.4 mm/h

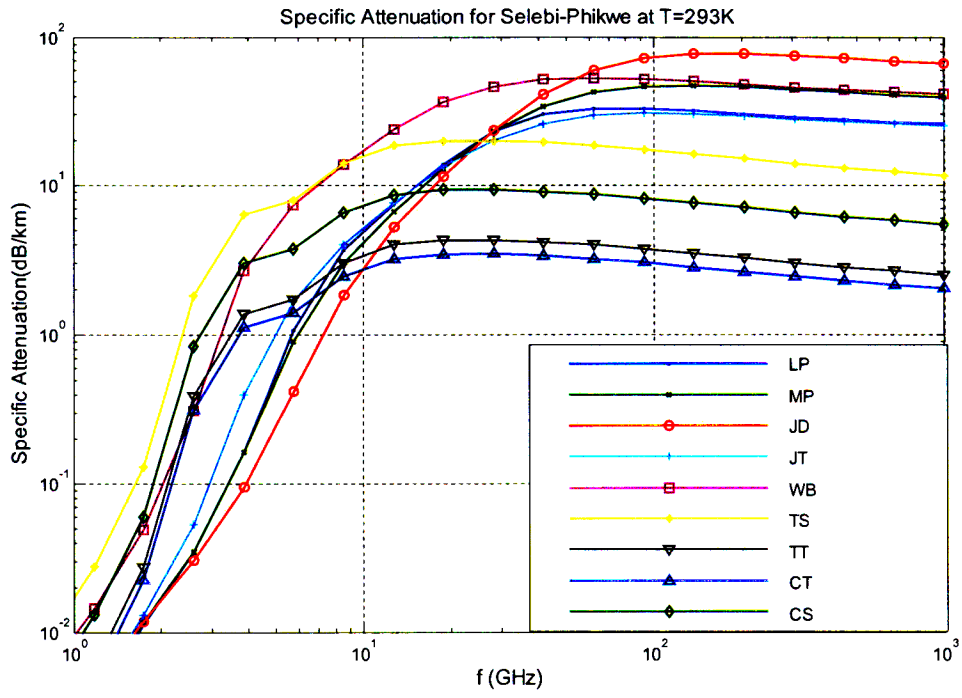

(d) $R_{0.01}$=137.06 mm/h

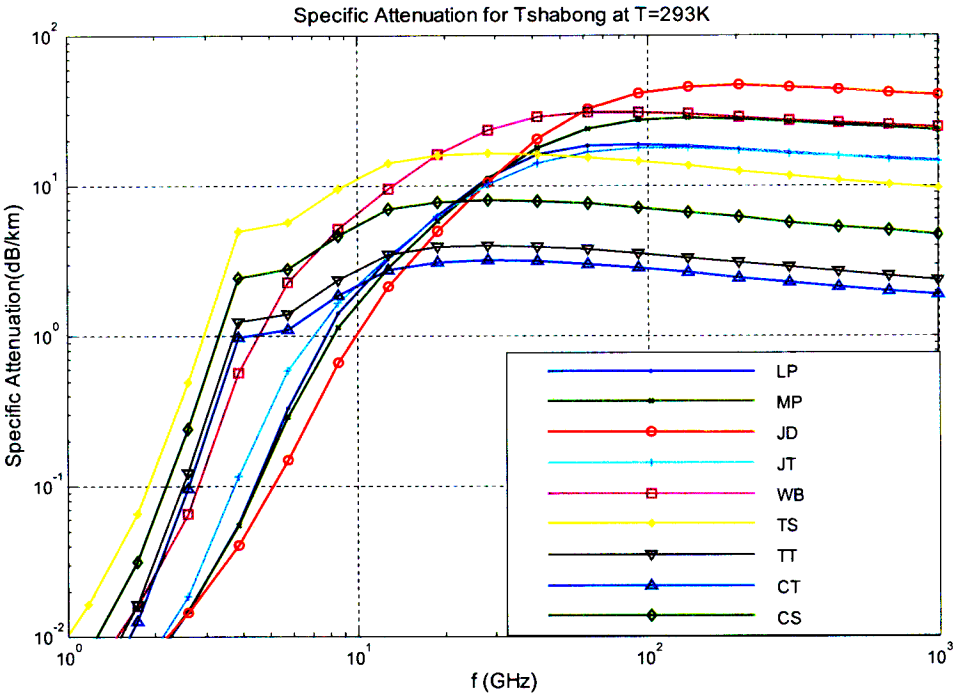

(e) $R_{0.01}$=64.2 mm/h

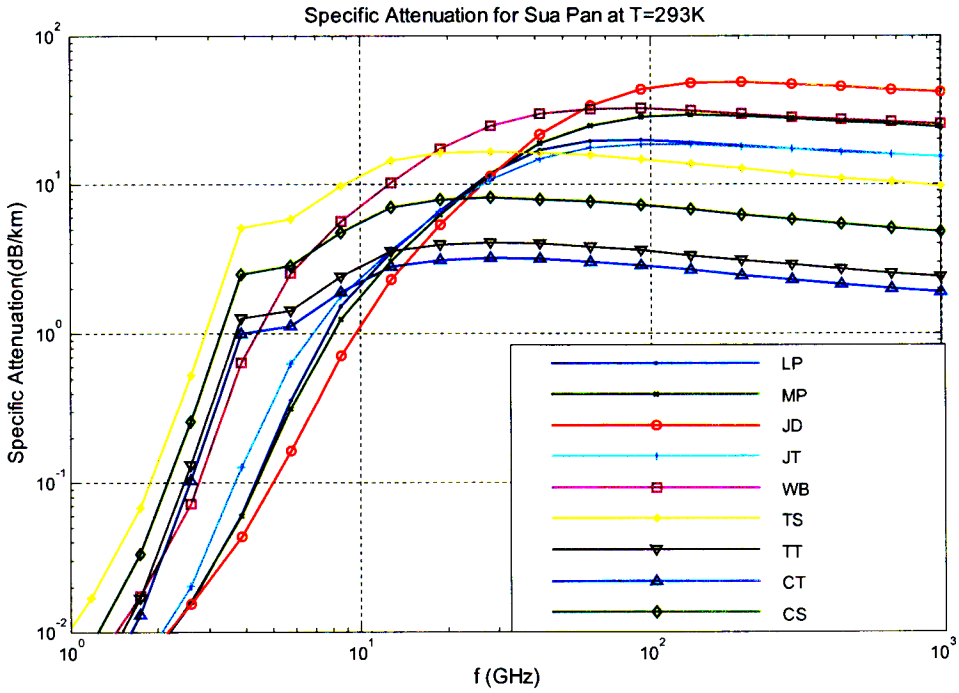

(f) $R_{0.01}$=67.89 mm/h

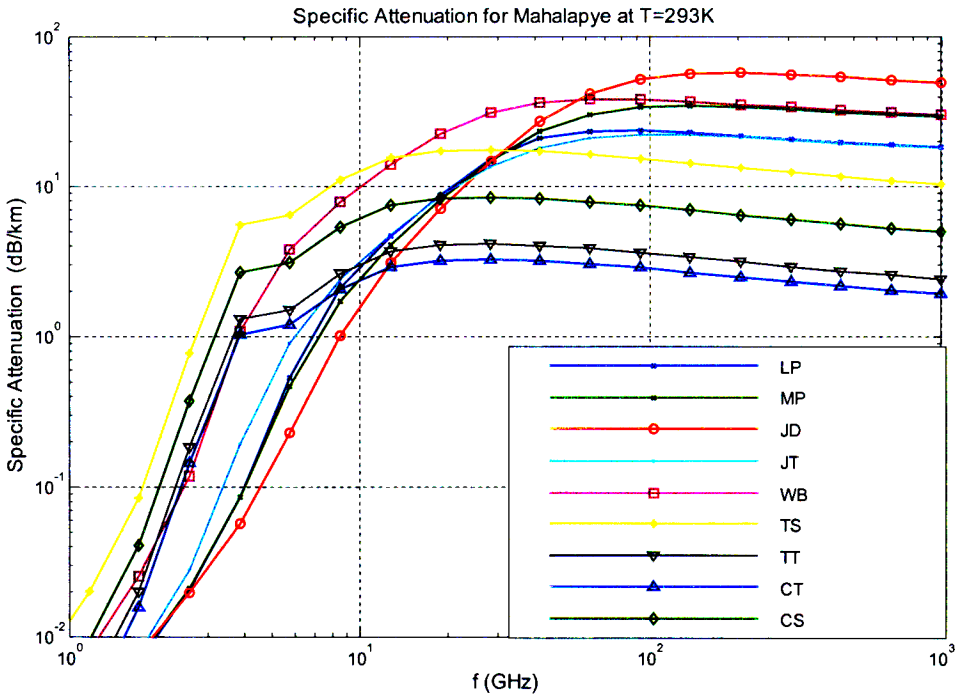

(g) $R_{0.01}$=87.7 mm/h

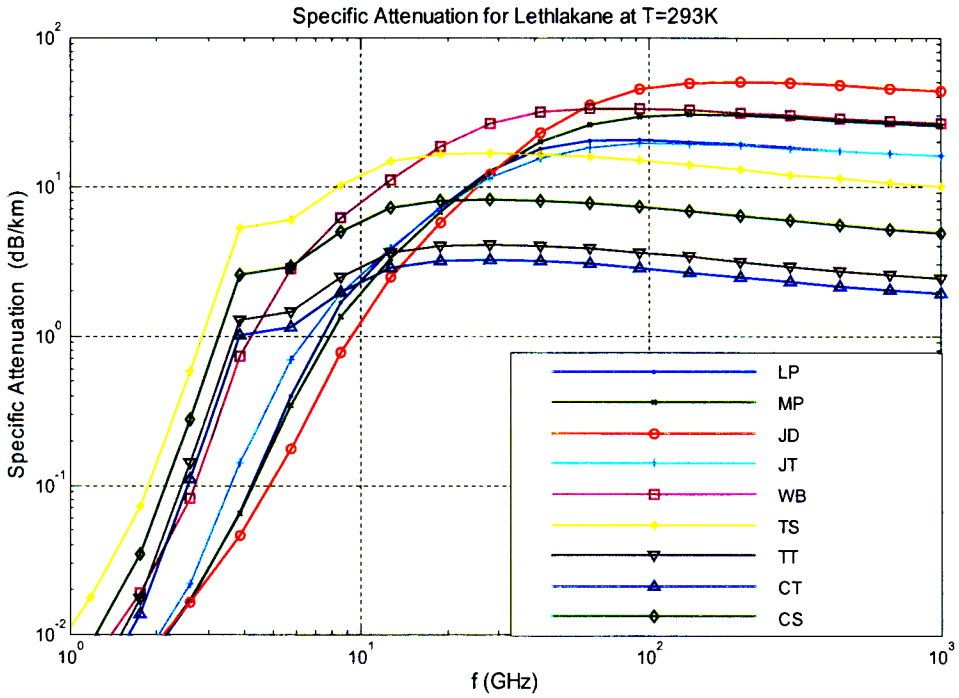

(h) $R_{0.01}$=72.31 mm/h

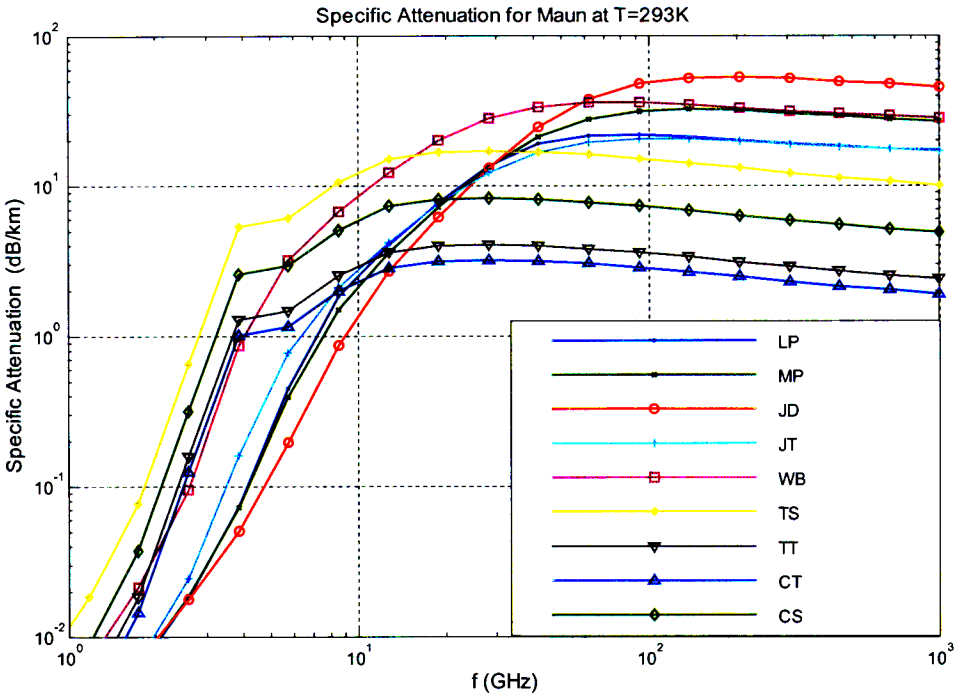

(i) $R_{0.01}$=78.44 mm/h

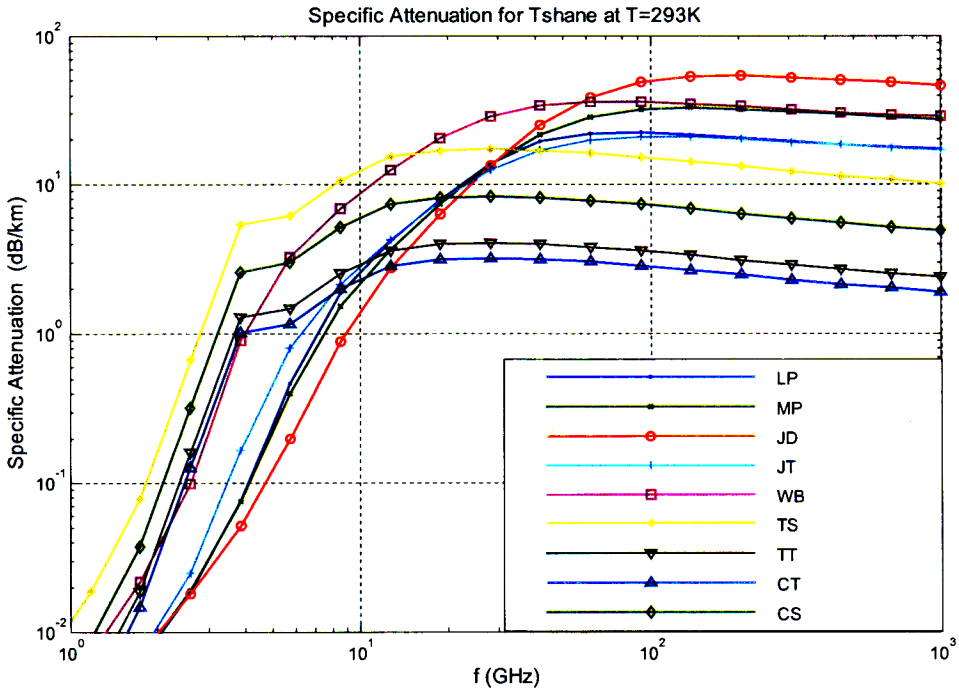

(j) $R_{0.01}$=79.77 mm/h

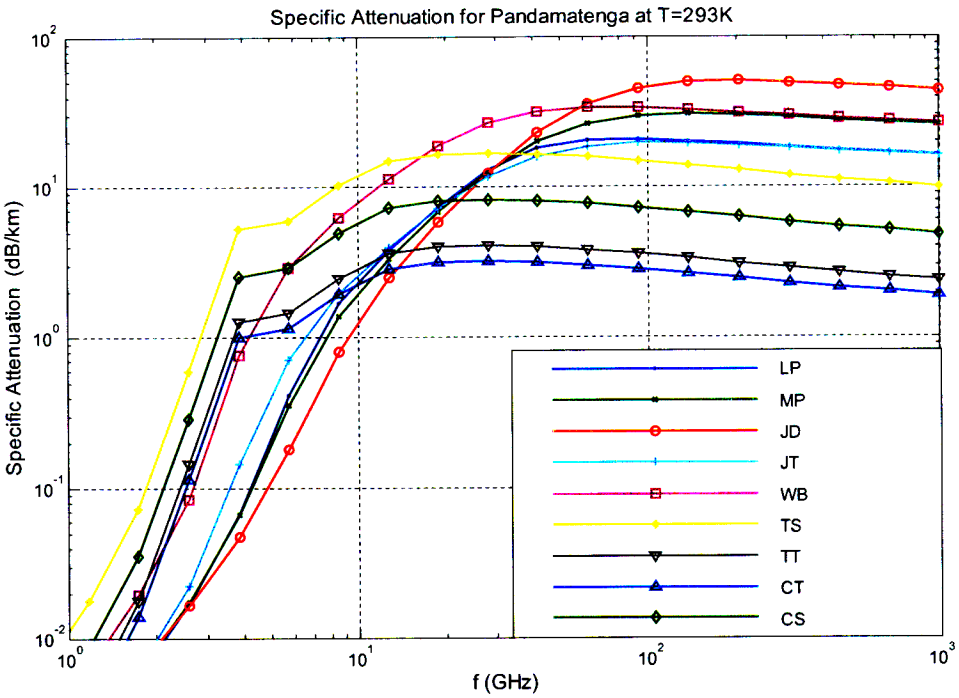

(k) $R_{0.01}$=73.64 mm/h

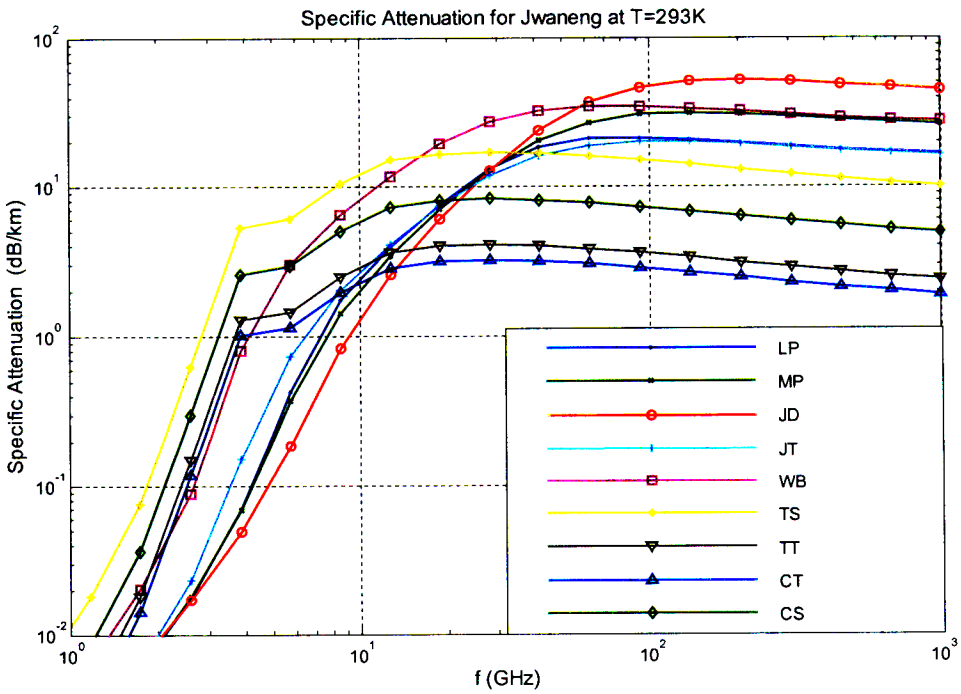

(l) $R_{0.01}$=75.74 mm/h

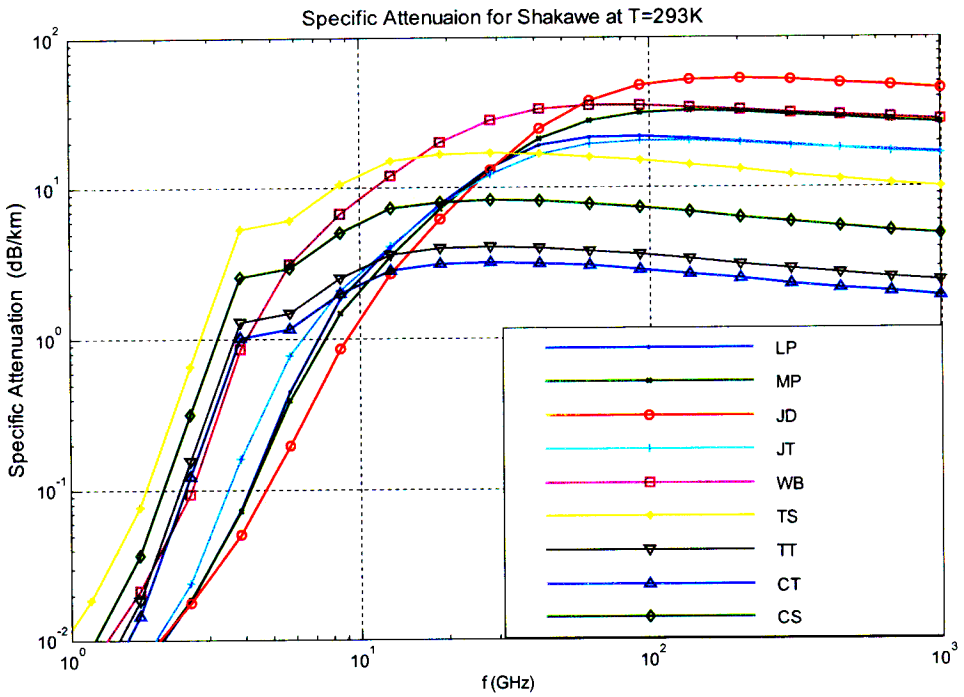

(m) $R_{0.01}$=78.14 mm/h

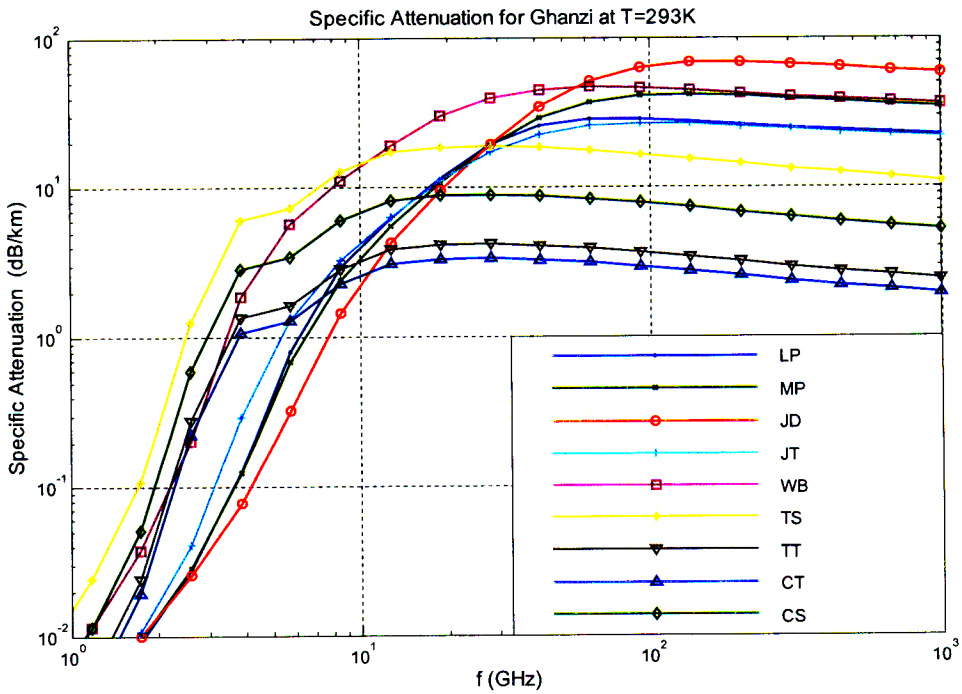

(n) $R_{0.01}$=114.37 mm/h

Figure 4-4: Specific attenuation due to rain, γ, for fourteen selected stations in Botswana, using the MP, JD, JT, LP, WB, CS, TS, CT and TT lognormal DSDs.

Compared to Figure 5 in [Olsen et al. 1978] as shown in Figure 4-1, the value of the specific attenuation due to rain for each of the fourteen stations should reasonably fall (between the curves for 50 mm/h and 150 mm/h) in the range of about 15-30 dB/km. This range is also confirmed for another tropical region (Nigeria) in Figure 4 of Adimula and Ajayi [1996]. For frequencies above 50 GHz, one observes that the JD (Joss-Drizzle) DSD does over-estimate the value of γ, as it rises above 50 dB/km, while the CT (Continental Thunderstorm) distribution underestimates γ with values of 2-3 dB/km. For the frequency range of 15 to 50 GHz, Figure 5 in Olsen et al [1978] shows that the range of γ should be about 10-25 dB/km. Again, this is over-estimated by the upper bound of WB (Weibull) DSD of 20-30 dB, while it is again under-estimated by the lower bound CT distribution of 2-3 dB/km.

We also compare Figure 4-4 plots for Gaborone ($R_{0.01}$=69 mm/h) and Kasane ($R_{0.01}$=64.4 mm/h) with the measurements of γ at 13 GHz in Fig.2 of [Moupfouma and Tiffon, 1982]. From Figure 4-4 plots, the specific attenuation range at 13 GHz extends between 2-13 dB/km, at both values of $R_{0.01}$. Through extrapolation of the measurements of [Moupfouma and Tiffon 1982] for vertical and horizontal polarization, as well as using their proposed model, one finds that γ falls within the range 3-4 dB/km for the two rain rates. The closest DSD model corresponding to this attenuation range in Figure 4-3 is the TT (Tropical Thunderstorm) model. Again, this result is consistent with the findings in Table 4-4, for rain rate range $21 < R < 72$ mm/h, as discussed below.

Figure 4-5 shows the variations of γ_j, $j = ext, abs, sca, b$ with temperature, for four (4) types of log-normal drop-size distribution, for frequencies of 1 GHz and 300 GHz. It is

seen from the figure that at lower frequencies, the absorption coefficient, γ_{abs}, contributes more strongly to the extinction coefficient, γ_{ext}, than the scattering coefficient, γ_{sca}, for all drop-size distributions. At higher frequencies, γ_{abs} and γ_{sca} are almost constant; thus making γ_{ext} depend just slightly on temperature. To illustrate this effect analysis was also performed for others stations such as: Francistown, Kasane, Selebi-Phikwe, Mahalapye, Shakawe, Tshane, Sua Pan, Maun, Lethlakane, Ghanzi, Tshabong, Pandamatenga and Jwaneng and the results are given in the Appendix B.

Table 4-4-4: RMS and χ^2 Statistic (1% significance level) for various DSD models

Rain Rate Range: $1 \leq R < 21 mm/h$			**Best Model**
DSD Model	**RMS test**	χ^2 Statistic Threshold=33.4	
L-P	3.012479	41.766236	**WB or ITU-R model for Horizontal Polarization**
MP	3.535579	121.0101	
JD	4.572003	110.4866	
JT	2.942713	40.14762148	
WB	3.154202	22.00830221	
ITU-R model for Hor. Pol	2.422586	23.85383	
ITU-R model for Vert. Pol	3.181751	36.40273666	
Rain rate Range: $21 \leq R \leq 79 mm/h$			
DSD Model	**RMS test**	χ^2 Statistic Threshold=13.3	**TT**
LP	6.698212	6.758705	
JT	7.176179	7.830554	
WB	21.96866	38.70068	
TT	4.209454	4.162024	
CT	4.424726	5.798952	
ITU-R model for Hor. Pol	10.05113	12.03571	
ITU-R model for Vert. Pol	5.574076	6.768724	

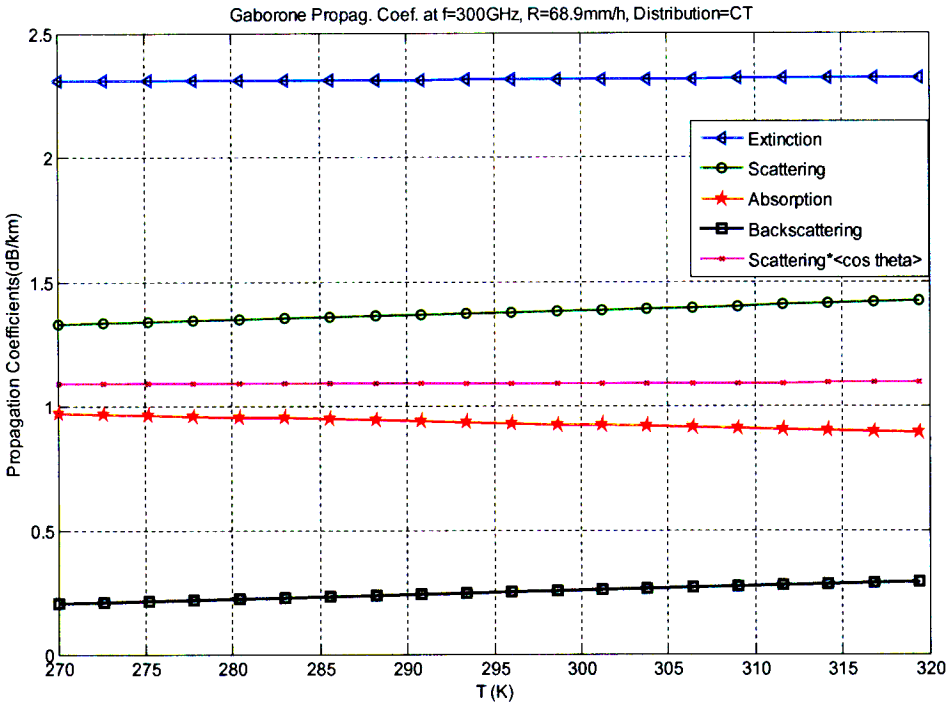
Gaborone Propag. Coef. at f=300GHz, R=68.9mm/h, Distribution=CT
Propagation Coefficients(dB/km)
T (K)
Extinction
Scattering
Absorption
Backscattering
Scattering*<cos theta>

(a)

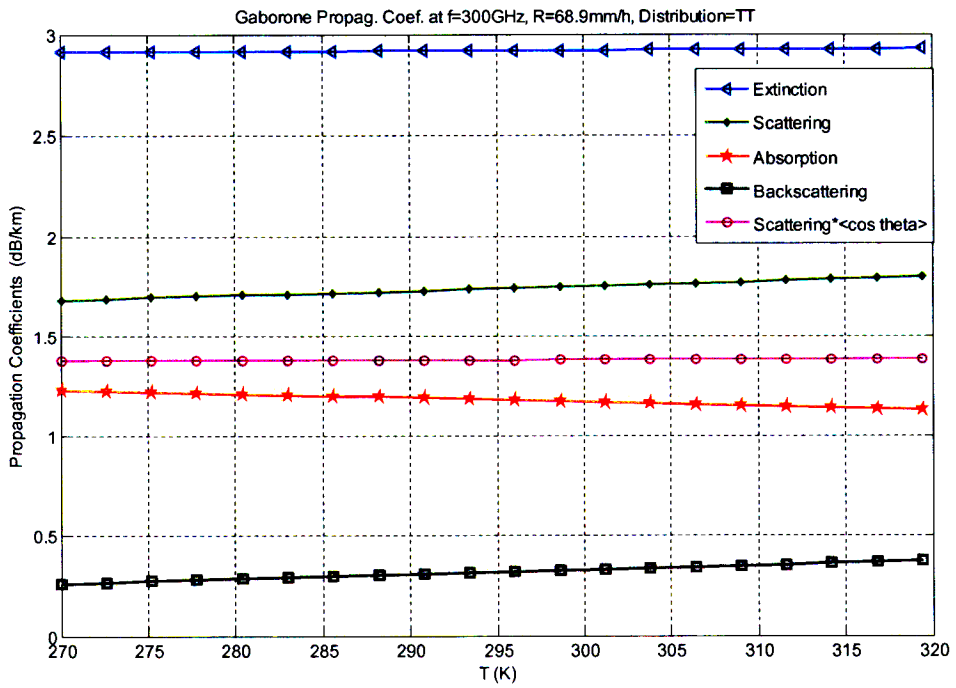
Gaborone Propag. Coef. at f=300GHz, R=68.9mm/h, Distribution=TT
Propagation Coefficients (dB/km)
T (K)
Extinction
Scattering
Absorption
Backscattering
Scattering*<cos theta>

(b)

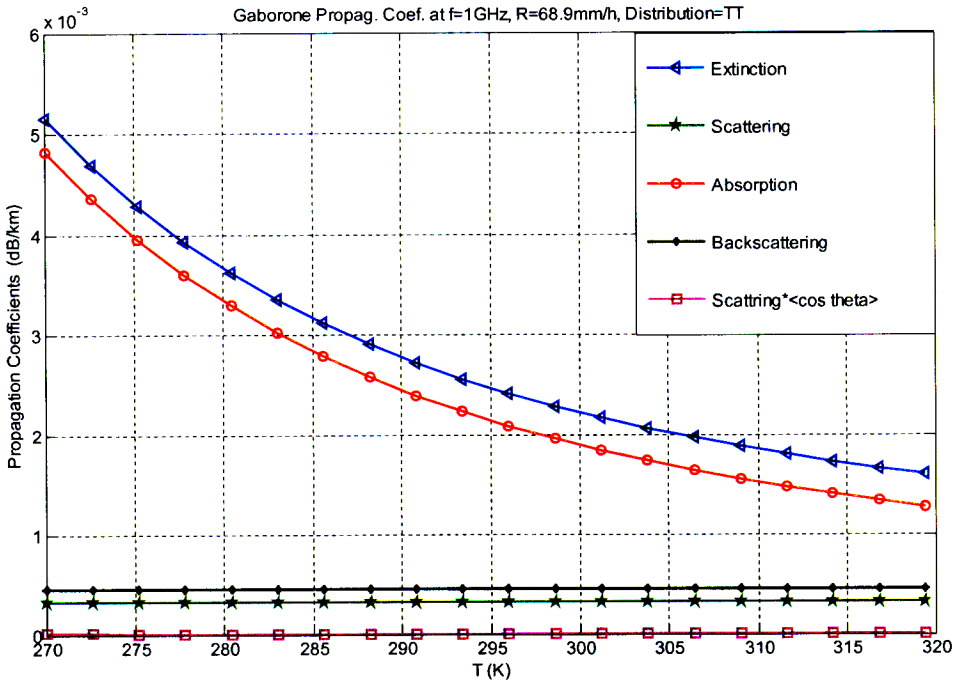

(c)

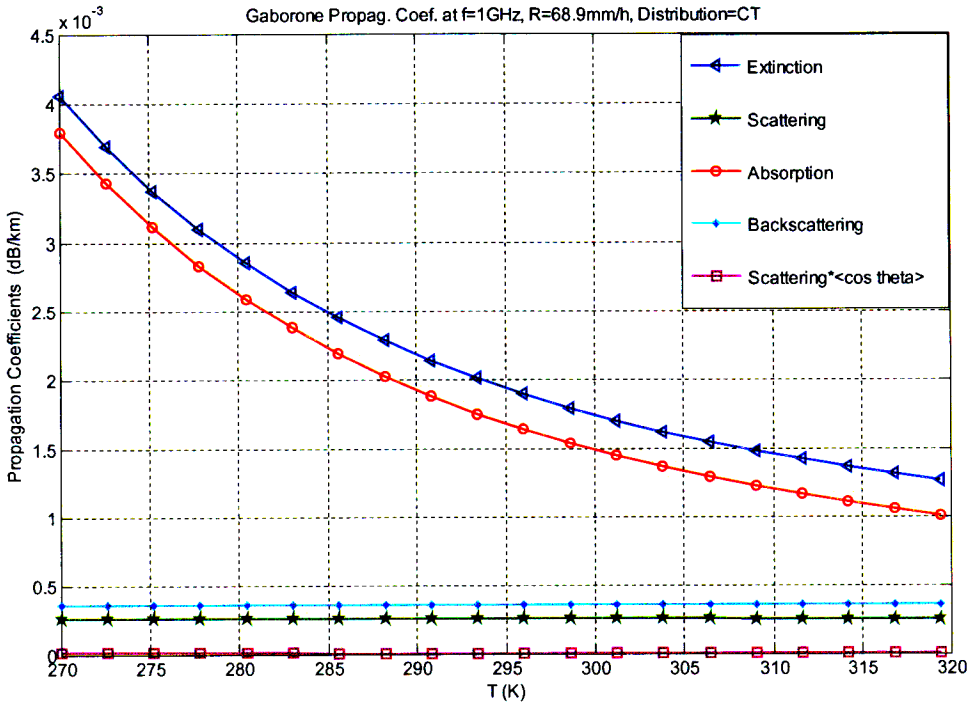

(d)

Figure 4-5 a, b, c and d: Attenuation coefficient due to rain versus Temperature for Gaborone using CT and TT lognormal distributions.

Finally, the analytical model is compared to the [Fashuyi et *al*, 2007] attenuation model based on the path profile for the 6.73-km terrestrial line-of-sight millimetric radio link between the Howard College campus and the Westville campus [Naicker, 2006]. The comparison of the attenuation using raindrop size distribution models by Mie scattering with rain attenuation measured is presented in Figure 4-6 according to ITU-R P530-12. ITU-R P.530-12 [ITU-R, 2007] gives a simple technique that may be used for estimating the long-term statistics of rain attenuation. To determine the effective path length, d_{eff}, of the link of path length d, use is made of a reduction factor r, given by ITU Recommendation 530-12 [ITU-R, 2007]:

$$r = 1/(1 + d/d_0)$$
$$d_0 = 35e^{-0.015R_{0.01}} \tag{4.11}$$

The above expression is valid for $R_{0.01} = 100$ *mm/h*. For $R_{0.01} > 100$ *mm/h*, use is made of the value 100 mm/h in place of $R_{0.01}$. In the case of the actual path in Durban, r is 0.61 and d_{eff} is 4.1. Thus the estimated path attenuation exceeded 0.01% of the time is:

$$A_{0.01} = \gamma_R d_{eff} = \gamma_R dr \ \text{(dB)} \tag{4.12}$$

Table 4-4 shows the values for the χ^2 statistic and the root mean square (RMS) error for L-P, MP, JT, JD, WB, ITU-R-Horizontal and ITU-R-Vertical models. For 17 degrees of freedom, the threshold value, t_α for α=1% significance level, is 33.4. The values of χ^2 statistic for the rain rate 1 = R < 21 mm/h, with the above distributions, when compared with the threshold value, show that the results for WB and ITU-R-Horizontal are the lowest and below the threshold value; and therefore, along with the RMS error test, the

ITU-R-Horizontal and the WB models give the best fit for 1 = R < 21 mm/h. Similarly, for the range 21 = R = 79 mm/h, with 4 degrees of freedom, the threshold value, t_α for α=1% significance level, is 13.3. With the same distributions, the lognormal model for tropical thunderstorm (TT) gives the best fit at 21 = R = 79 mm/h, with a χ^2 statistic of 4.16, and an RMS error of 4.21. The plots are displayed in Figure 4.6, where the curves for the ITU-R-Horizontal model and the TT DSD model are seen to fall within the minimum and maximum bounds of the measured rain attenuation for the Howard College-Westville campus radio link, for their respective rain rates.

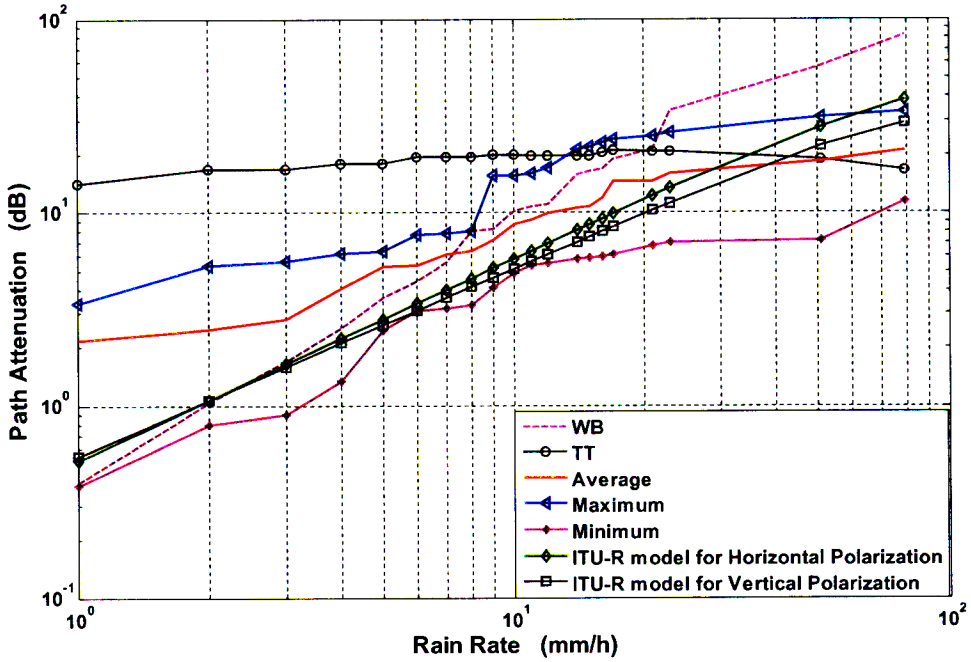

Figure 4-6: Rain attenuation for Durban along the 6.73 km link at 19.5 GHz for the year 2004: Maximum, minimum and average measured values versus the analytical plots using WB, TT, and ITU-R models.

4.4 Conclusion

In this chapter, the extinction coefficient γ_{ext}, is seen to depend more strongly on temperature at lower frequencies than at higher frequencies for lognormal rain drop-size distribution as confirmed by Olsen (1978) and Mätzler (2002b-2002c) using exponential distributions. The variation of the specific rain attenuation, γ, for Botswana (a tropical area) at 5 GHz and 1000 GHz shows a very close agreement with the results obtained by Roger and Olsen, at three temperatures of 263°K, 273°K, and 293°K, even though the latter used the less accurate Ray model for Mie scattering parameter evaluation, while we have employed the Liebe model. Plots of γ for fourteen different values of $R_{0.01}$ in Botswana for different rain drop-size distributions and varying frequencies show that while they are comparable to results obtained by Olsen et al. [1978] and Ajayi and Adimula [1996], at frequencies above 50 GHz, the Joss-Drizzle distribution over-estimates the attenuation, while the Continental Thunderstorm model under-estimates it. In the frequency range 15-50 GHz, the upper bound of γ is provided by the Weibull DSD, while the lower bound is due again to the CT model. In comparing these results with the measurements over a 13 GHz microwave link by Moufpouma and Tiffon [1982], it is seen that the appropriate model for Gaborone and Kasane in Botswana is the Tropical Thunderstorm. Finally, applying the model to measurements over the 6.73-km 19.5 GHz line-of-sight link in Durban, it is concluded that the TT model would again be the most suitable for Durban, for rain rates greater than 21 mm/h.

Chapter 5

Effects of Rain on Ground-based Radars in Durban

5.1 Introduction

In Chapter 2, we introduced the dielectric properties of water at microwave frequencies and studied hydrometeors that are essentially particles of water within the atmosphere, which take the form of liquid water as in rain, mist and fog or ice as in clouds, hail and snow. Plane electromagnetic waves traveling through air containing precipitation are scattered and absorbed by the particles of ice, snow or water. Water, with its larger dielectric constant, scatters electromagnetic wave more strongly than ice, [Nemarich et al., (1988), Manabe et al., (1987) and Kharadly, (1989)]. In addition, it has a much larger dielectric loss and the attenuation due to thermal dissipation is therefore much greater for water particles than for ice particles [Ishimaru, 1978 and Jiang et al., 2004]. Thus rain degrades the performance of millimeter waves and microwave radars more than ice. Radiowave propagating through a rain zone will be scattered, depolarized, absorbed and delayed in time. All these effects of rain on the wave propagation are related to the frequency at which the signal is transmitted, and polarization of the wave as well as to the rain rate, which influences the form and size distribution of the raindrop.

In this chapter we investigate the impact of rain on sensor systems at microwave frequencies in Durban. As there is no measurement on radar, we have used the rain attenuation measurement for the path profile for the 6.73km terrestrial line-of-sight from the Howard College campus to the Westville campus [Naicker et al., 2006 and Fashuyi et *al.*, 2007], since the hydrometeors act in the same way for both links. We investigate the specific backscattering for that link which could be applied to radar systems in Durban and can be used as an indicator of the degree of possible degradation of system performance.

5.2 Experimentation Configuration

In the previous Chapter, we determined specific attenuation for various locations in Botswana; we learned that the specific attenuation varies with rain rate, size parameter and refractive index. We now consider a practical case of attenuation due to rain at a given distance d in Durban and compare it with our model.

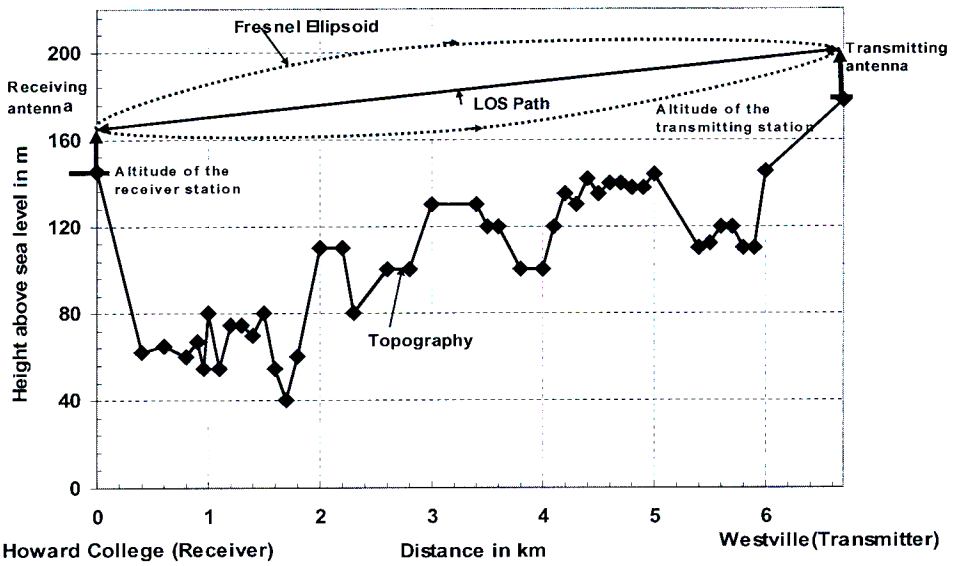

Figure 5-1: The path profile for the 6.73km terrestrial line-of-sight from the Howard College campus to the Westville campus [Naicker, 2006 and Naicker et al., 2006, Fashuyi and Afullo, 2007].

The line-of-sight link was established between the Howard College and the Westville campuses of the University of KwaZulu-Natal, Durban, as in Figure 5-1. The details on the link setup at the receiver and the transmitter end can be seen in [Naicker, 2006 and Naicker et al., 2006, Fashuyi and Afullo, 2007]. The terrestrial link parameters are shown in Table 5-1. Figure 5-1 shows the topography of the path between two campuses in Durban.

Calculating for the received power P_r we have:

$$\begin{aligned} P_r &= P_t - FSL + G_t + G_r - Losses \\ &= 20\ dBm - 135\ dB + 2 \times 38.6\ dBi - 2.2\ dB - 1\ dB \\ &= -41\ dBm \end{aligned} \tag{5.1}$$

where, P_t = transmitted Power (taken as $100\ mW = 20\ dBm$); FSL= Free space loss; G_r = Receive antenna gain; G_t = Transmit antenna gain.

Thus the received power P_r expected at the receiver end of the link when a transmitting power of 100 mW is employed between Howard College and Westville campuses should be -41 dBm when there is no rain to cause any attenuation.

Table 5-5-1: Terrestrial link parameters for the LOS SHF systems [Naicker, 2006]

Parameter	**Description**
Path length	6.73 km
Height of transmitting antenna above the ground	24 m
Altitude of transmitter station	178 m
Height of receiving antenna above the ground	20 m
Altitude of receiver station	145 m
Carrier frequency	19.5 GHz
Bandwidth under investigation	200 MHz
Transmitting power	10-100 mW
Transmitting/receiver antenna gain	38.6 dBi
Transmitting/receiver antenna beam width	1.9 degrees
Free space loss	135 dBm
Total cabling and connection losses	~ 2.2 dB
Clear air attenuation	~ 1dB
Receiver bandwidth	100 kHz 1 GHz

Consider now Figure 5-2, where the total field, at a distance r from a reference point in the particle, in the direction of a unit vector k_s consists of the incident field $E_i(r)$ and

the field $E_s(r)$ scattered by the particle. Within a distance $r < D^2/\lambda$ where D is a typical dimension of the particle such as its diameter, the field $E_s(r)$ has complicated amplitude and phase variations because of interference between contributions from different parts of the particle. So, the observation point r is said to be in the near field of the particle. When $r > D^2/\lambda$ however, the scattered field $E_s(r)$ behaves as a spherical wave and is given, according to [Ishimaru, 1978 Page 279], by

$$E_s(r) = f(j_i, k_s)\frac{e^{-jkr}}{r} \tag{5.2}$$

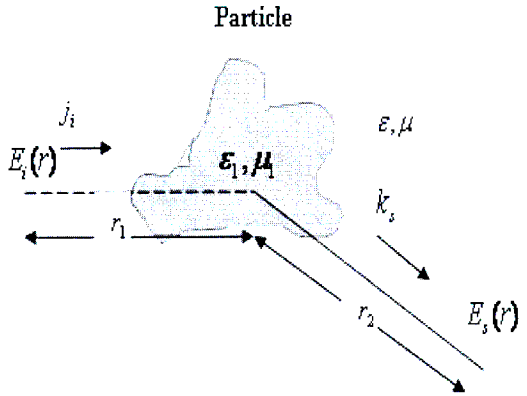

Figure 5-2: A plane wave is incident upon a dielectric scatterer and the scattered field is observed in the direction k_s at a distance r, [Ishimaru, (1978) Page 279].

$f(j,k)$ represents the amplitude, phase and polarization of the scattered wave in the far field in the direction k_s when the particle is illuminated by a plane wave propagating in the direction j_i with unit amplitude. It is known as the scattering amplitude. Based on the Rayleigh and Mie scattering theory, we have the total sum of the cross sections of all particles per unit volume, such as $\rho < \sigma_s >$, $\rho < \sigma_a >$, $\rho < \sigma_b >$ and, $\rho < \sigma_t >$ [Ishimaru, 1978 (pp 46)] as presented in Appendix A.3.

The computation of the rain attenuation must therefore be based on the exact formulation for spheres as developed by Mie. In Appendix A.1, it was stated that the key parameters

for Mie calculations are Mie coefficients, a_n, b_n, c_n and d_n which are expansion coefficients given by Sadiku (1992) on p.100. The backscattering efficiency, applicable to monostatic radar, [Meador and Weaver, 1980] is given in equation (3.42), as

$$Q_b = \frac{\sigma_b}{\pi a^2}\frac{1}{x^2}\left|\sum_{n=1}^{\infty}(2n+1)(-1)^n(a_n - b_n)\right|^2. \tag{5.3}$$

In Section 2.2.5, we discussed dielectric properties of water at higher frequencies. The more accurate dielectric model of due to Liebe, with refraction index of water for wavelengths from 10 nm to 10 m as given in [Segelstein, 1981] where at $f = 19.5\ GHz$ $\lambda = 15\ mm$, m is $6.70992+2.7608j$.

For an incident plane electromagnetic wave of unit amplitude traveling in the positive z direction with the electric vector polarized along de x axis, the backscattered far fields are given by [strantton, 1941 and Inada, 1973]:

$$E_\theta = [\exp(j\omega t - jkr)/jkr]S(\pi)\cos\phi, \tag{5.4}$$

$$E_\phi = [\exp(j\omega t - jkr)/jkr]S(\pi)\sin\phi, \tag{5.5}$$

where

$$S(\pi) = \sum_{n=1}^{\infty}(-1)^n(n+1/2)(a_n - b_n). \tag{5.6}$$

The Mie scattering coefficients, a_n and b_n, are expressed in terms of the spherical Bessel functions, with a_n related to the amplitudes of the oscillations of magnetic type, while the coefficients b_n are related to the amplitudes of electric oscillations, [Inada, (1973)].

5.3 Radar Equations

Consider T_X as a transmitter illuminating a particle at a large distance r_1 with a total transmitted power P_t and $G_t(j_i)$ is the gain of transmitter in the incidence direction. Consider again R_X as a receiver of the scattered wave at a large distance r_2 with the received power P_r. Assume that r_1 and r_2 are large and that the particle is in the far field of both antennas. The incident power flux density Π_i at the particle in term of gain of transmitter, is given by

$$\Pi_i = \frac{G_t(j_i)}{4\pi r_1^2} P_t. \tag{5.7}$$

At the receiver, the power flux density Π_r is given by

$$\Pi_r = \frac{\sigma_{bi}(k_s, j_i)}{4\pi r_2^2} \Pi_i, \tag{5.8}$$

where $\sigma_{bi}(k_s, j_i)$ is the measure of the amount of incident power intercepted by the target (particle) and re-radiated back in the direction of receiving radar, and is denoted as the radar bistatic cross section. Then the received power is given by

$$P_r = A_r(k_s)\Pi_r, \tag{5.9}$$

where $A_r(k_s)$ is the receiving cross section given by [Ishimaru, 1978]

$$A_r(k_s) = \frac{\lambda^2}{4\pi} G_r(-k_s) \tag{5.10}$$

Equations (5.7) to (5.10) give a ratio of the received to the transmitted power

$$\frac{P_r}{P_t} = \frac{\lambda^2 G_t(j_i) G_r(-k_s) \sigma_{bi}(j_i, k_s)}{(4\pi)^3 r_1^2 r_2^2}. \tag{5.11}$$

When $k_s = -j_i$ and $r_1 = r_2 = r$, the ratio of the received to the transmitted power will be

$$\frac{P_r}{P_t} = \frac{\lambda^2 (G_r(j_i))^2 \sigma_b(-j_i, j_i)}{(4\pi)^3 r^4}. \tag{5.12}$$

Equation (5.11) is applied to bistatic radar while equation (5.12) is for monostatic radar. For the rest of this section we are going to concentrate on monostatic radar.

5.4 First-Order Multiple Scattering

The First-order multiple scattering takes into account attenuation by scattering and absorption of a wave propagating along a path. This method is often used in millimeter and optical wave propagation through rain, fog, smog, and snow [Ishimaru, 1978]. The first order multiple scattering can be easily considered as an extension of the radar equations for the single scattering approximation, discussed earlier in the preceding section.

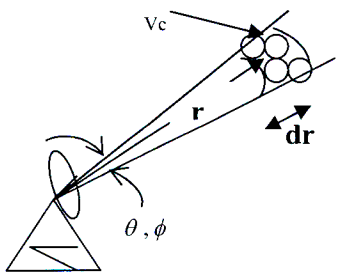

Figure 5-3: Narrow beam monostatic radars, [Hassen, 2006].

The received power P_r given in equation (5.9) can then be modified for the first-order multiple scattering case as follows [Skolnik, 1962]:

$$P_r = \frac{\pi^5 P_t A_e h}{32 r^2 \lambda^4} \exp(-2\gamma r) \sum_i D^6 |K|^2, \quad (5.13)$$

where A_e is the transmitting cross section, D is the rain drop diameter, P_t is the total transmitted power, $|K|^2 = (\delta - 1)/(\delta + 2)$, and δ = dielectric constant of the scattering particles, h is the radar pulse-extent and γ is the one-way attenuation coefficient, given by

$$\gamma = \int_0^r \rho < \sigma_{ext} > ds. \quad (5.14)$$

The number of particles (or density) $\rho(s)$ and the total cross section $\sigma_{ext}(s)$ can be a function of the position along the path from the transmitter to dr. This can be easily incorporated in the equation (5.13) by substituting the total cross section σ_{ext} and the backscattered cross section σ_b with their average value defined in the following manner [Ishimaru, 1978]

$$\rho < \sigma_{ext} \geq \int_0^\infty n(D,r)\sigma_{ext} dD, \text{ and} \quad (5.15)$$

$$\rho < \sigma_b \geq \int_0^\infty n(D,r)\sigma_b dD. \quad (5.16)$$

where *n(D, r)* is the number of particles per unit volume located at *r* having a range of sizes between *D* and *D* + *dD*, and ρ is the number of particles per unit volume given by:

$$\rho(r) = \int_0^\infty n(D,r) dD. \quad (5.17)$$

The two-way attenuation of radar signal in traversing the distance ***r*** and back is an exponential function of the distance given by:

$$\psi = \exp(-2\int_0^r \gamma\, dr)\,. \tag{5.18}$$

For the backscattering radar equation (5.16), we obtain the rain cell volume, V_c, (figure 5-3)

$$V_c = (\pi r^2 \theta\phi / 4\ln 2)dr\,. \tag{5.19}$$

We then write equation (5.12) as:

$$\frac{\Pr}{Pt} = (2.855\times10^{-4})\lambda^2[G_t(i_0)]^2\theta\phi\int_{r_0}^{r}\frac{\rho\sigma_b}{r^2}e^{-2\gamma}dr, \tag{5.20}$$

where $(2.855\times10^{-4}) = \pi/(4\pi)^3(8\ln 2)$.

The gains $G_t(j_i)$ and $G_r(k_s)$ are related to the actual aperture areas A_t and A_r of the transmitter and receiver:

$$G_t(j_i) = \xi_t 4\pi A_t/\lambda^2,\quad G_r(k_s) = \xi_r 4\pi A_r/\lambda^2, \tag{5.21}$$

where ξ_t and ξ_r are the aperture efficiencies of the transmitter and the receiver, and are typically 0.5-0.6. The half-power beamwidths, θ and ϕ are related to the diameters of the apertures. θ is given in terms of the diameter D_1 in the θ plane:

$$\theta = \alpha_1\lambda/D_1 \qquad \text{radians.} \tag{5.22}$$

The constant α_1 is typically 1.3-1.6, depending on the field distribution over the aperture. We may combine equations (5.21) and (5.22) and obtain the following formula for the gain:

$$G_t(j_i) = (\xi_t \alpha_1 \alpha_2)(\pi^2 / \theta\phi) \approx \pi^2 / \theta\phi \tag{5.23}$$

The total backscattering cross section $\rho < \sigma_b >$ per cubic meter of rain cell volume V_c in the beam can obviously be equated from (5.20) as follows, [Hassen, 1973]:

$$\rho<\sigma_b>=\frac{114}{\lambda^2[G_t(j_i)]^2\theta\phi e^{(-2\rho<\sigma_t>r)}\int_r^{r+dr}\frac{e^{(-2\rho<\sigma_t>r)}}{r^2}dr}\left(\frac{P_r}{P_t}\right) \tag{5.24}$$

So far, the attenuating effect of the precipitation $e^{-2\gamma}$, through which the signal may have to pass, has been considered. It shows that the influence of the rain intensity over the attenuation makes it difficult to determine the backscattering cross section $\rho < \sigma_b >$ of the rain using equation (5.24) by only measuring the received power. Most of parameters in equation (5.24) are either known or measured. At frequencies higher than 10 GHz, the calculations of the cross-sections must be made by using the Mie theory. We return to the specific backscattering γ_b given by equation (4.1),

$$\gamma_b = 4.343\int_0^{\infty} D^2 Q_b N(D) dD \qquad \text{(dB/km)} \tag{5.25}$$

γ, attenuation coefficient in dB, can be found in [Naicker et al., 2006 and Fashuri et al., 2007] where it is characterized by path attenuation due to rain in Durban between two campuses.

In absence of precipitation (dry weather), the received signal-to-noise ratio (S/N_o) is given by, [Silver, 1949]:

$$(S/N_0)_d = \frac{P_d}{N_r} = \frac{K_1 \sigma_T / r_d^4}{N_r}. \tag{5.26}$$

where P_d = received echo power from a target of cross-section σ_T at a range r_d in dry air; K_1= a constant representing the parameters of radar equation $K_1 = P_t G^2 \lambda^2 / (4\pi)^3$ and

N_o = receiver noise power.

In inclement weather the signal-to-noise ratio is,

$$(S/N_0)_w = \frac{P_w}{N_r + P_r} = \frac{K_1 \sigma_T \psi / r_w^4}{N_r + P_r}. \tag{5.27}$$

where P_w = received echo power from a target of cross section σ_T at a range r_w in inclement weather.

P_r = received echo power from rain is equal to equation (5.13), $\psi = \exp(-2\gamma r_w)$ and γ = attenuation coefficient.

When received echo power from rain becomes significant, it contributes to rise in the noise floor and the radar can lose its target.

5.5 Specific Rain Backscattering for Durban

Based on measurements realized by Naicker [Naicker et al., 2006], we establish the specific rain backscattering (dB/km) using equation (5.25) for the Marshall-Palmer (MP), Joss-Drizzle (JD), Joss-Thunderstorm (JT), Law-Parson (LP), Continental-Showers (CS), Tropical Showers (TS), Continental Thunderstorms (CT) and Tropical Thunderstorm (TT) distributions at 19.5 GHz as shown in Figure 5.4.

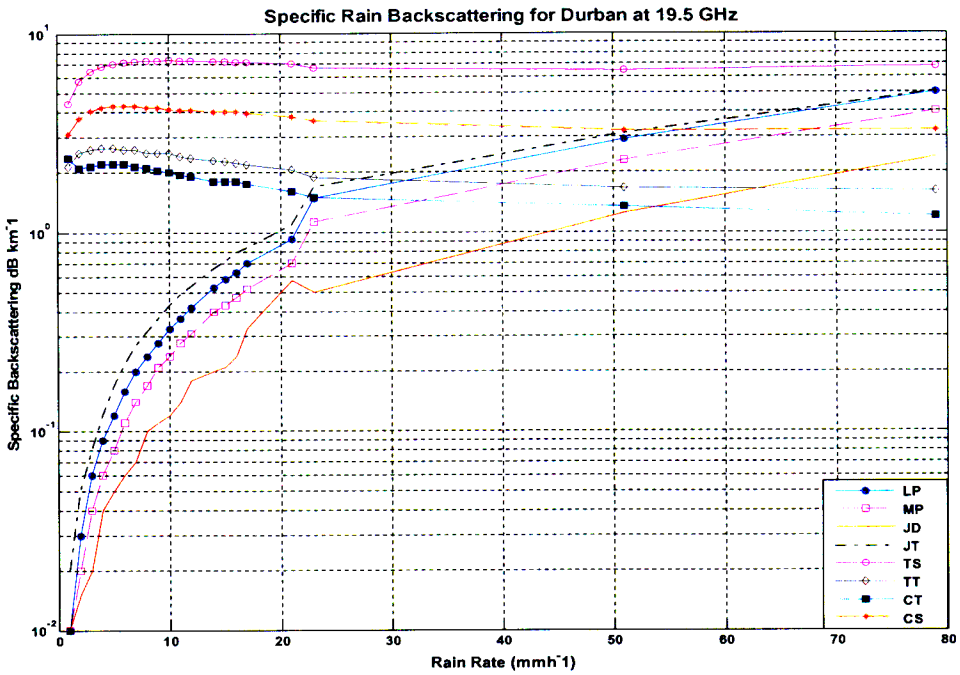

Figure 5-4: Specific Rain backscattering in Durban for different distributions.

From Figure 5-4, we observe that for MP, JT, JD and LP distributions the specific backscattering increases more strongly with rain rate up to 10 mm/h and after that the increment is not significant while the rain rate is increasing; the maxima are 5dB/km, 4 dB/km, 2.5 dB/km and 5 dB/km, respectively.

On the other hand, for the log-normal DSDs, γ_b remains almost constant for rain rates above 4 mm/h. Thus the lognormal distribution (TS, CS, TT, and CT) has much higher values of γ_b than the exponential distributions (MP, JT, JD, LP). As the rain rates increase, towards 50-80 mm/h, γ_b values tend to merge for the two groups of DSD.

According to Laws and Parsons [Alfred et *al.*, 1989], a very large fraction of raindrops are larger than $D \geq 1mm$ at rainfall intensities $R \geq 2.5mm/h$. Therefore based on the scattering matrix by Bohren and Huffman (1978, pp 111), the angular diagrams for Mie scattering on raindrops at 19.5 GHz, T = 293^0 K in Durban will appear as shown in Figure 5-5. Mie scattering intensities $|S_1|^2$ and $|S_2|^2$ as a function of $\cos\theta$, and the result as a polar diagram of θ on the upper part of the curves ($0 < \theta < \pi$) are for polarization perpendicular to the scattering plane. The lower part of the curves ($\pi < \theta < 2\pi$) are for

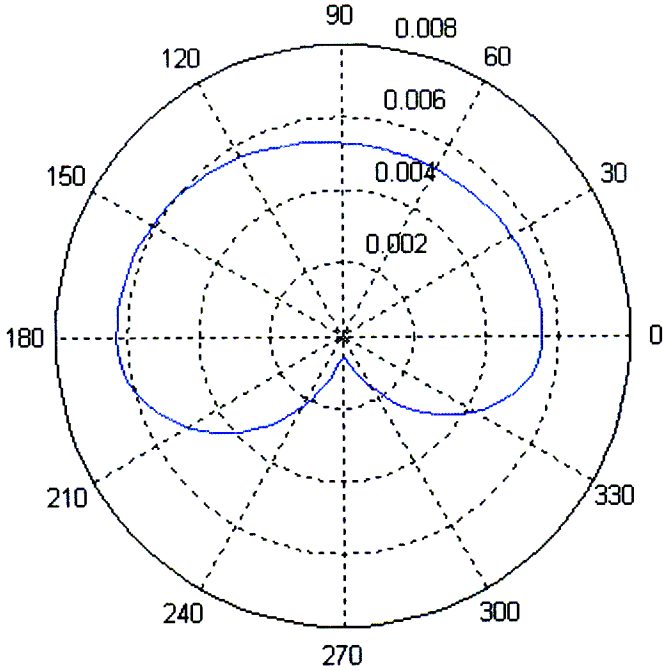

(a) D = 2 mm

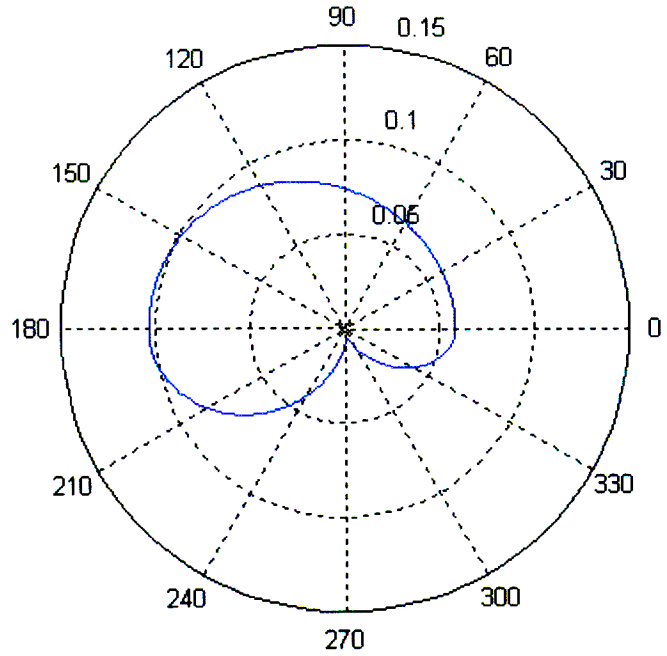

(b) D = 3 mm

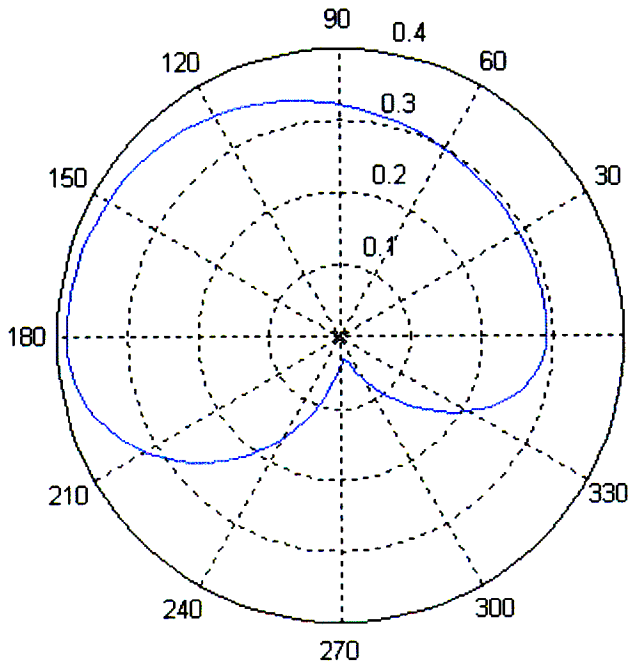

(c) D = 4 mm

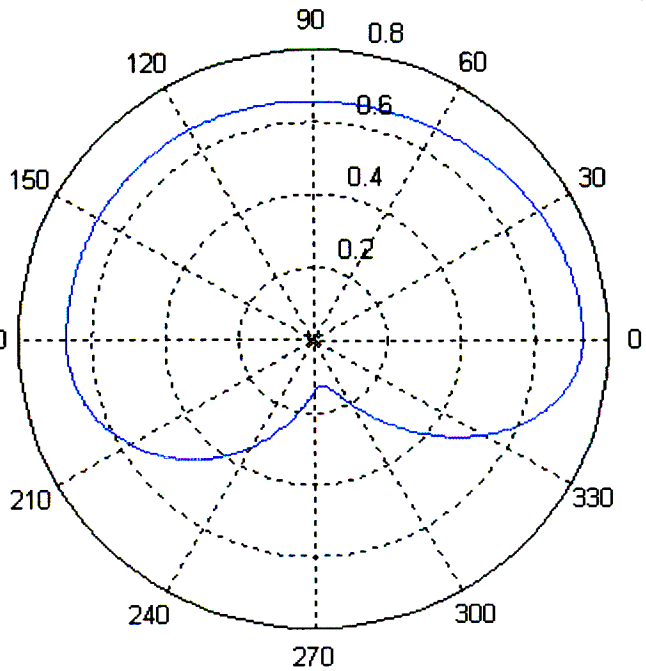

(d) D = 5 mm

polarization parallel to the scattering plane, and both functions are symmetric with respect to two half circles.

For raindrop diameter equal to 2 mm there is little change in intensity with angle in the upper part while the lower part strongly changes and reaches the maximum at 0 ^{0}C. For a diameter equal to 3 mm or size parameter ($x = k\,a$), equal 0.63, scattering in the backward hemisphere is much larger than in the forward hemisphere.

At a diameter equal to *4 mm* or size parameter ($x = k\,a$) equal to 0.84, $|S_1|^2$ and $|S_2|^2$ have large amplitudes in backward direction at $\theta = \pi$. At diameter equal to 5 mm or size parameter ($x = k\,a$) equal to 1.26, $|S_1|^2$ and $|S_2|^2$ have much larger amplitudes in the forward direction at $\theta = 0$.

Figure 5-5 a, b, c, d: Polar plots for magnitudes of Mie scattering on raindrops at f =19.5 GHz, T= 293K for different diameters.

The Mie backscattering efficiency variation with raindrop size, Q_b (Figure 5-6) shows different maxima according to raindrop diameter. While the monostatic radar signal from rain is not directly influenced by the changing diagram, the modeling of microwave transmission signals depends on the angular diagram, i.e. on the phase function [Ishimaru, 1978].

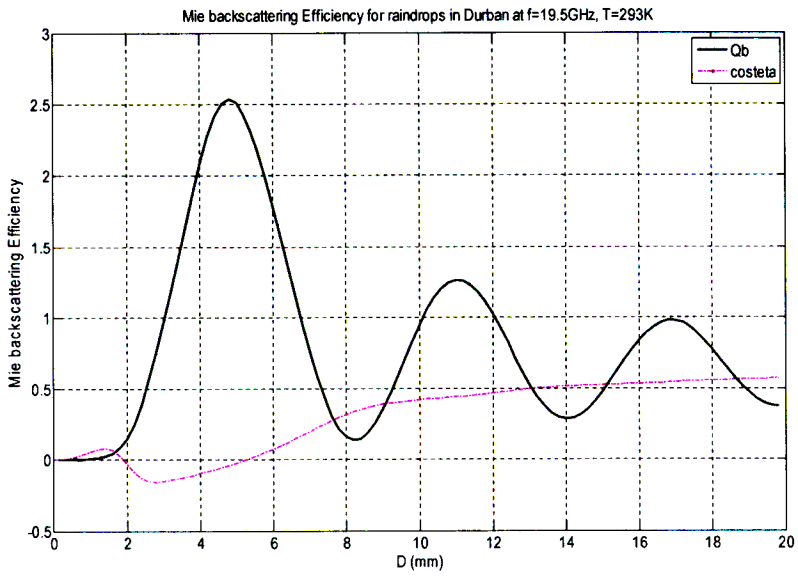

Figure 5-6: Mie efficiencies on raindrop in Durban at f= 19.5 GHz and T= 293K.

It is observed that the peak value of Q_b occurs at a raindrop size of 4.7 mm. Thus, at 19.5 GHz, the highest attenuation for radar system occurs for this raindrop size (4.7 mm).

5.6 Conclusion

For rainfall intensity below about 10 mm/h for JD, JT, MP and LP distributions, and below about 4 mm/h for TS, TT, CT and CS distributions, the rain drops are small with respect to the wavelength at 19.5 GHz; the specific backscattering follows Rayleigh scattering law where the average backscattering cross-section is proportional to the sixth power of the drop diameter [Ishimaru, 1978, Chap. 3]. This can be seen in the curve observed in Figure 5-5. For rainfall intensity above about 10 mm/h, the diameters of raindrops are in the order of the wavelength, so backscattering is predominantly due to Mie scattering law where the average backscattering cross-section depends weakly on raindrop diameter. Since the raindrop diameter D appears as the sixth power in equation (5.13), it follows that in any raindrop size distribution, the small number of large drops will contribute the largest amount of received echo power of the rain. Then there is a reduction of the signal-to-noise ratio and the radar can lose the target according to equation (5.27). Figure 5-6 shows that the highest Mie backscattering on raindrops in Durban at $f = 19.5\ GHz$ occurs when D equals 4.7 mm, and the lowest when D falls below 1.5 mm.

Chapter 6

Conclusion and Future Work

6.1 Conclusion

Radio wave attenuation due to rain has been studied in this work, with specific focus on Southern Africa. While the ITU-R recommendation 837-1 had three rain climatic zones for Botswana (C, E and J), and Recommendation 837-4 had three zones (J, L and N), in this work, we have two (2) rain zones (Q and M). This derivation is based on comparison of CDFs for South African and Botswana sites. Thus the corresponding values of $R_{0.01}$ have been derived.

The extinction coefficient γ_{ext}, is seen to depend more strongly on temperature at lower frequencies than at higher frequencies for lognormal rain drop-size distribution as confirmed by Olsen (1978) and Mätzler (2002b-2002c) using exponential distributions. The variation of the specific rain attenuation, γ, for Botswana (a tropical area) at 5 GHz and 1000 GHz shows a very close agreement with the results obtained by Roger and Olsen, at three temperatures of 263°K 273°K, and 293°K, even though the latter used the less accurate Ray model for Mie scattering parameter evaluation, while we have employed the Liebe model. Plots of γ for fourteen different values of $R_{0.01}$ in Botswana

for different rain drop-size distributions and varying frequencies shows that while they are comparable to results obtained by Olsen et al. [1978] and Ajayi and Adimula [1996], at frequencies above 50 GHz, the Joss-Drizzle distribution over-estimates the attenuation, while the Continental Thunderstorm model under-estimates it. In the frequency range 15-50 GHz, the upper bound of γ is provided by the Weibull DSD, while the lower bound is due again to the CT model. In comparing these results with the measurements over a 13 GHz microwave link by Moufpouma and Tiffon [1982], it is seen that the appropriate model for Gaborone and Kasane in Botswana is the Tropical Thunderstorm. Finally, applying the model to measurements over the 6.73-km 19.5 GHz line-of-sight link in Durban, it is concluded that the TT model would again be the most suitable for Durban, for rain rates greater than 21 mm/h.

For rainfall intensity below about 10 mm/h for JD, JT, MP and LP distributions, and below about 4 mm/h for TS, TT, CT and CS distributions, the rain drops are small with respect to the wavelength at 19.5 GHz; the specific backscattering follows Rayleigh scattering law where the average backscattering cross-section is proportional to the sixth power of the drop diameter [Ishimaru, 1978, Chap. 3]. This can be seen in the curve observed in Figure 5-5. For rainfall intensity above about 10 mm/h, the diameters of raindrops are in the order of the wavelength, so backscattering is predominantly due to Mie scattering law where the average backscattering cross-section depends weakly on raindrop diameter. Since the raindrop diameter D appears as the sixth power in equation (5.13), it follows that in any raindrop size distribution, the small number of large drops will contribute the largest amount of received echo power of the rain. Then there is a reduction of the signal-to-noise ratio and the radar can lose the target according to equation (5.27). Figure 5-6 shows that the highest Mie backscattering on raindrops in Durban at $f = 19.5\ GHz$ occurs when D equals 4.7 mm, and the lowest when D falls below 1.5 mm.

6.2 Future Work

Note that the R values for Ghanzi and Tshabong are not close enough to 1 (they are 0.0885 and 0.932, respectively), since these are in desert region of Botswana. A more accurate fit may be required.

To get more reliable results, long-term constant measurement of rain events is required. Most of the raindrop size distribution models used in Southern Africa are analytic. In the future, the event should be measured and studied constantly; thus there is need to measure the appropriate distribution for each of the locations, and based on that the rain attenuation is determined.

To this end, the school of Electrical, Electronic and Computer Engineering at the UKZN has recently installed a distrometer – an instrument that will help us model the actual DSDs.

Appendix A

Absorption, Scattering, Backscattering, and Extinction by Precipitation

A.1 Scattered Far Field

The parameter efficiency coefficient $Q(D)$, because of the interaction of the cross-section (σ) over a scattering sphere of radius a [Mätzler, 2002a]. According to cross section of the particle we can have extinction efficiency, Q_{ext}, absorption efficiency, Q_{abs}, scattering efficiency, Q_{sca} and backscattering efficiency, Q_b. Raindrops are assumed to be randomly distributed within rain cell volume, so that there are no coherent phase relationships between the fields scattered by the individual particles, thereby allowing the use of incoherent theory for computing the extinction coefficient (the absorption and the scattering) by a volume containing many particles. Since the assumption that shadowing of one particle by another is ignored, because of the microwave frequency is used, the wavelength and the particle size is equivalent. Then the high-order scattering effect can be ignored. Thus the total extinction cross-section of a given volume is equal to the algebraic sum of the extinction cross-sections of all particles per unit volume. As a result, the attenuation due to rain can be estimated by calculating the extinction coefficient over all of the rain drops within the antenna beam volume, [Sadiku (1992) and Crane (1996)]. Figure A1 shows all the individual particles contained in that volume.

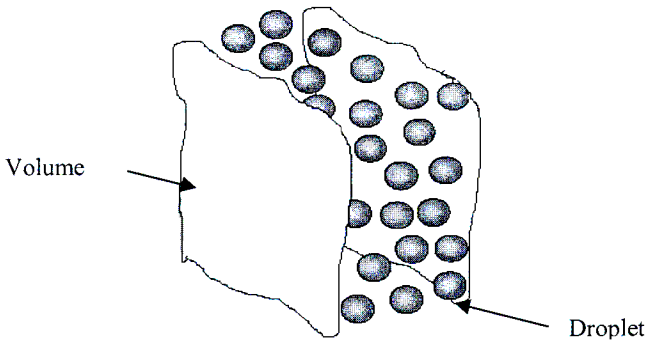

Figure A 1: Raindrops volume.

It has been pointed out on several occasions (e.g. Sadiku 1992 and Ulaby et al., 1981) that the extinction coefficient can be a function of the size and shape of rain drops, the wavelength of electromagnetic wave, and the complex refractive index of water.

Two approaches are used to approximate the extinction coefficient. First, we assume the scattering mechanism following the Mie scattering approximation, while the rain drops are all spherical as shown by Sadiku (1992). Second, Mishchenko (2002) uses the T-Matrix method to estimate the coefficient. The latter was initially a technique for computing electromagnetic scattering by single, homogeneous and arbitrarily shaped particles based on the Huygens principle. Actually, the T-Matrix method is one of the most dominant and generally used tools for computing electromagnetic scattering by single and compounded particles. In this study, we assume that raindrops are spherical so that Mie theory will be applied throughout this thesis.

The key parameters for Mie calculations are the Mie Coefficients a_n and b_n to compute the amplitudes of the scattered field, and c_n and d_n for the internal field, respectively. a_n, b_n, c_n and d_n are expansion coefficients which are given by Sadiku (2002, p.100).

$$a_n = \frac{j_n(mx)[xj_n(x)]' - j_n(x)[mxj_n(mx)]'}{j_n(mx)[xh_n^{(2)}(x)]' - h_n^{(2)}(x)[mxj_n(mx)]'} \tag{A.1}$$

$$b_n = \frac{j_n(mx)[xj_n(x)]' - m^2 j_n(x)[mxj_n(mx)]'}{h_n^{(2)}(x)[mxj_n(mx)]' - m^2 j_n(mx)[xh_n^{(2)}(x)]'} \tag{A.2}$$

$$c_n = \frac{j/x}{h_n^{(2)}(x)[mxj_n(mx)]' - j_n(mx)[xh_n^{(2)}(x)]'} \tag{A.3}$$

$$d_n = \frac{j/x}{h_n^{(2)}(x)[mxj_n(mx)]' - m^2 j_n(mx)[xh_n^{(2)}(x)]'} \tag{A.4}$$

where j_n is spherical Bessel function of first kind, and $h_n^{(2)}$ is spherical Hankel function of second kind.

Consider an arbitrary particle that is illuminated by a plane harmonic wave (Figure A2). The direction of propagation of the incident wave propagation is along the z axis, the forward direction. Any point in the particle may be chosen as the origin of a Cartesian coordinate system (x, y, z), where the x and y axes are orthogonal to the z axis and to each other but are otherwise arbitrary. The scattering direction e_r and the forward direction e_z define a plane called the scattering plane, which is analogous to the plane of incidence in problems of reflection at an interface. The scattering plane is uniquely determined by the azimuthal angle ϕ except when e_r is parallel to the z axis. In these two instances ($e_r \pm e_z$) any plane containing the z axis is a suitable scattering plane. Its components parallel ($E_{//i}$) and perpendicular ($E_{\perp i}$) to the scattering plane are:

$$E_i = (E_{0//}\, e_{//i} + E_{0\perp} e_{\perp i}) \exp(-ikz) = E_{//i}\, e_{//i} + E_{\perp i}\, e_{\perp i} \tag{A.5}$$

The orthogonal basis vectors are $e_{//i}$ and $e_{\perp i}$, where

$$e_{//i} = \cos\phi\ e_x + \sin\phi\, e_y, \quad e_{\perp i} = \sin\phi\, e_x - \cos\phi\, e_y \tag{A.6}$$

Form a right-handed triad with e_z:

$$e_{\perp i} \times e_{//i} = e_z \tag{A.7}$$

We also have

$$e_{//i} = -e_\phi, \quad , \ e_{\perp i} = \sin\theta\, e_r + \cos\theta\, e_\theta \tag{A.8}$$

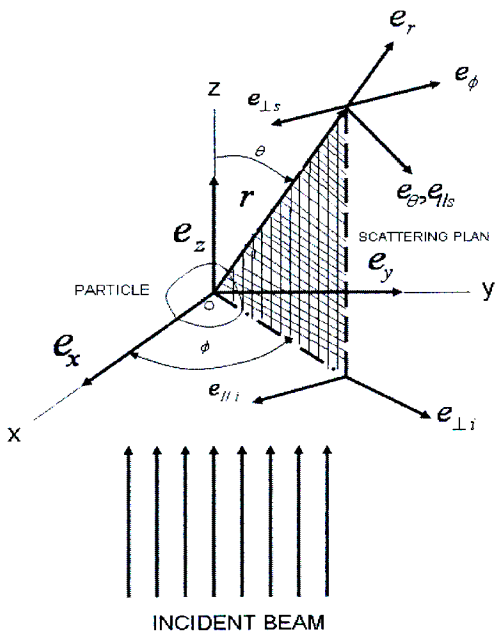

Figure A 2: Coordinate system for a single particle [Bohren, pp62].

where e_r, e_θ, e_ϕ are the orthogonal basis vectors associated with the spherical polar coordinate system (r, θ, ϕ). If the x and y components of the incident field are denoted by E_{xi} and E_{yi}, then

$$E_{//i} = \cos\phi E_{xi} + \sin n\phi E_{yi}, \tag{A.9}$$

$$E_{\perp i} = \sin\phi E_{xi} - \cos\phi E_{yi}. \tag{A.10}$$

In the far-field region, the scattered field E_s is approximately transverse ($e_r \cdot E_s \cong 0$) and thus may be written as:

$$E_s = E_{//s}\, e_{//s} + E_{\perp s}\, e_{\perp s}$$

where $e_{//s} = -e_\theta$, $e_{\perp s} = -e_\phi$ and $e_{\perp s} \times e_{//s} = e_r$ (A.11)

The basis vector $e_{//s}$ is parallel and $e_{\perp s}$ is perpendicular to the scattering plane. Note, nevertheless, that E_s and E_i are specified relative to different sets of basis vectors. If the detailed shape of the angular scattering pattern is required, e.g. to get the phase matrix or phase function for radiative-transfer calculations (e.g. Chandrasekhar, 1960), Mie scattering intensities $|S_1|^2$ and $|S_2|^2$ as a function of $\cos\theta$, (and the result as a polar diagram of θ on the upper part of the curves $(0 < \theta < \pi)$ are for polarization perpendicular to the scattering plane. The lower part of the curves $(\pi < \theta < 2\pi)$ are for polarization parallel to the scattering plane, and both functions are symmetric with respect to two half circles), are required. These functions describe the scattered field E_s. The scattered far field in spherical coordinates $(E_{s\theta}, E_{s\phi})$ for a unit amplitude incident field (where the time variation $\exp(-i\omega t)$ has been omitted) is given by

$$E_{s\theta} = E_0 \frac{e^{ikr}}{-ikr} \cos\phi \cdot S_2(\cos\theta) \tag{A.12}$$

$$E_{s\phi} = -E_0 \frac{e^{ikr}}{-ikr} \sin\phi \cdot S_1(\cos\theta) \tag{A.13}$$

With the scattering amplitudes S_1 and S_2

$$S_1(\cos\theta) = \sum_{n=1}^{\infty} \frac{2n+1}{n(n+1)} (a_n \pi_n + b_n \tau_n) \tag{A.14}$$

$$S_2(\cos\theta) = \sum_{n=1}^{\infty} \frac{2n+1}{n(n+1)} (a_n \tau_n + b_n \pi_n) \tag{A.15}$$

$E_{s\theta}$ is the scattered far-field component in the scattering plane, defined by the incident and scattered directions, and $E_{s\phi}$ is the orthogonal component. The angle ϕ is the angle between the incident electric field and the scattering plane. The functions $\pi_n(\cos\theta)$ and $\tau_n(\cos\theta)$ describe the angular scattering patterns of the spherical harmonics used to describe S_1 and S_2 and follow from the recurrence relations

$$\pi_n = \frac{2n-1}{n-1}\cos\theta\cdot\pi_{n-1} - \frac{n}{n-1}\pi_{n-2};\ \tau_n = n\cos\theta\cdot\pi_n - (n+1)\pi_{n-1} \tag{A.16}$$

starting with (Deirmendjian, 1969)

$$\pi_0 = 0;\ \pi_1 = 1;\ \pi_2 = 3\cos\theta;\ \tau_0 = 0;\ \tau_1 = \cos\theta;\ \tau_2 = 3\cos(2\theta) \tag{A.17}$$

The internal field E_1 for an incident field with unit amplitude is given by

$$E_1 = \sum_{n=1}^{\infty}\frac{2n+1}{n(n+1)}(c_n M_{o1n}^{(1)} - d_n N_{e1n}^{(1)}) \tag{A.18}$$

where the vector-wave harmonic fields are given in spherical (r,θ,ϕ) coordinates by

$$M_{o1n}^{(1)} = \begin{pmatrix} 0 \\ \cos\phi\cdot\pi_n(\cos\theta)j_n(rmx) \\ -\sin\phi\cdot\tau_n(\cos\theta)j_n(rmx) \end{pmatrix} \tag{A.19}$$

$$N_{e1n}^{(1)} = \begin{pmatrix} n(n+1)\cos\phi\cdot\sin\theta\cdot\pi_n(\cos\theta)\dfrac{j_n(rmx)}{rmx} \\ \cos\phi\cdot\tau_n(\cos\theta)\dfrac{[rmxj_n(rmx)]'}{rmx} \\ -\sin\phi\cdot\pi_n(\cos\theta)\dfrac{[rmxj_n(rmx)]'}{rmx} \end{pmatrix} \tag{A.20}$$

where operator j_n is spherical Bessel function of first kind, operator $h_n^{(1)}$ is spherical Hankel function of first kind. (Note that the function $j_n(mx)$ and its derivative cannot be eliminated in (3.20), the size parameter is given by $x = ka$, a is the radius of the sphere and $k = 2\pi/\lambda$ is the wave number, λ. However, as they appear in the denominator only, their divergence just leads to diminishing values of c_n and d_n.

A.2 Rayleigh Approximation Applied to Rain

At frequencies below $6\,GHz$ ($\lambda = 5\,cm$), most rain droplet sizes satisfy the condition $ka \le 0.1$ and therefore the Rayleigh scattering theory is applicable. Even at $10\,GHz$ ($\lambda = 3\,cm$), ka is much smaller than unity, except for heavy rain, and Rayleigh scattering gives a good approximation. In Rayleigh scattering, the total sum of the cross sections of all particles per unit volume, such as $\rho < \sigma_s >, \rho < \sigma_a >, \rho < \sigma_t >$ and $\rho < \sigma_b >$ are given by Akira (1978, pp 46) as:

$$\rho < \sigma_s >= \frac{128}{3}\frac{\pi^5}{\lambda^4}|K|^2 \int_0^\infty a^6 n(a)da \tag{A.21}$$

$$\rho < \sigma_a >= \frac{8\pi^2}{\lambda}\mathrm{Im}(K)\int_0^\infty a^3 n(a)da \tag{A.22}$$

$$\rho < \sigma_t >= \rho < \sigma_s > + \rho < \sigma_a > \tag{A.23}$$

$$\rho < \sigma_b >= \frac{64\pi^5}{\lambda^4}|K|^2 \int_0^\infty a^6 n(a)da \tag{A.24}$$

where t, a, s and b stand for extinction, absorption, scattering and backscattering, respectively, and $K = (\varepsilon_r - 1)/(\varepsilon_r + 2)$. The value of K depends on wavelength and

temperature. In the range of $\lambda = 3$ to $10cm$, $|K|^2$ is almost constant at temperatures between 0° and 20°C and is equal to 0.93. The imaginary part $\mathrm{Im}(K)$ ranges from 0.0074 at 20°C to 0.00688 at 10°C. Since rain attenuation is usually small and unimportant at the longer wavelengths where this expression is valid, the simplicity offered by the Rayleigh scattering approximation is of limited use for predicting the attenuation through rain [(Skolnik, 1962) and Kerr (1951)] suggested that the computation of the rain attenuation must therefore be based on the exact formulation for spheres as developed by Mie.

A.3 Mie Approximation Applied to Rain

When diameter of a rain drop is in the order of millimeter; this is equivalent to the wavelength in microwave frequencies; therefore, the scattering mechanism following the Mie scattering approximation is valid here. Assume the rain droplet is a dielectric sphere; and considering a dielectric sphere illuminated by a plane wave. The efficiencies Q_i for the interaction of radiation with a sphere of radius a are cross sections σ_i normalized to the geometrical particle cross section, $\sigma_g = \pi a^2$, where i stands for extinction $(i = ext)$, absorption $(i = abs)$, scattering $(i = sca)$, and backscattering. Energy conservation requires that [see Mätzler (2002b)]:

$$Q_{ext} = Q_{sca} + Q_{abs},\ or\ \sigma_{ext} = \sigma_{sca} + \sigma_{abs} \tag{A.25}$$

$$Q_{sca} = \frac{2}{x^2}\sum_{n=1}^{\infty}(2n+1)(|a_n|^2 + |b_n|^2) \tag{A.26}$$

$$Q_{ext} = \frac{2}{x^2}\sum_{n=1}^{\infty}(2n+1)\,\mathrm{Re}(a_n + b_n) \tag{A.27}$$

The asymmetry parameter is given by (Bohren and Huffman, 1978):

$$Q_{sca} < \cos\theta >= \frac{4}{x^2}\left[\sum_n \frac{n(n+2)}{n+1}\mathrm{Re}\{a_n a_{n+1}^* + b_n b_{n+1}^*\} + \sum_n \frac{2n+1}{n(n+1)}\mathrm{Re}\{a_n b_n^*\}\right] \quad \text{(A.28)}$$

And, the backscattering efficiency, applicable to monostatic radar, is given by [Bohren and Huffman, 1978]:

$$Q_b = \frac{1}{x^2}\left|\sum_{n=1}^{\infty}(2n+1)(-1)^n (a_n - b_n)\right|^2 \quad \text{(A.29)}$$

A. 4 Comparison with Rayleigh Theory [Mätzler, (2002a)]

At two different frequencies, Mätzler came up with the observation that Rayleigh theory underestimates absorption at $f = 5\,GHz$ at $D = 2\,mm$ $(x = 0.1)$ by a factor of 1/2, and computations with an accuracy of 10 % only reach to $D = 0.7\,mm$. For accurate modeling of microwave transmission signals, absorption should be known to the 1 % level. Thus Mie Theory is needed in microwave radiometry of rain at higher than $5\,GHz$.

The Rayleigh approximation is applicable up to $D = 6\,mm$ for scattering and backscattering. Since radar data are usually needed with an accuracy of about $1\,dB$ (26%), the Rayleigh approximation is enough for radar observations at $5\,GHz$. Note the little fluctuation behavior of the Mie backscattering efficiency around the Rayleigh curve in Figure A.3.

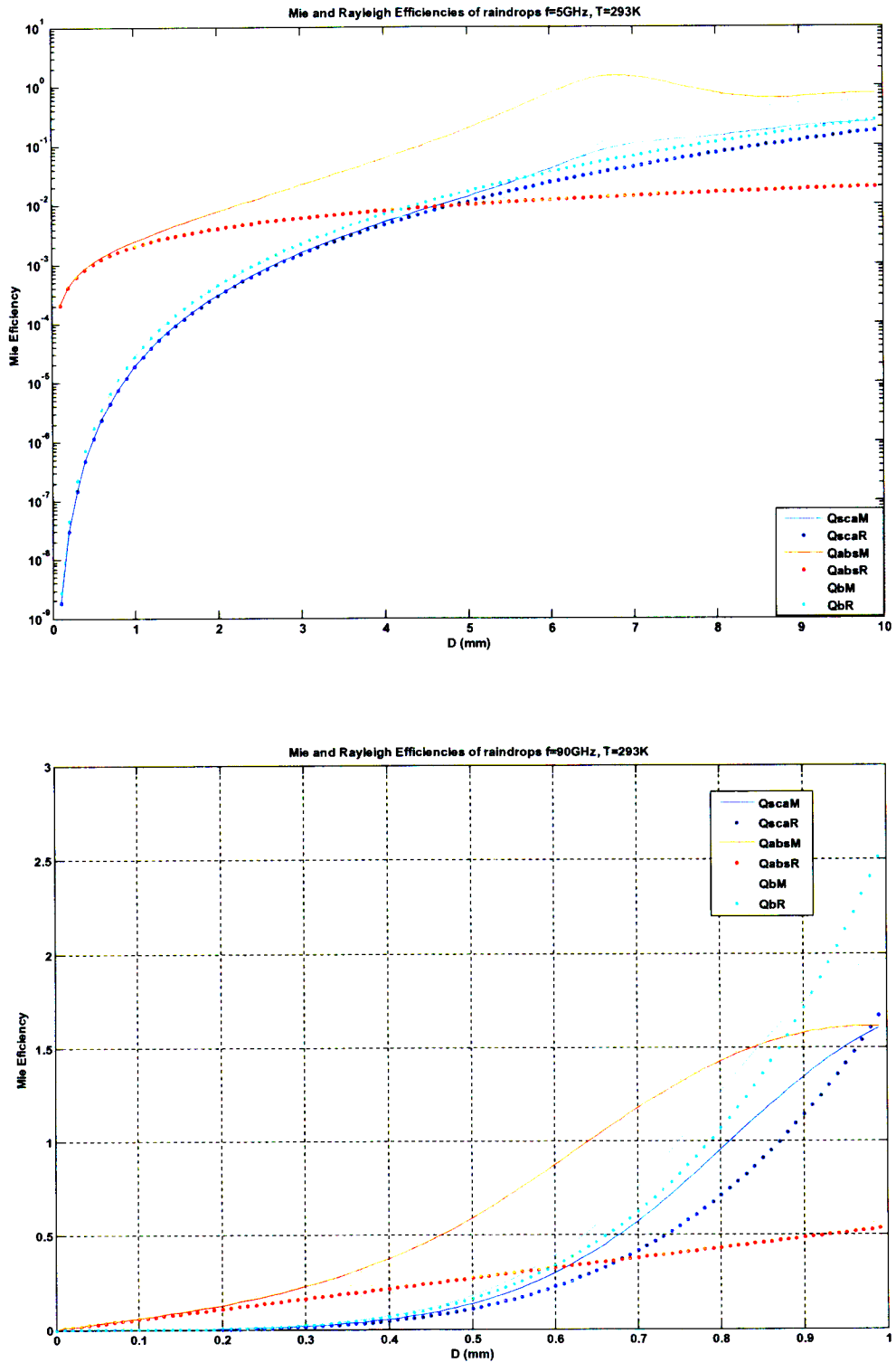

Figure A 3: Mie efficiencies of rain drops versus drop diameter in Mie (M) and Rayleigh (R) Theory at T=293^0 K, f=6 (Top) and 90 GHz (Bottom), respectively.

Similar results are found at $90\,GHz$ (bottom graph of Figure 10). The underestimate of absorption of the Rayleigh curve by a factor of 1/2 is reached at $D = 0.5\,mm$ $(x = 0.5)$, i.e. at a 4 times lower value of D than at $5\,GHz$, while the frequency is higher by a factor of 19. This behavior is due to the relaxation spectrum of water.

A.5 Size-Distribution Effects in Mie Computations

The index n in equations 3.25 to 3.29 runs from 1 *to* ∞, but the infinite series occurring in Mie formulas can be truncated at a maximum, $n_{\max}$. For this number, Bohren and Huffman (1983, p.477) have proposed:

$$n_{\max} = x + 4x^{1/3} + 2 \tag{A.30}$$

and this value is used here as well. The size parameter is given by $x = ka$, a is the radius of the sphere and $k = 2\pi/\lambda$ is the wave number, λ the wavelength in the ambient medium, $m = (\varepsilon_1\mu_1)^{1/2}/(\varepsilon\mu)^{1/2}$ is the refractive index with respect to the ambient medium, ε_1 and μ_1 are the permittivity and permeability of the sphere and ε and μ are the permittivity and permeability of the ambient medium.

Note that, in case of nonspherical raindrop, T-Matrix method [Mishchenko (2002)] is better to use for estimation of coefficients than Mie scattering approximation.

Appendix B

Supplementary Graphs

B.1 Attenuation due to Rain and Fog

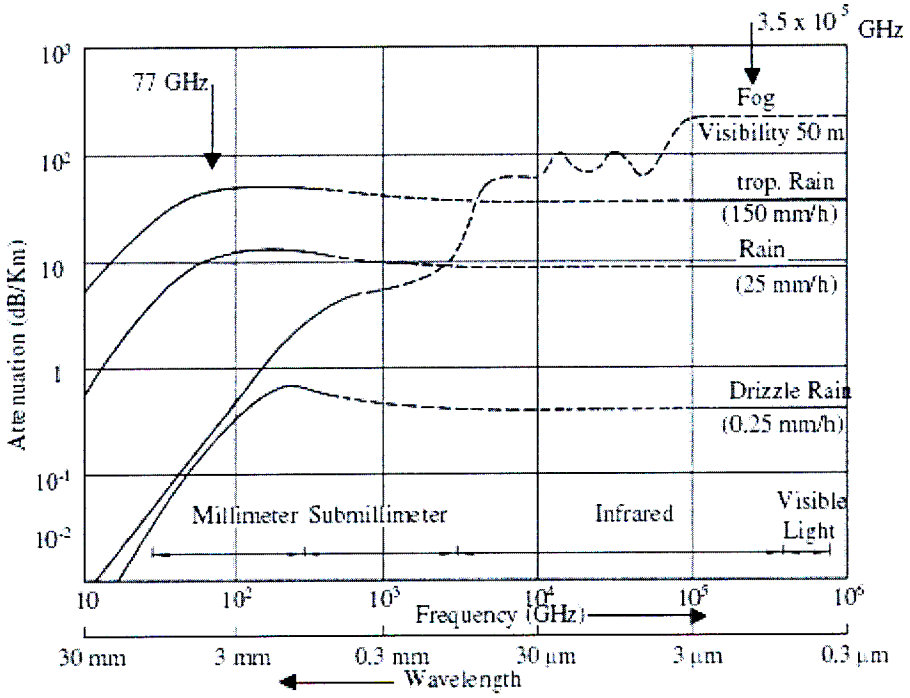

Figure B 1: Attenuation of Radiowave through rain and fog, Source: [Detlefsen, (1989)].

B.2 Attenuation due to Variation of Rain Temperature in Botswana

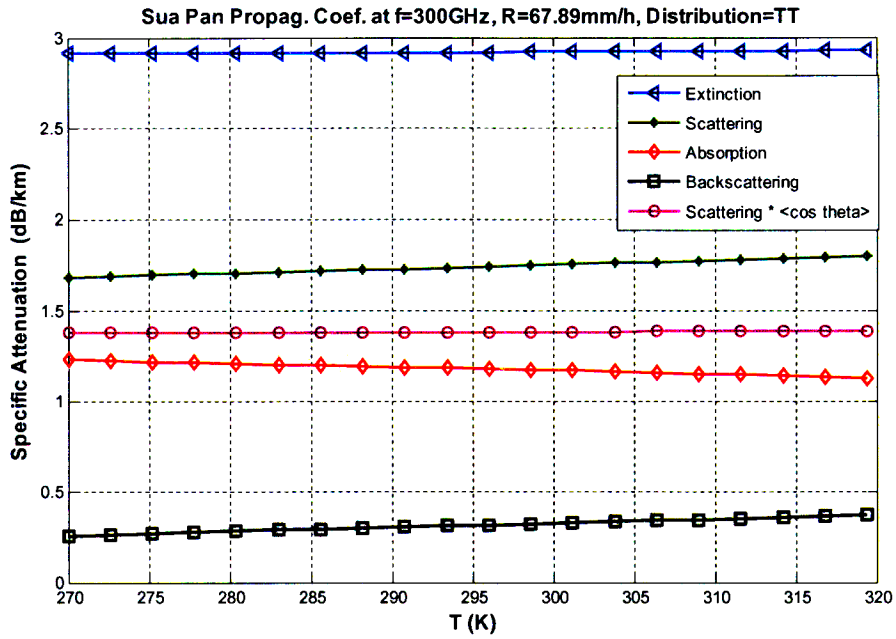

(a)

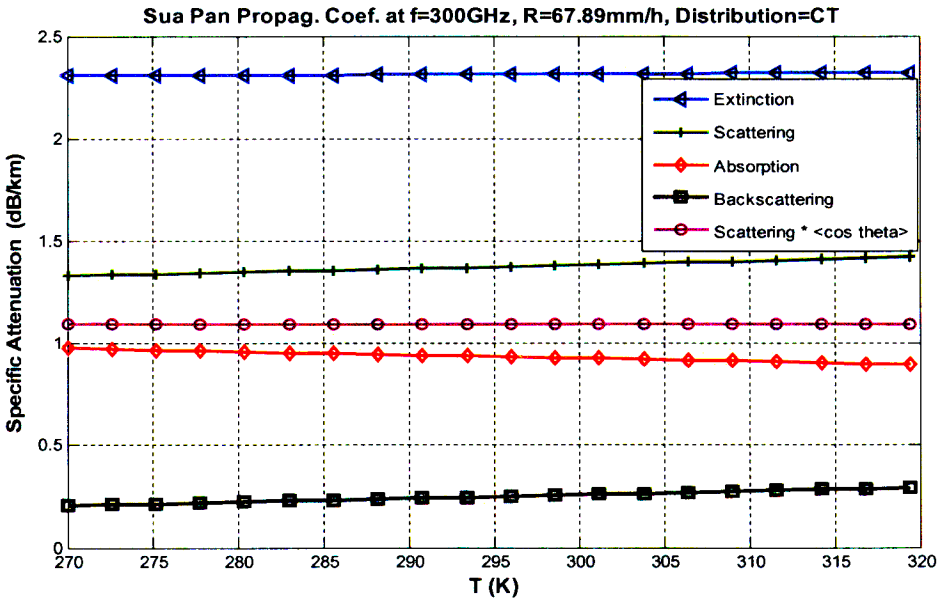

(b)

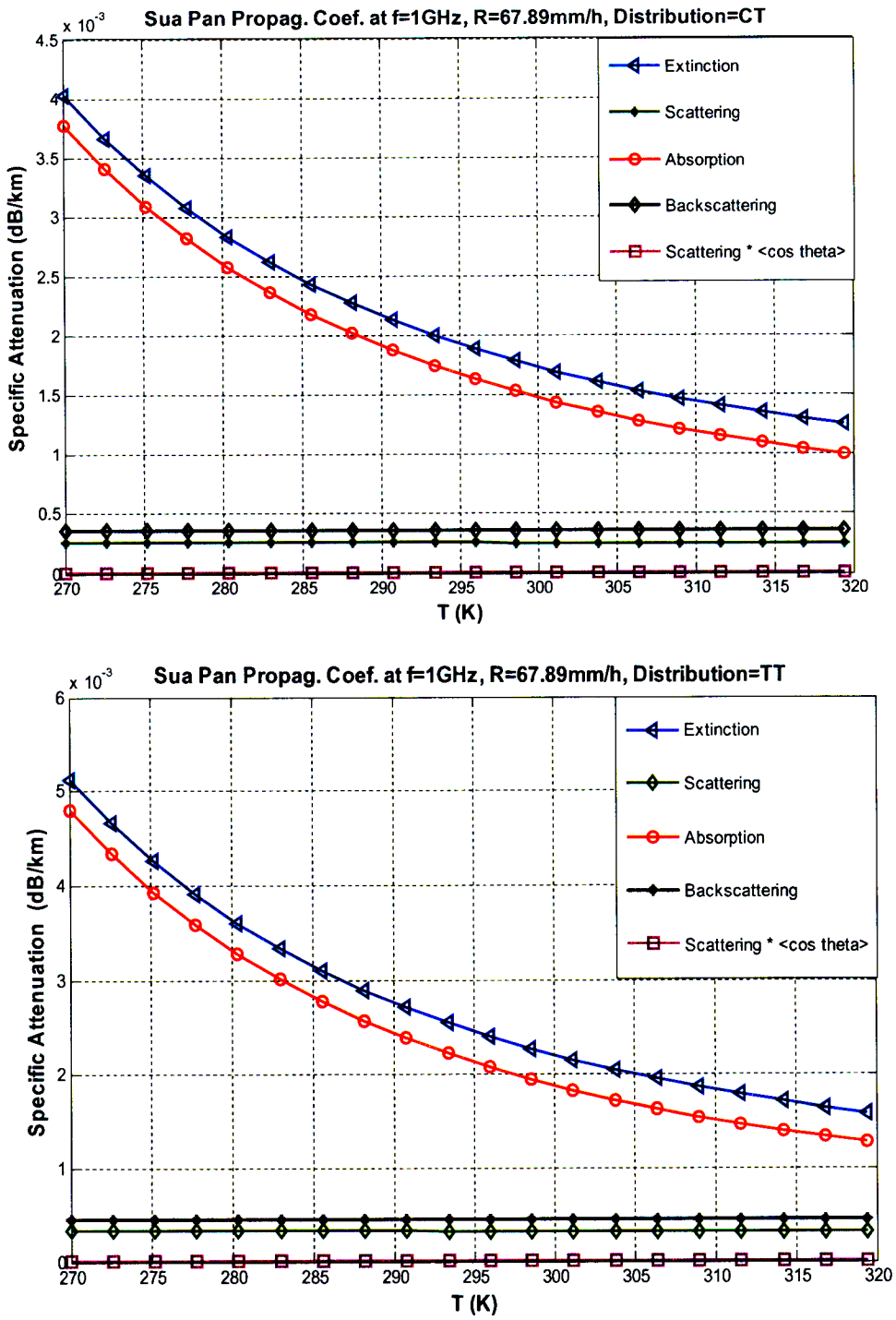

Figure B 2 a, b, c, d: Attenuation coefficient due to rain versus Temperature for Gaborone using CT and TT lognormal distributions.

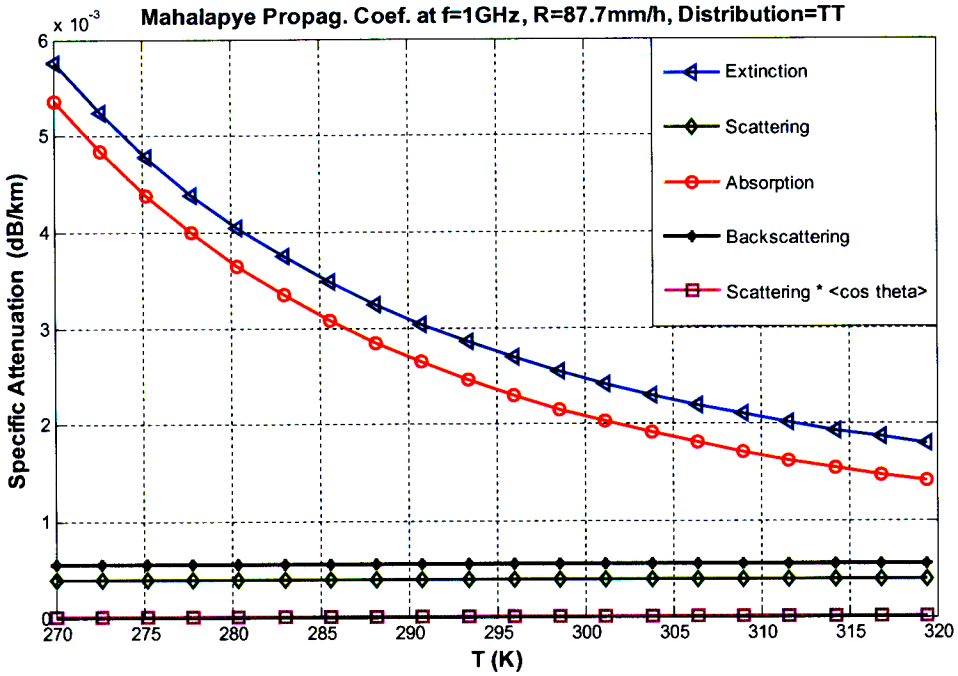
Mahalapye Propag. Coef. at f=1GHz, R=87.7mm/h, Distribution=TT
x 10^-3
Specific Attenuation (dB/km)
T (K)
Extinction
Scattering
Absorption
Backscattering
Scattering * <cos theta>
0
1
2
3
4
5
6
270
275
280
285
290
295
300
305
310
315
320

(e)

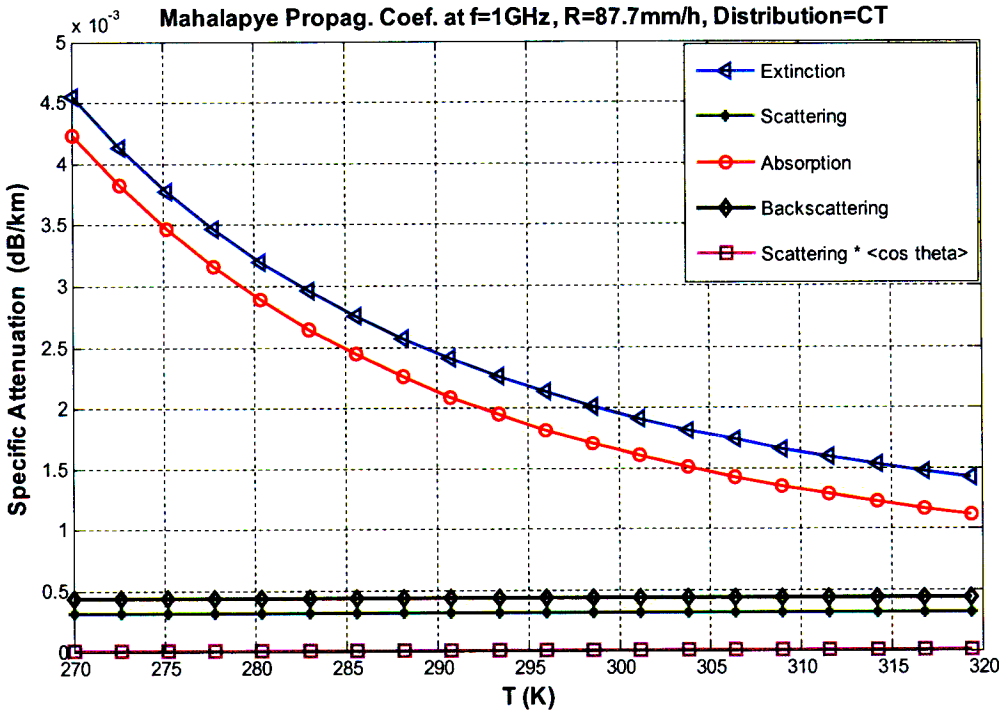
Mahalapye Propag. Coef. at f=1GHz, R=87.7mm/h, Distribution=CT
x 10^-3
Specific Attenuation (dB/km)
T (K)
Extinction
Scattering
Absorption
Backscattering
Scattering * <cos theta>
0
0.5
1
1.5
2
2.5
3
3.5
4
4.5
5
270
275
280
285
290
295
300
305
310
315
320

(f)

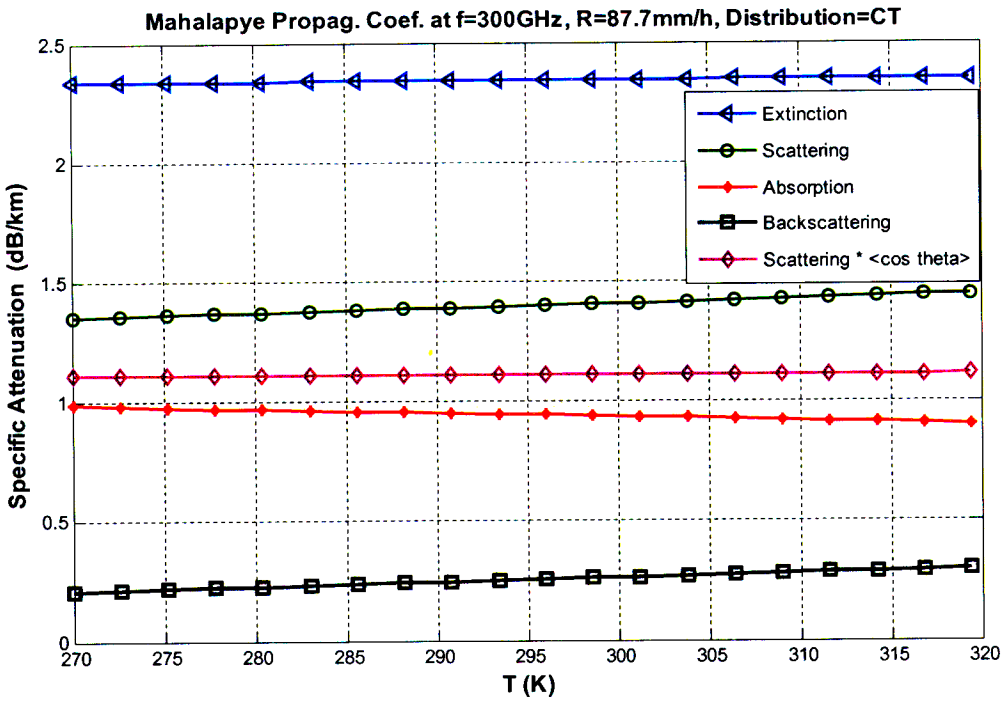

(g)

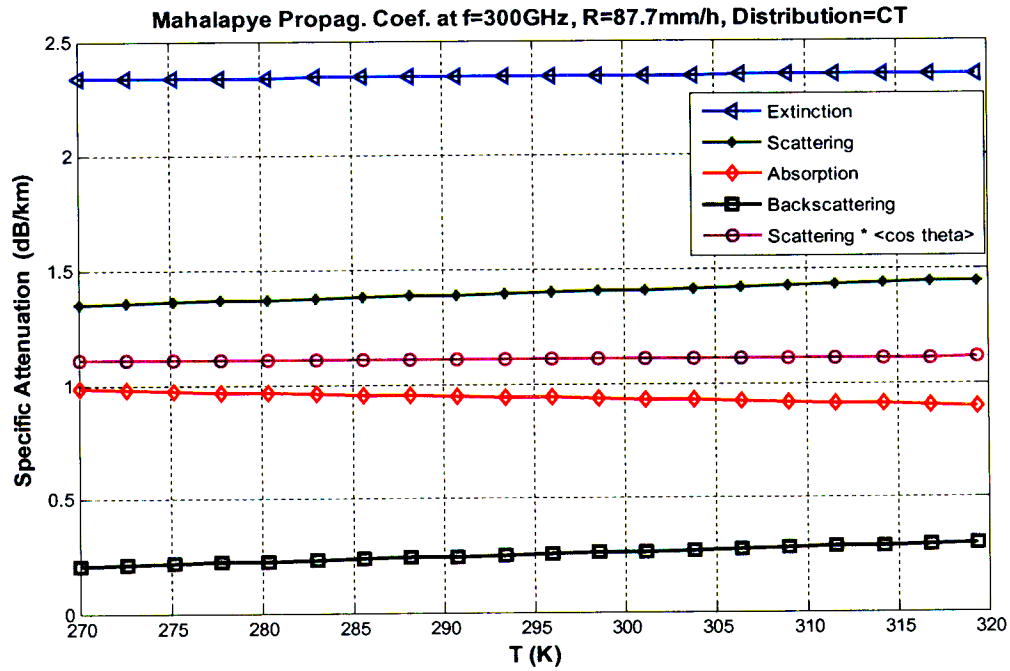

(h)

Figure B 3 e, f, g, h: Attenuation coefficient due to rain versus Temperature for Mahalapye using CT and TT lognormal distributions.

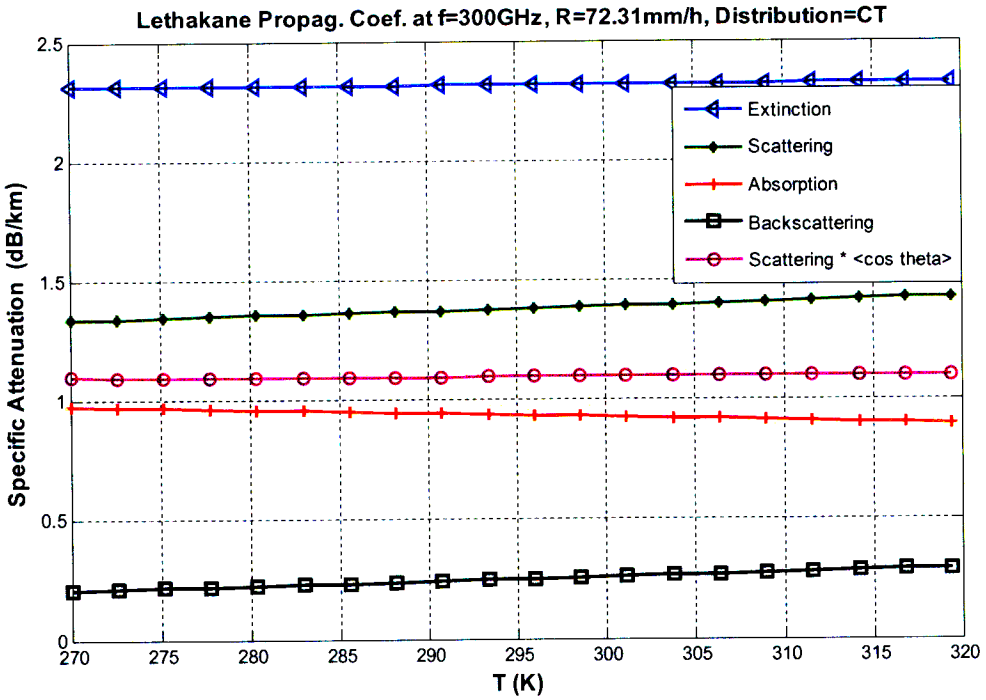
Lethakane Propag. Coef. at f=300GHz, R=72.31mm/h, Distribution=CT
Specific Attenuation (dB/km)
T (K)
Extinction
Scattering
Absorption
Backscattering
Scattering * <cos theta>
0
0.5
1
1.5
2
2.5
270
275
280
285
290
295
300
305
310
315
320

(i)

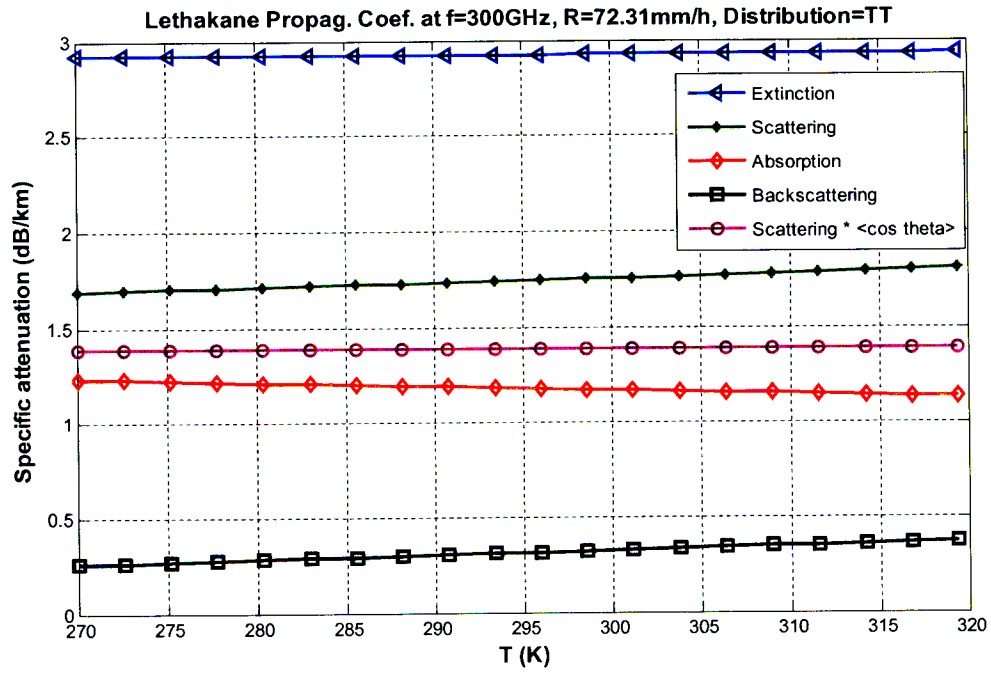
Lethakane Propag. Coef. at f=300GHz, R=72.31mm/h, Distribution=TT
Specific attenuation (dB/km)
T (K)
Extinction
Scattering
Absorption
Backscattering
Scattering * <cos theta>
0
0.5
1
1.5
2
2.5
3
270
275
280
285
290
295
300
305
310
315
320

(j)

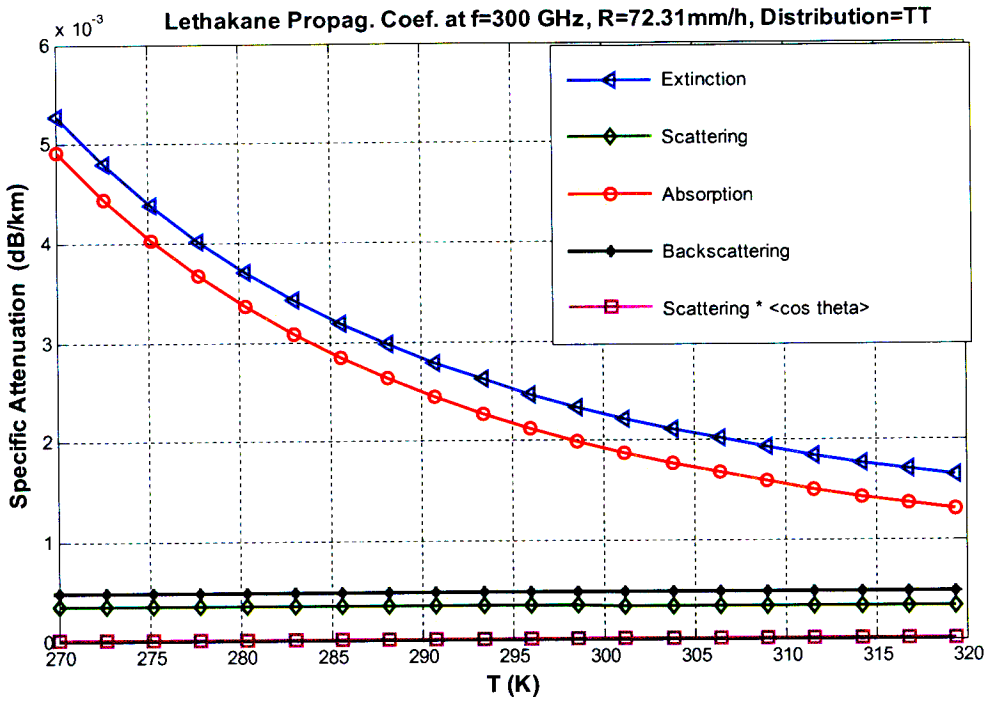

(k)

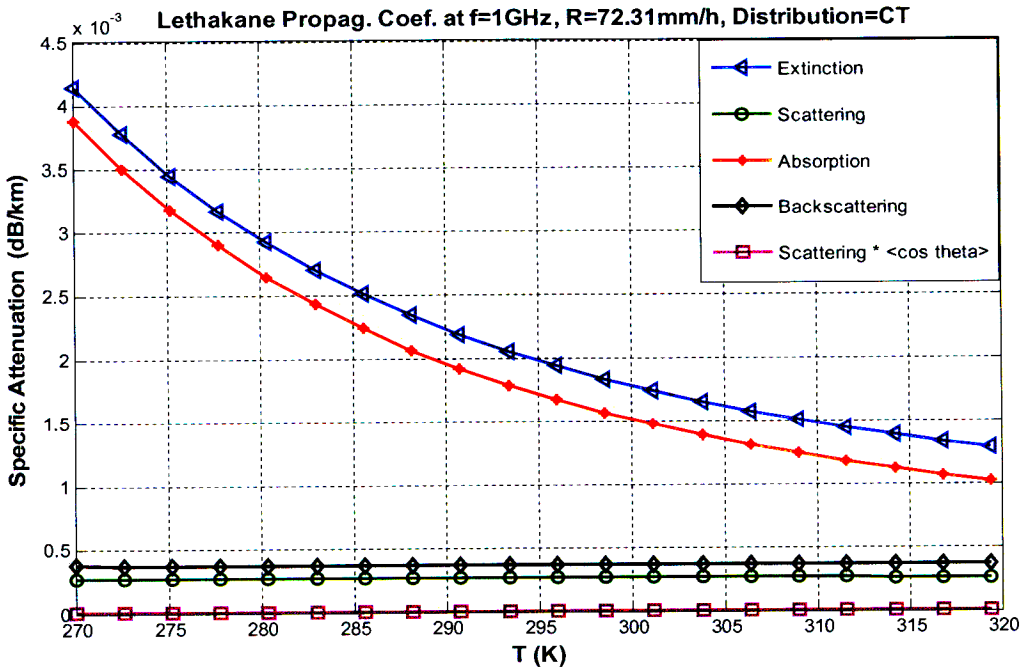

(l)

Figure B 4 i, j, k, l: Attenuation coefficient due to rain versus Temperature for Lethlakane using CT and TT lognormal distributions.

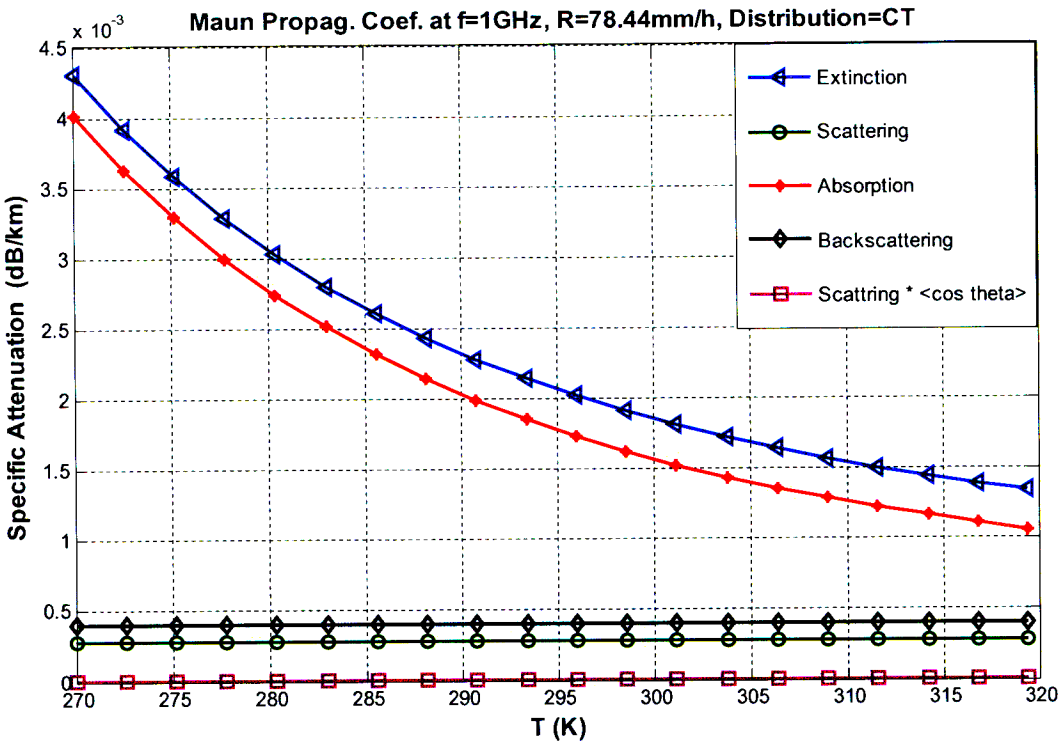
Maun Propag. Coef. at f=1GHz, R=78.44mm/h, Distribution=CT
x 10^-3
Specific Attenuation (dB/km)
T (K)
Extinction
Scattering
Absorption
Backscattering
Scattring * <cos theta>
4.5
4
3.5
3
2.5
2
1.5
1
0.5
0
270
275
280
285
290
295
300
305
310
315
320

(m)

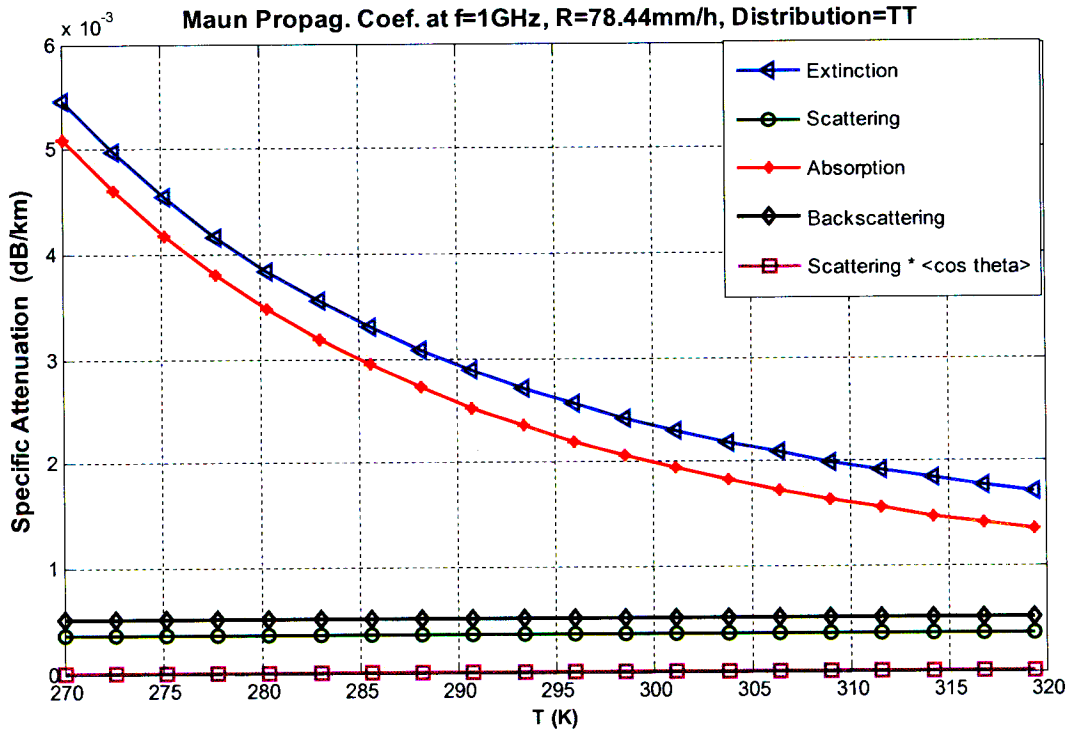
Maun Propag. Coef. at f=1GHz, R=78.44mm/h, Distribution=TT
x 10^-3
Specific Attenuation (dB/km)
T (K)
Extinction
Scattering
Absorption
Backscattering
Scattering * <cos theta>
6
5
4
3
2
1
0
270
275
280
285
290
295
300
305
310
315
320

(n)

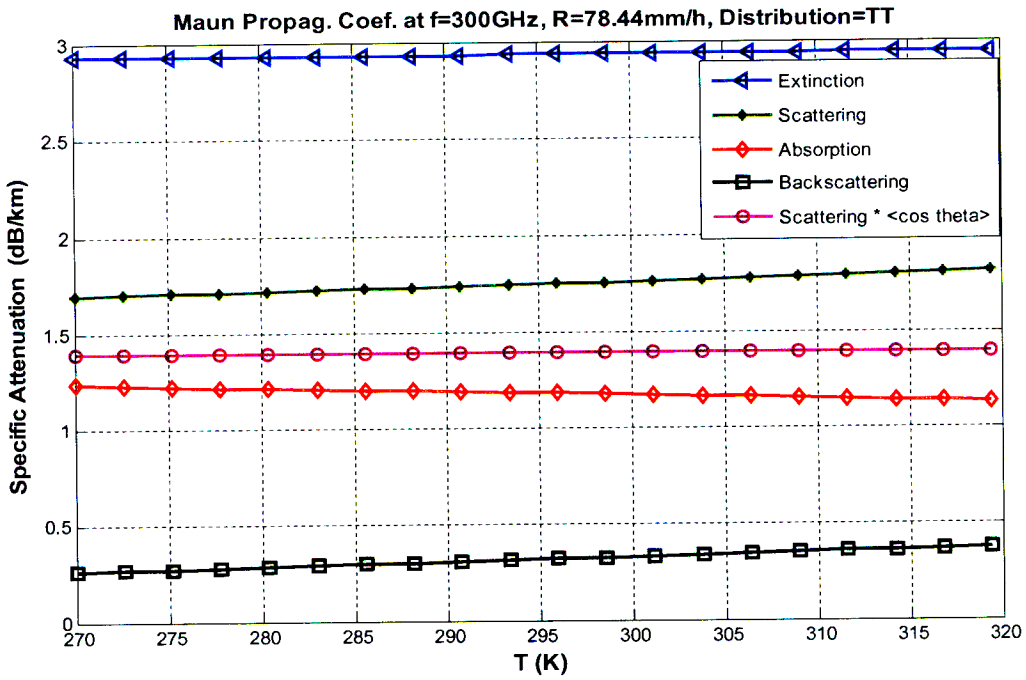

(o)

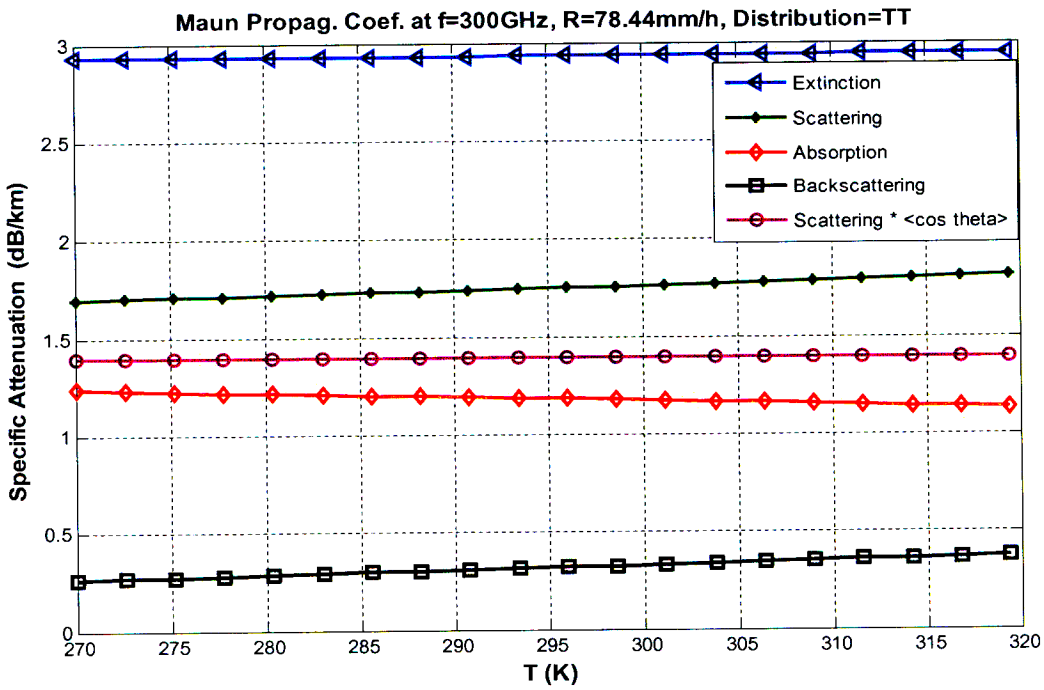

(p)

Figure B 5 m, n, o, p: Attenuation coefficient due to rain versus Temperature for Maun using CT and TT lognormal distributions.

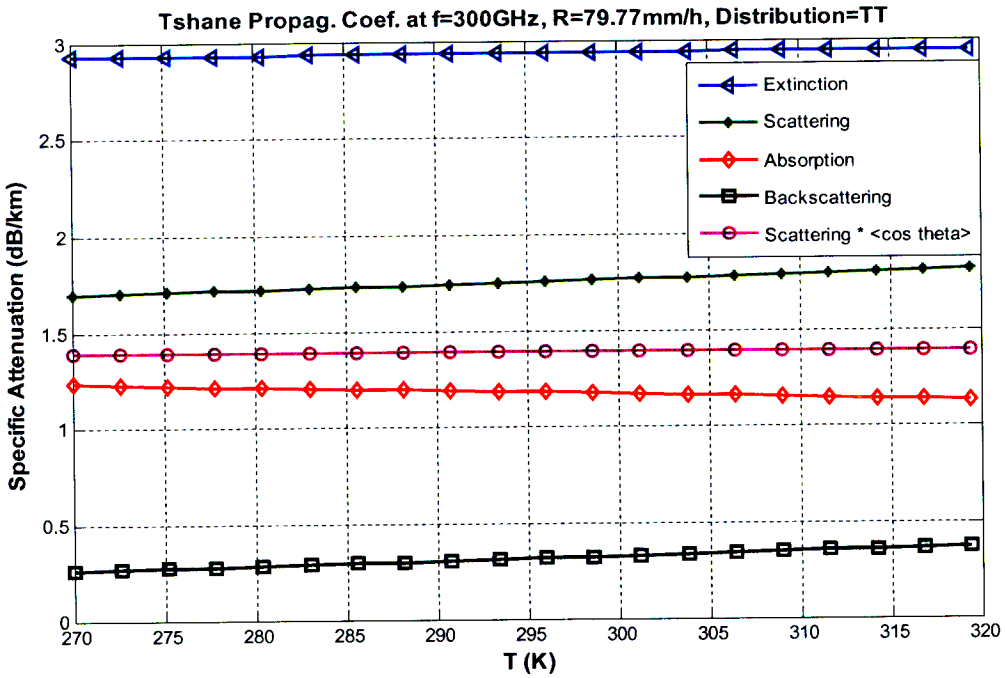
Tshane Propag. Coef. at f=300GHz, R=79.77mm/h, Distribution=TT
Specific Attenuation (dB/km)
T (K)
Extinction
Scattering
Absorption
Backscattering
Scattering * <cos theta>
0
0.5
1
1.5
2
2.5
3
270
275
280
285
290
295
300
305
310
315
320

(q)

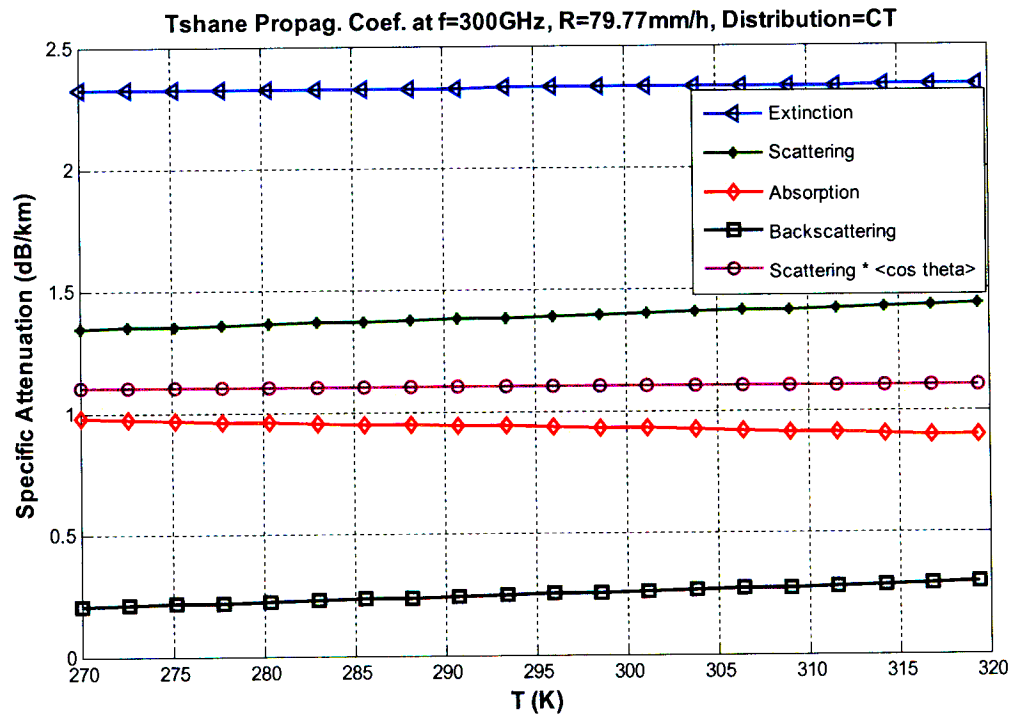
Tshane Propag. Coef. at f=300GHz, R=79.77mm/h, Distribution=CT
Specific Attenuation (dB/km)
T (K)
Extinction
Scattering
Absorption
Backscattering
Scattering * <cos theta>
0
0.5
1
1.5
2
2.5
270
275
280
285
290
295
300
305
310
315
320

(r)

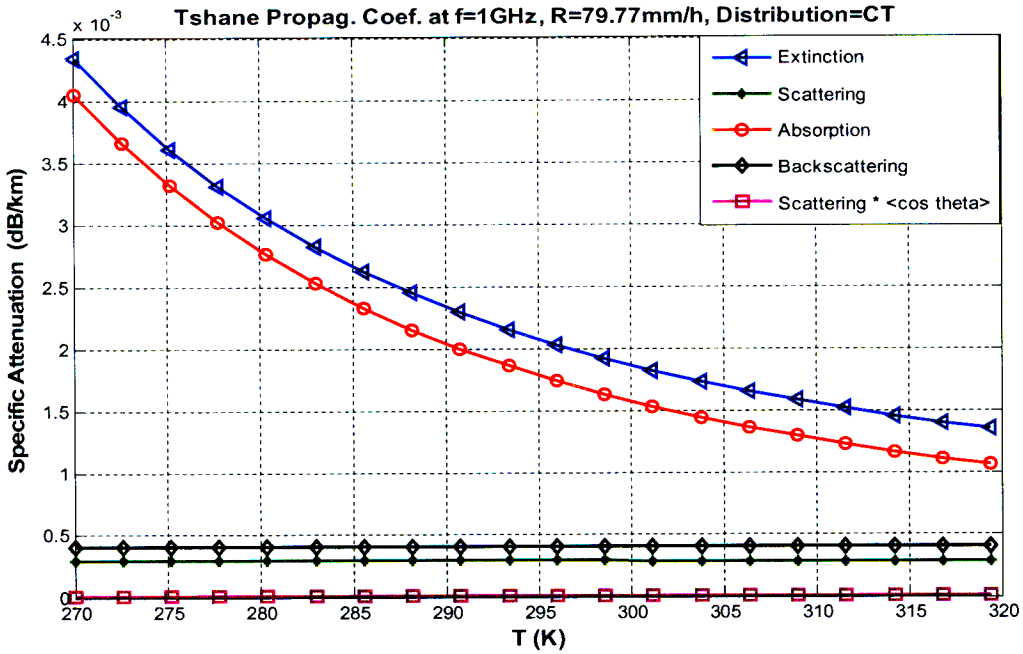

(s)

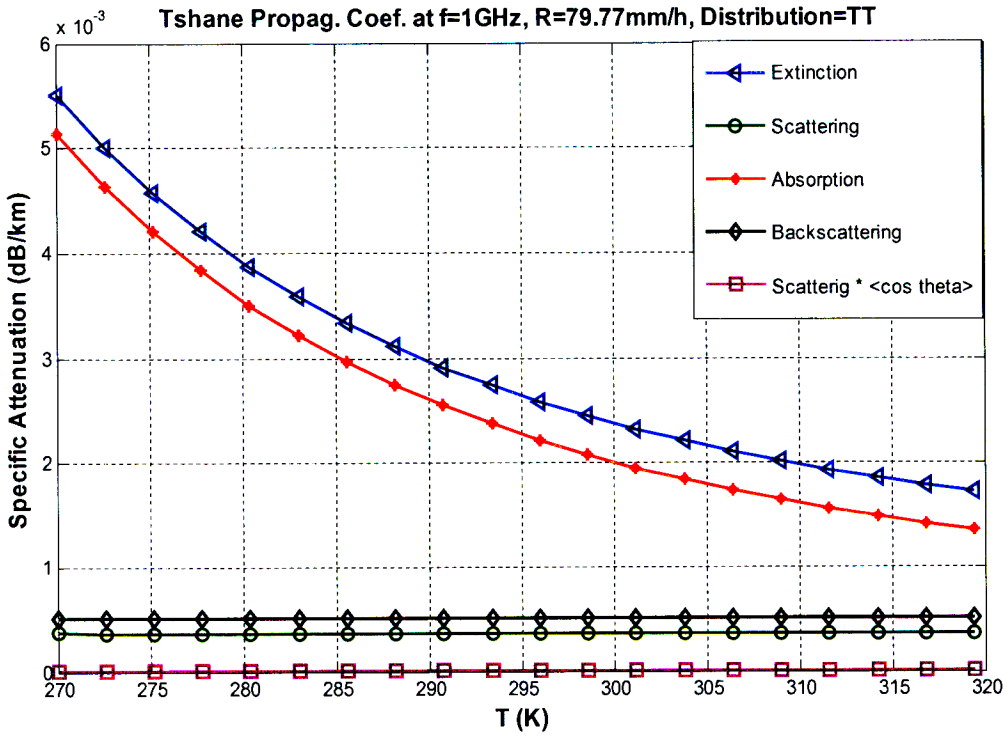

(t)

Figure B 6 q, r, s, t: Attenuation coefficient due to rain versus Temperature for Tshane using CT and TT lognormal distributions.

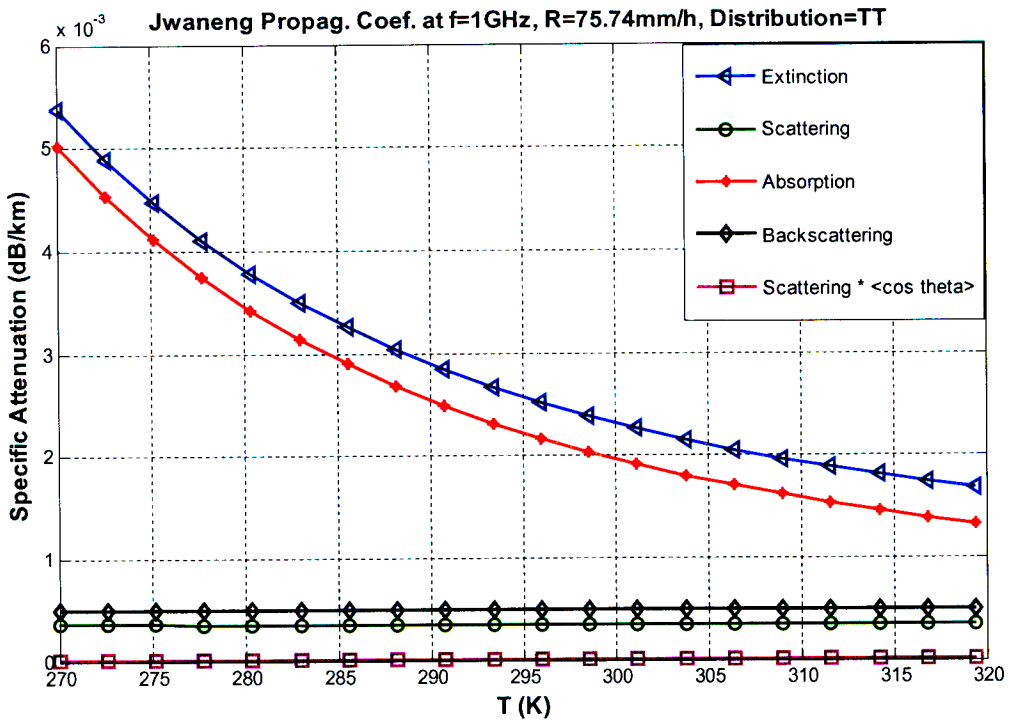
Jwaneng Propag. Coef. at f=1GHz, R=75.74mm/h, Distribution=TT
x 10^-3
Specific Attenuation (dB/km)
T (K)
Extinction
Scattering
Absorption
Backscattering
Scattering * <cos theta>
0
1
2
3
4
5
6
270
275
280
285
290
295
300
305
310
315
320

(u)

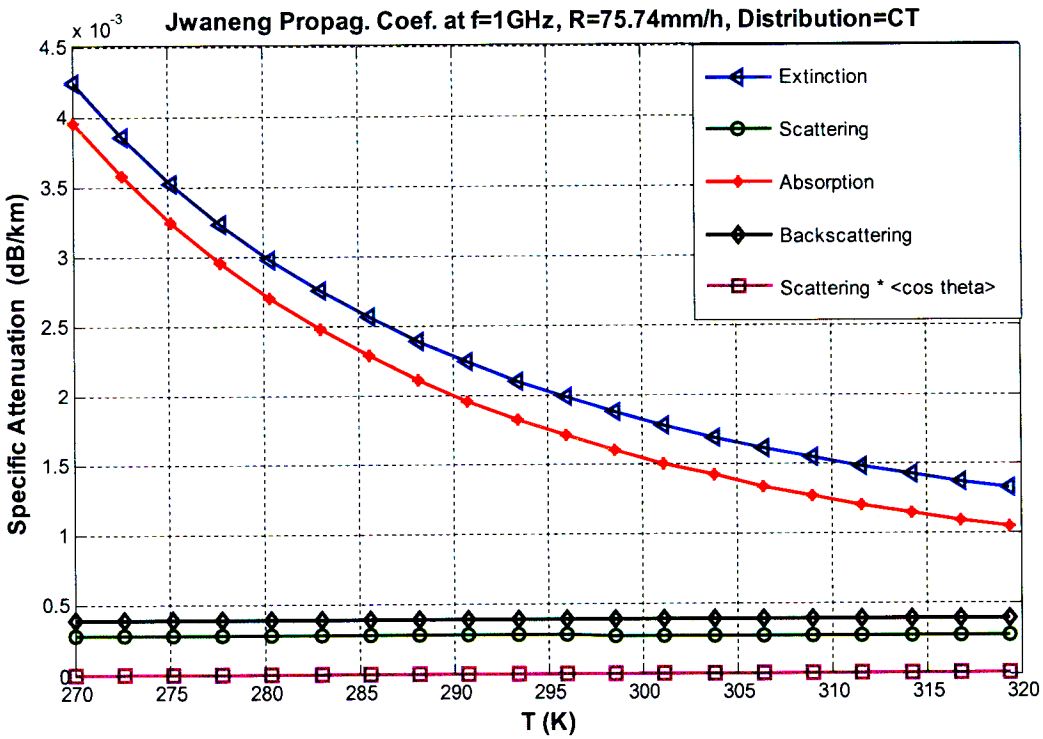
Jwaneng Propag. Coef. at f=1GHz, R=75.74mm/h, Distribution=CT
x 10^-3
Specific Attenuation (dB/km)
T (K)
Extinction
Scattering
Absorption
Backscattering
Scattering * <cos theta>
0
0.5
1
1.5
2
2.5
3
3.5
4
4.5
270
275
280
285
290
295
300
305
310
315
320

(v)

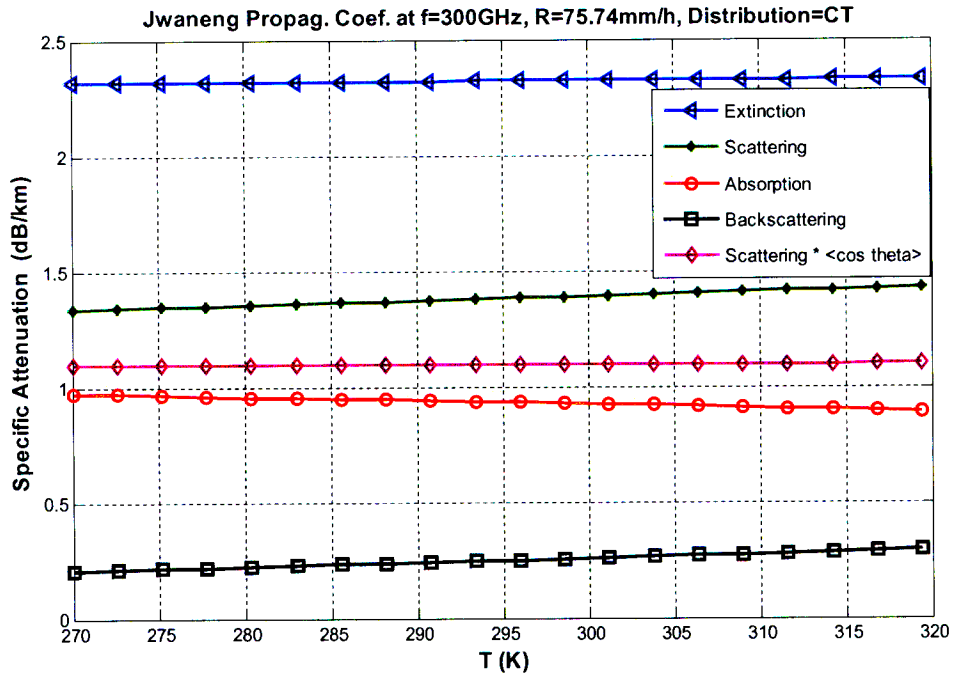

(w)

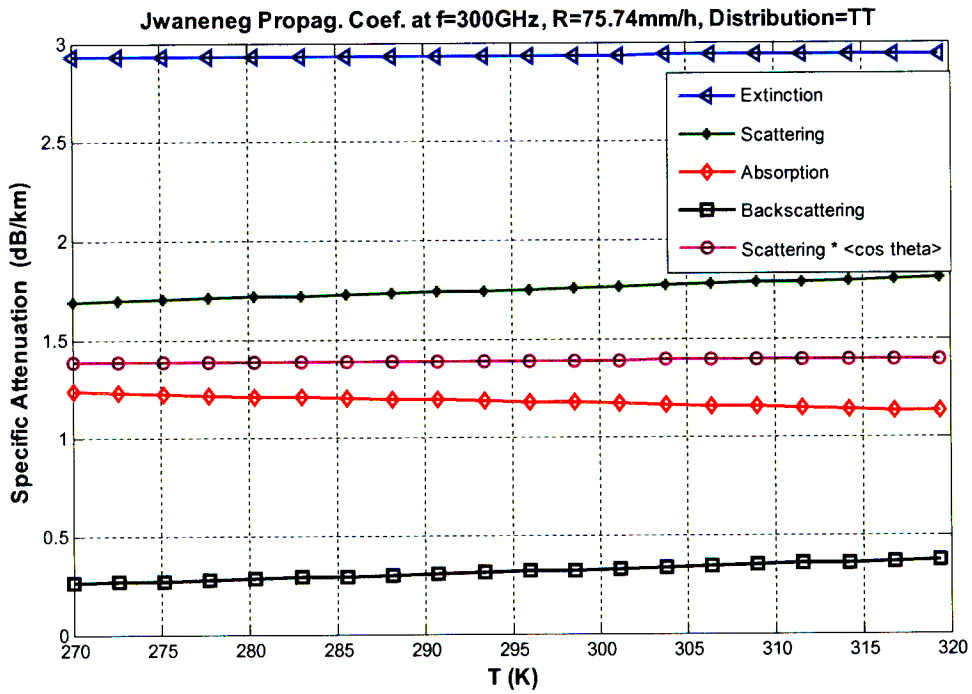

(y)

Figure B 7 u, v, w, y: Attenuation coefficient due to rain versus Temperature for Jwaneng using CT and TT lognormal distributions.

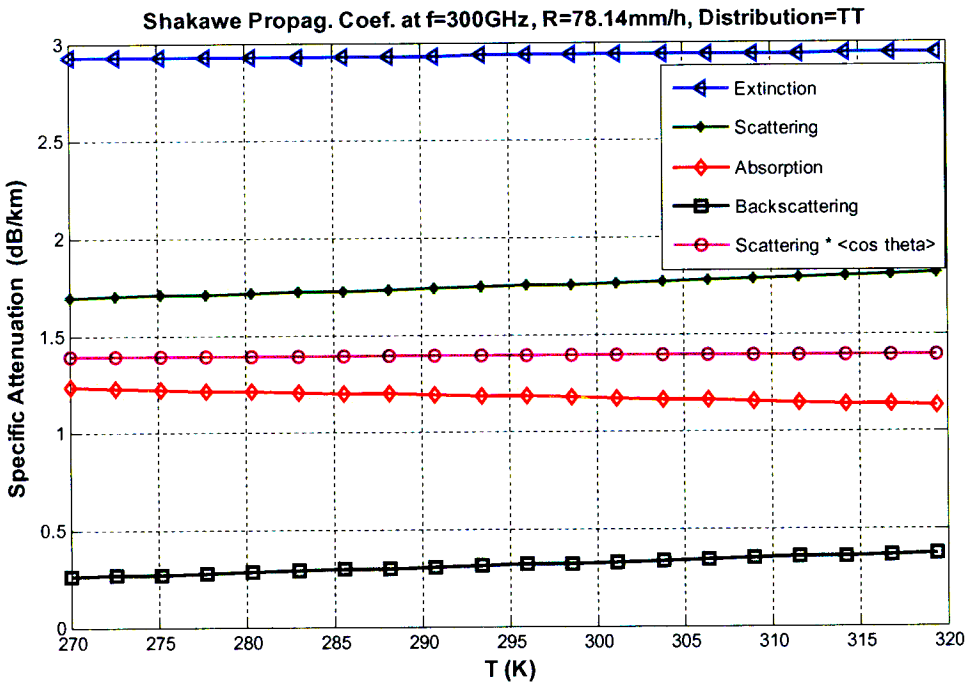
Shakawe Propag. Coef. at f=300GHz, R=78.14mm/h, Distribution=TT
Specific Attenuation (dB/km)
T (K)
Extinction
Scattering
Absorption
Backscattering
Scattering * <cos theta>
0
0.5
1
1.5
2
2.5
3
270
275
280
285
290
295
300
305
310
315
320

(z)

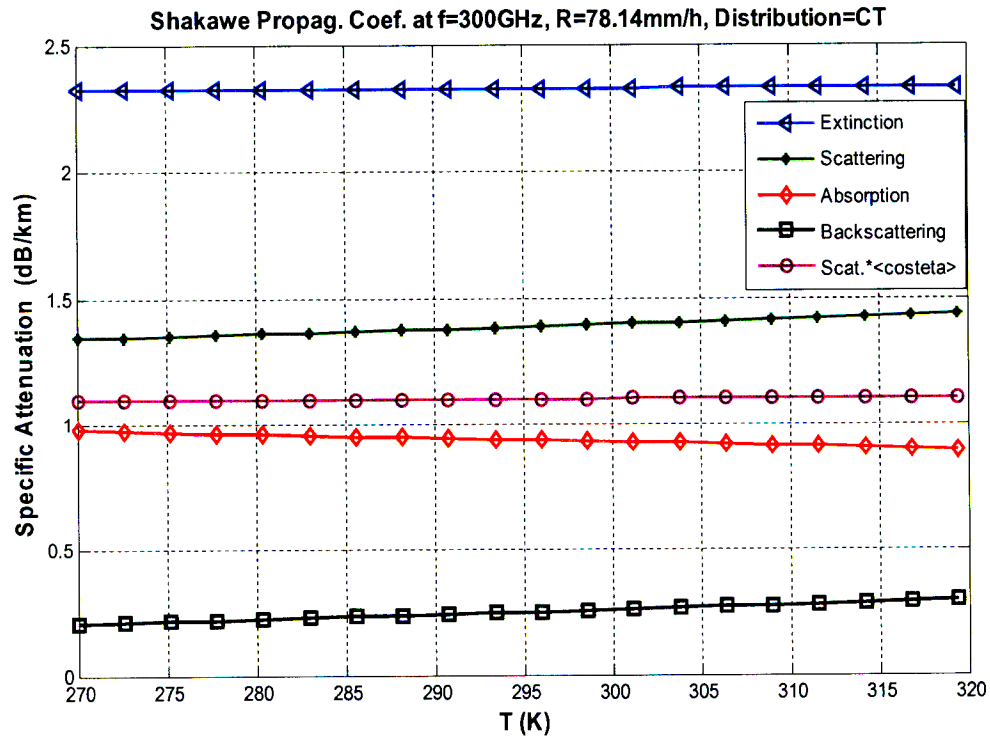
Shakawe Propag. Coef. at f=300GHz, R=78.14mm/h, Distribution=CT
Specific Attenuation (dB/km)
T (K)
Extinction
Scattering
Absorption
Backscattering
Scat.*<costeta>
0
0.5
1
1.5
2
2.5
270
275
280
285
290
295
300
305
310
315
320

(aa)

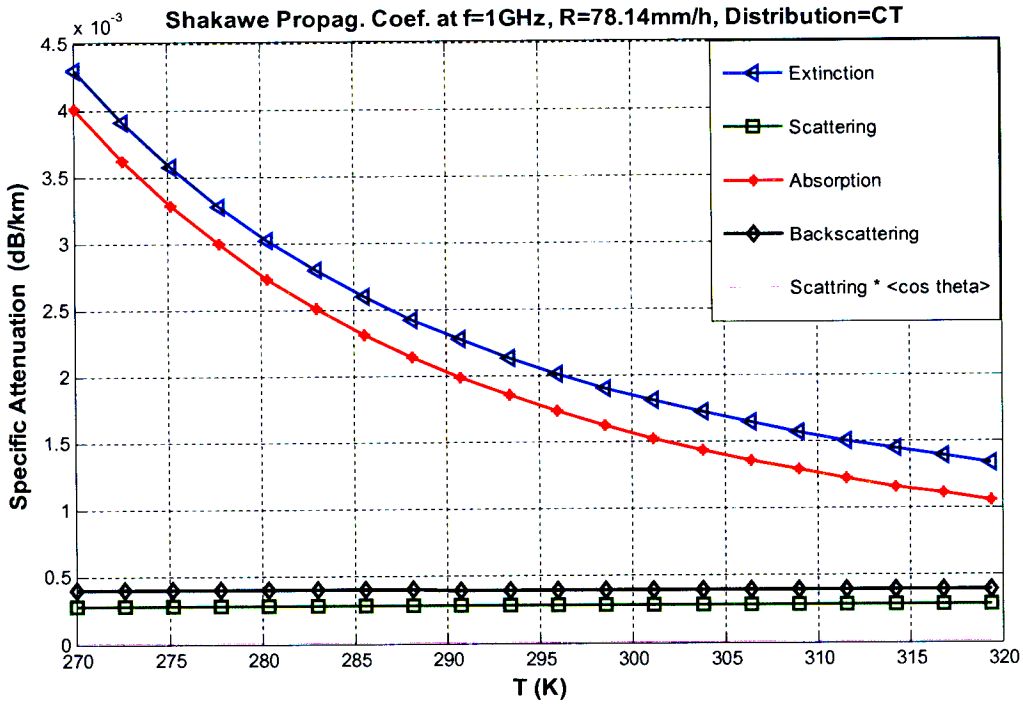

(bb)

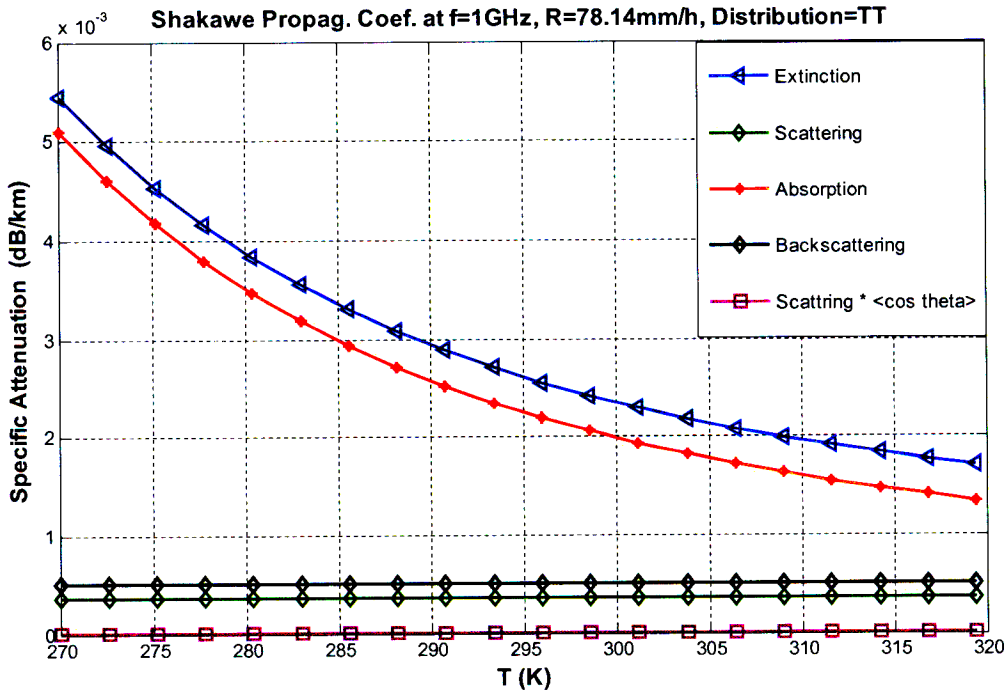

(cc)

Figure B 8 z, aa, bb, cc: Attenuation coefficient due to rain versus Temperature for Shakawe using CT and TT lognormal distributions.

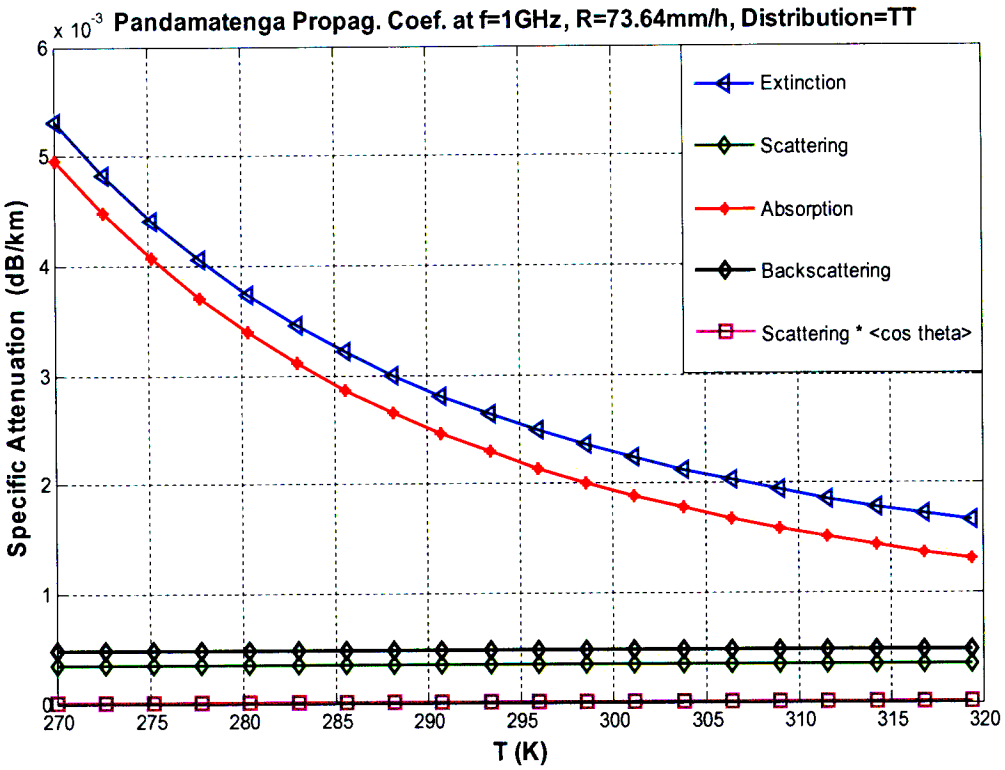
x 10^-3 Pandamatenga Propag. Coef. at f=1GHz, R=73.64mm/h, Distribution=TT
Specific Attenuation (dB/km)
T (K)
Extinction
Scattering
Absorption
Backscattering
Scattering * <cos theta>

(dd)

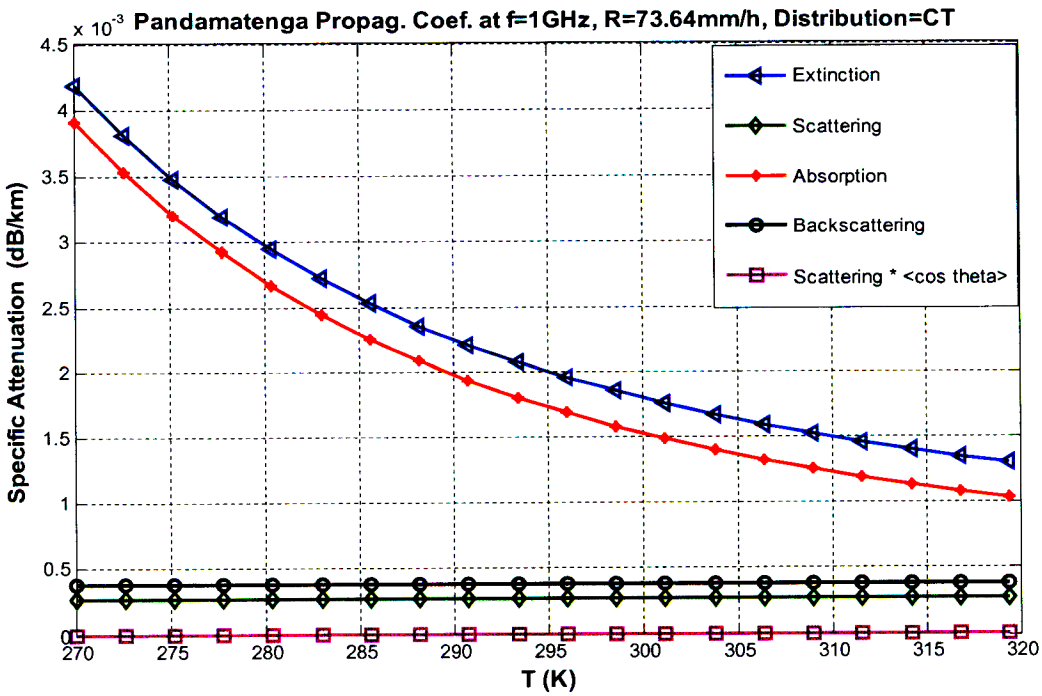
x 10^-3 Pandamatenga Propag. Coef. at f=1GHz, R=73.64mm/h, Distribution=CT
Specific Attenuation (dB/km)
T (K)
Extinction
Scattering
Absorption
Backscattering
Scattering * <cos theta>

(ee)

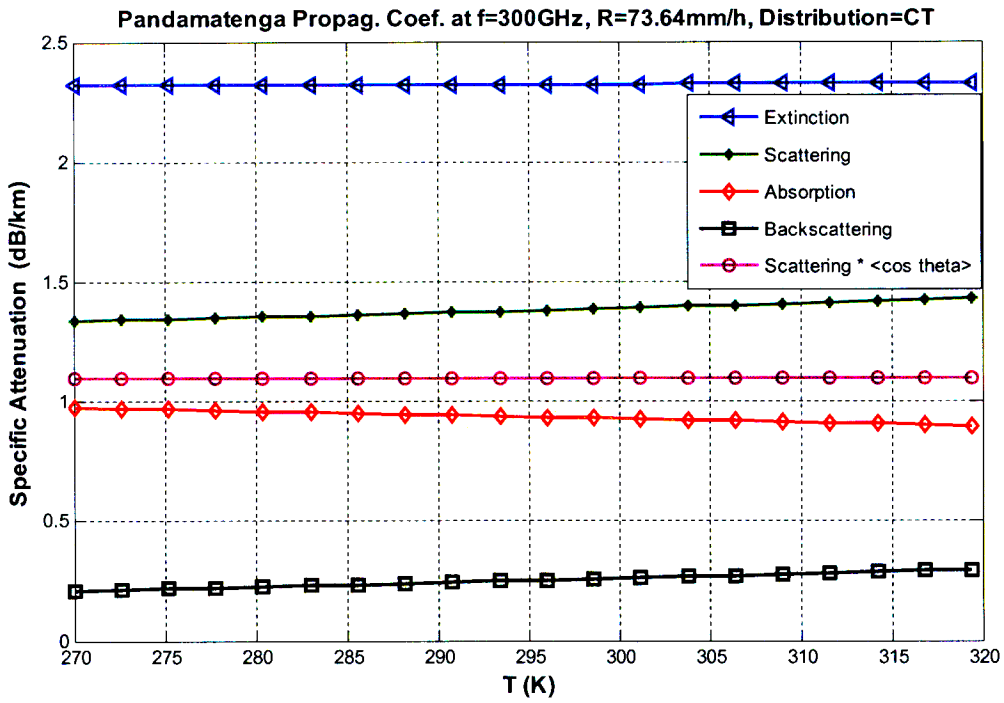

(ff)

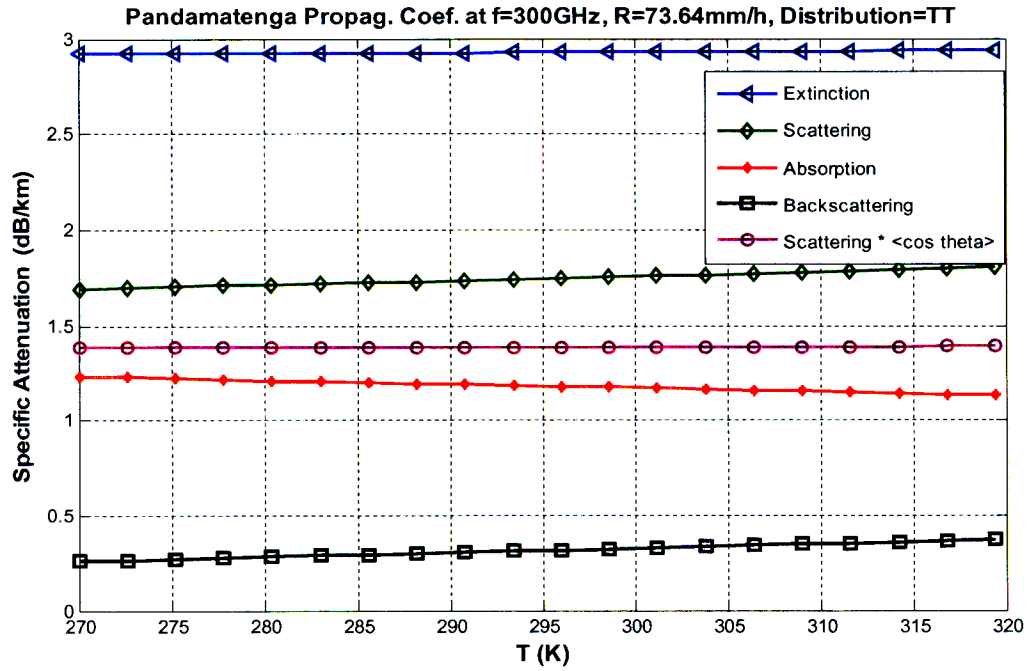

(gg)

Figure B 9 dd, ee, ff, gg: Attenuation coefficient due to rain versus Temperature for Pandamatenga using CT and TT lognormal distributions.

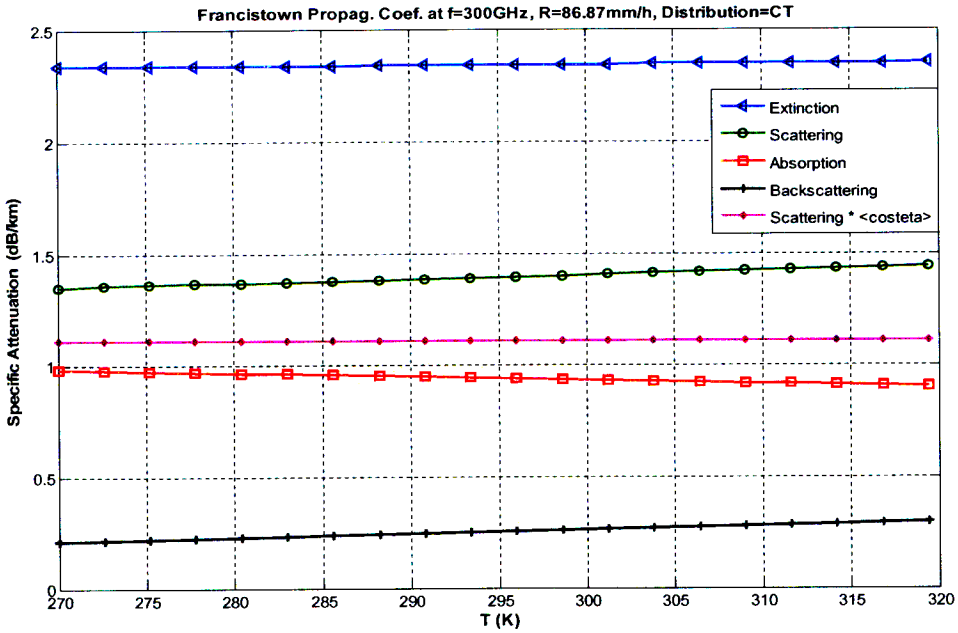
Francistown Propag. Coef. at f=300GHz, R=86.87mm/h, Distribution=CT
Specific Attenuation (dB/km)
T (K)
Extinction
Scattering
Absorption
Backscattering
Scattering * <costeta>

(hh)

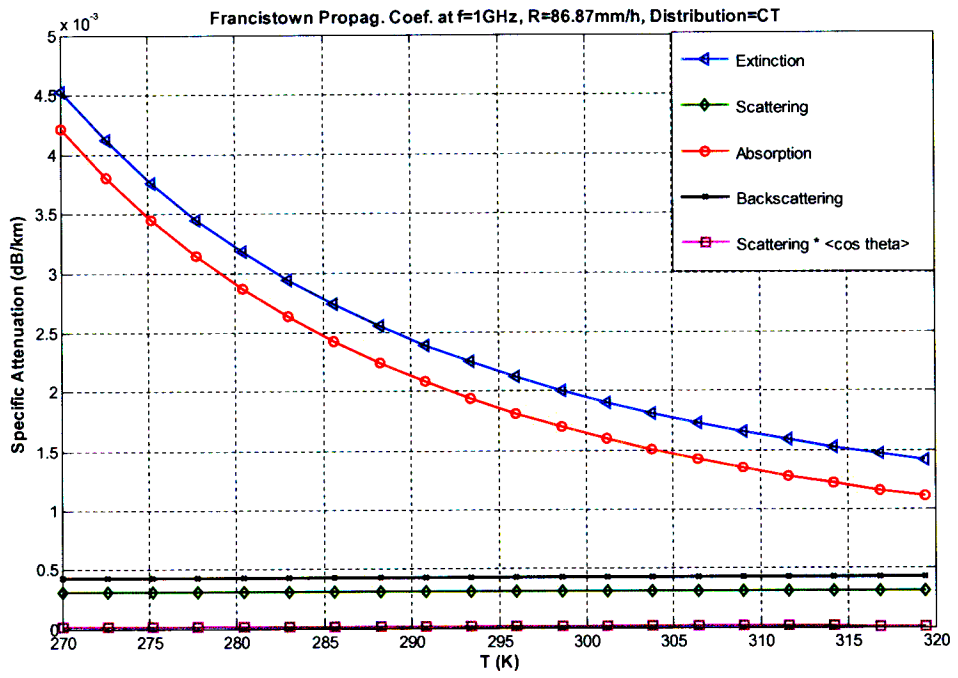
Francistown Propag. Coef. at f=1GHz, R=86.87mm/h, Distribution=CT
x 10^-3
Specific Attenuation (dB/km)
T (K)
Extinction
Scattering
Absorption
Backscattering
Scattering * <cos theta>

(ii)

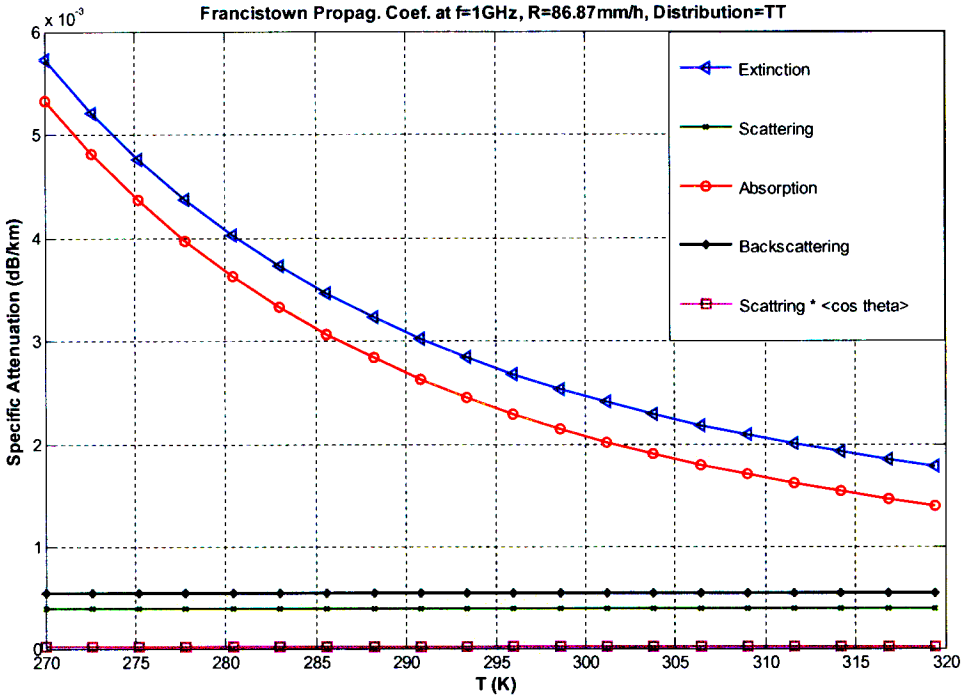

(jj)

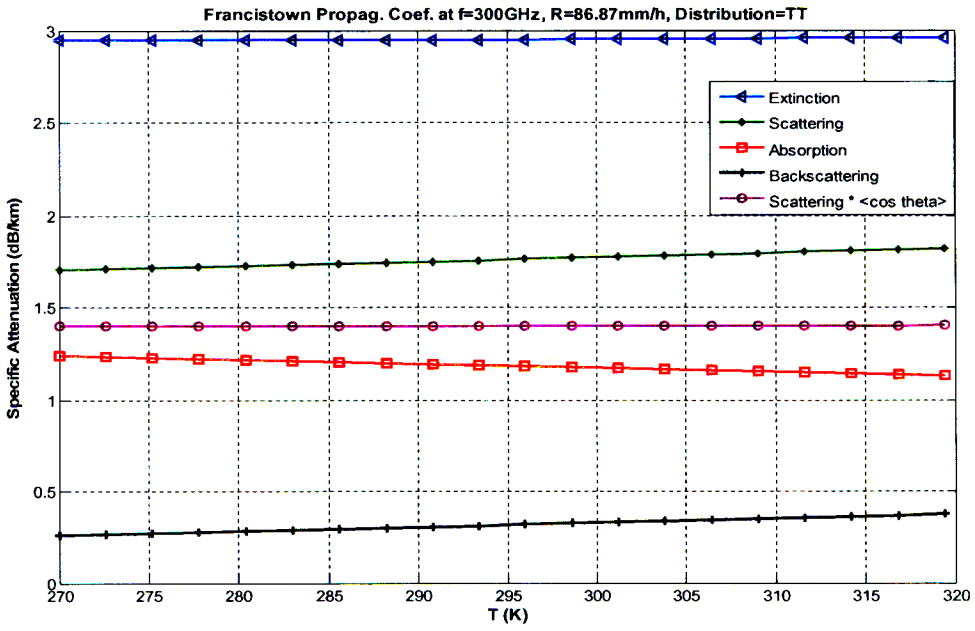

(kk)

Figure B 10 hh, ii, jj, kk: Attenuation coefficient due to rain versus Temperature for Francistown using CT and TT lognormal distributions.

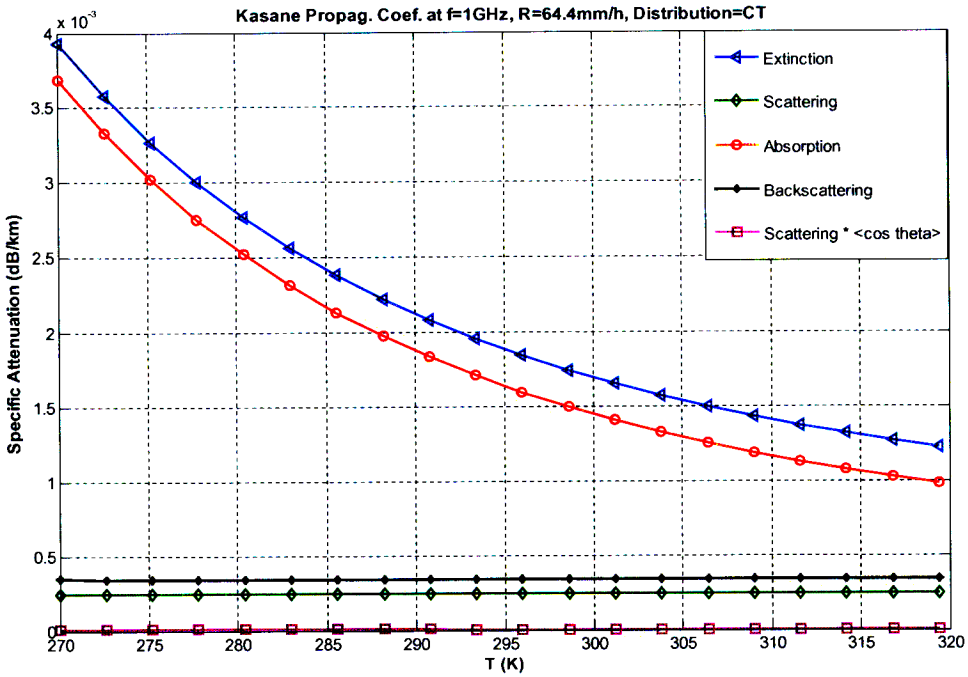
Kasane Propag. Coef. at f=1GHz, R=64.4mm/h, Distribution=CT
x 10^-3
Specific Attenuation (dB/km)
T (K)
Extinction
Scattering
Absorption
Backscattering
Scattering * <cos theta>
0
0.5
1
1.5
2
2.5
3
3.5
4
270
275
280
285
290
295
300
305
310
315
320

(ll)

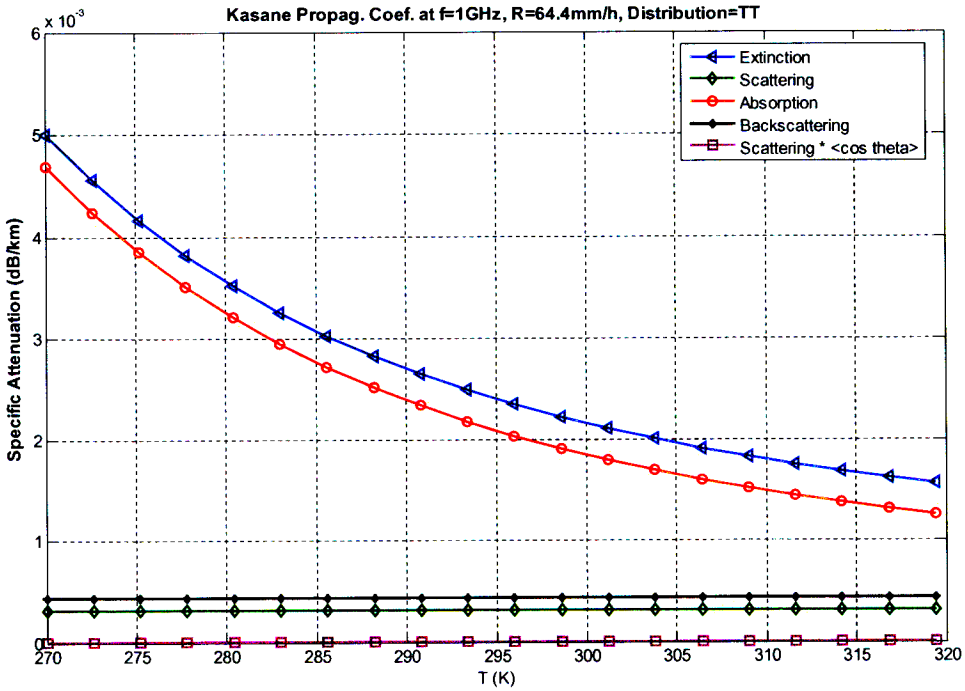
Kasane Propag. Coef. at f=1GHz, R=64.4mm/h, Distribution=TT
x 10^-3
Specific Attenuation (dB/km)
T (K)
Extinction
Scattering
Absorption
Backscattering
Scattering * <cos theta>
0
1
2
3
4
5
6
270
275
280
285
290
295
300
305
310
315
320

(mm)

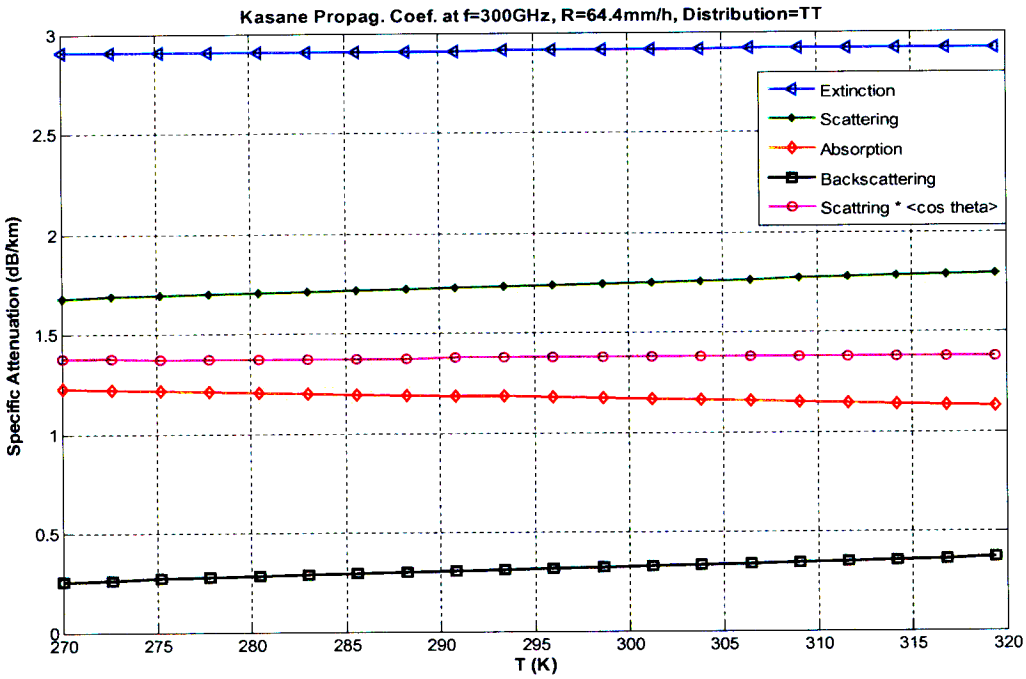

(mm)

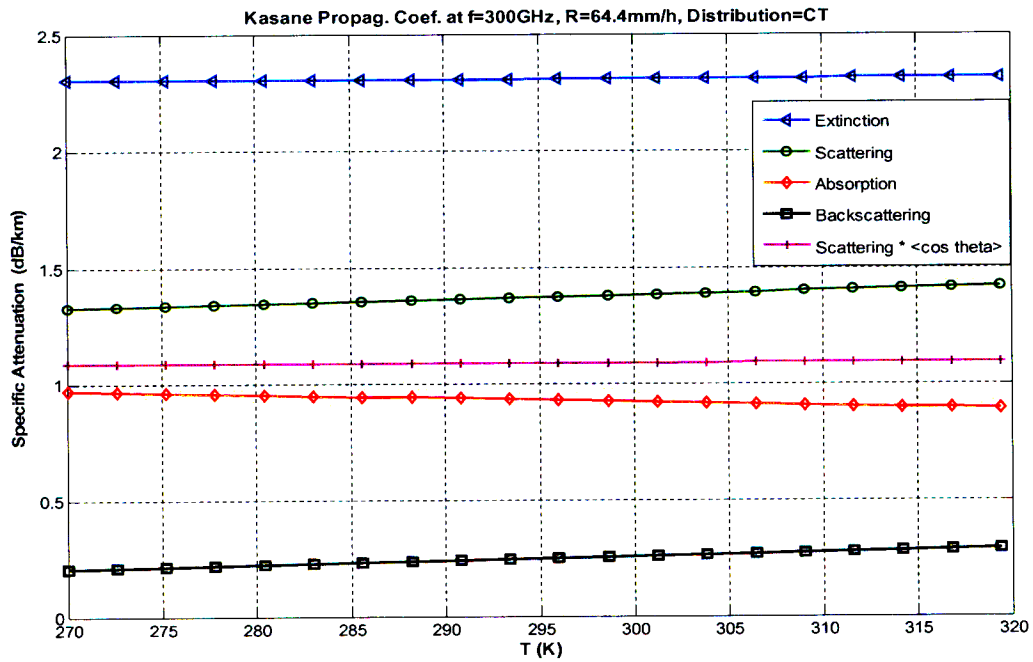

(oo)

Figure B 11 ll, mm, nn, oo: Attenuation coefficient due to rain versus Temperature for Kasane using CT and TT lognormal distributions.

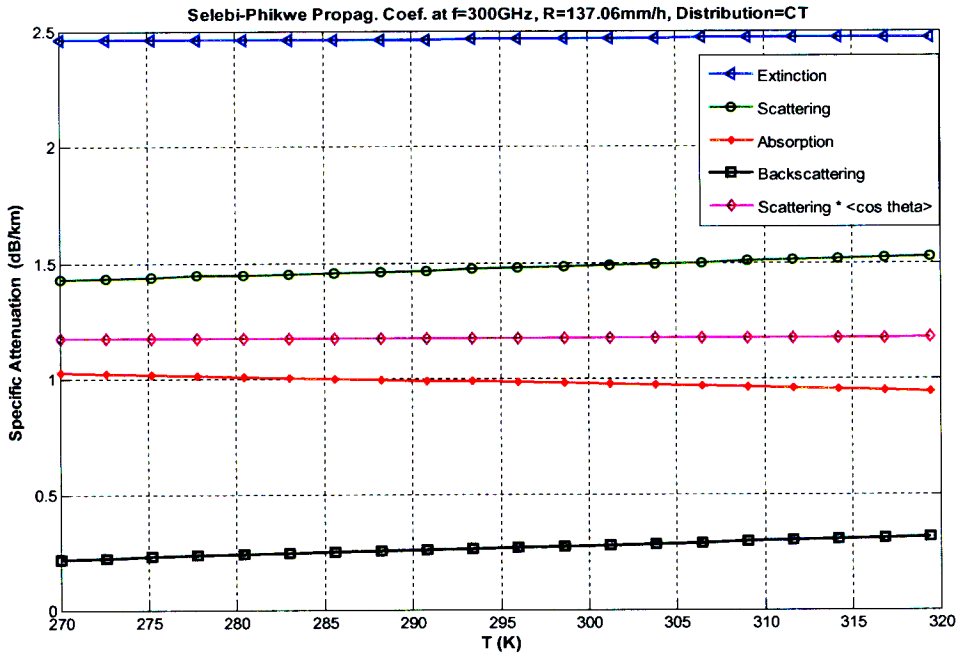
Selebi-Phikwe Propag. Coef. at f=300GHz, R=137.06mm/h, Distribution=CT
Specific Attenuation (dB/km)
T (K)
Extinction
Scattering
Absorption
Backscattering
Scattering * <cos theta>
0
0.5
1
1.5
2
2.5
270
275
280
285
290
295
300
305
310
315
320

(pp)

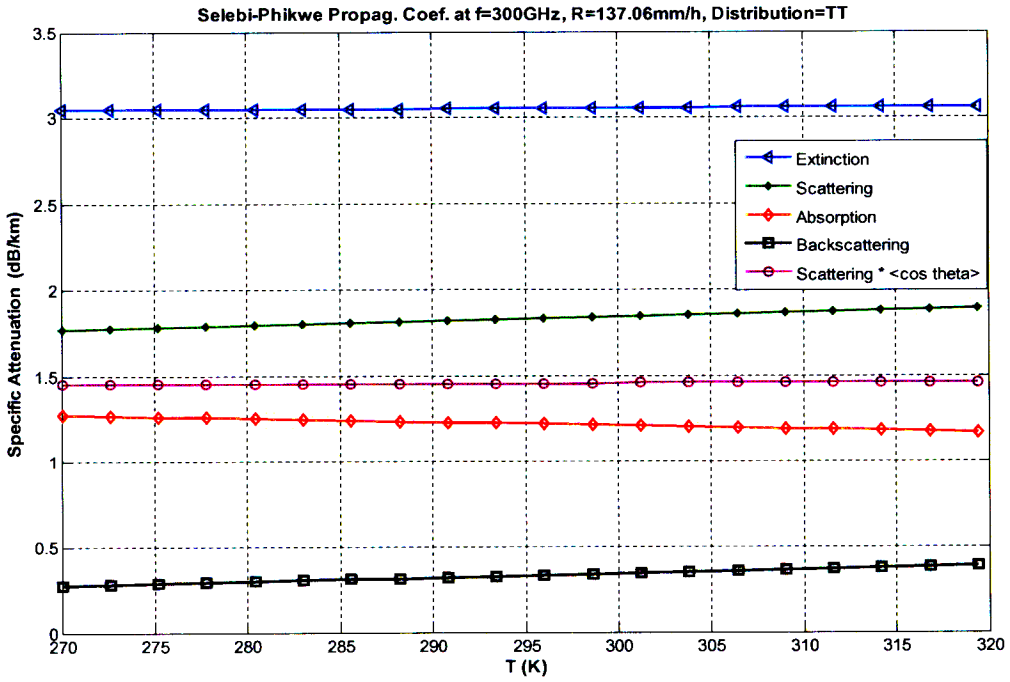
Selebi-Phikwe Propag. Coef. at f=300GHz, R=137.06mm/h, Distribution=TT
Specific Attenuation (dB/km)
T (K)
Extinction
Scattering
Absorption
Backscattering
Scattering * <cos theta>
0
0.5
1
1.5
2
2.5
3
3.5
270
275
280
285
290
295
300
305
310
315
320

(qq)

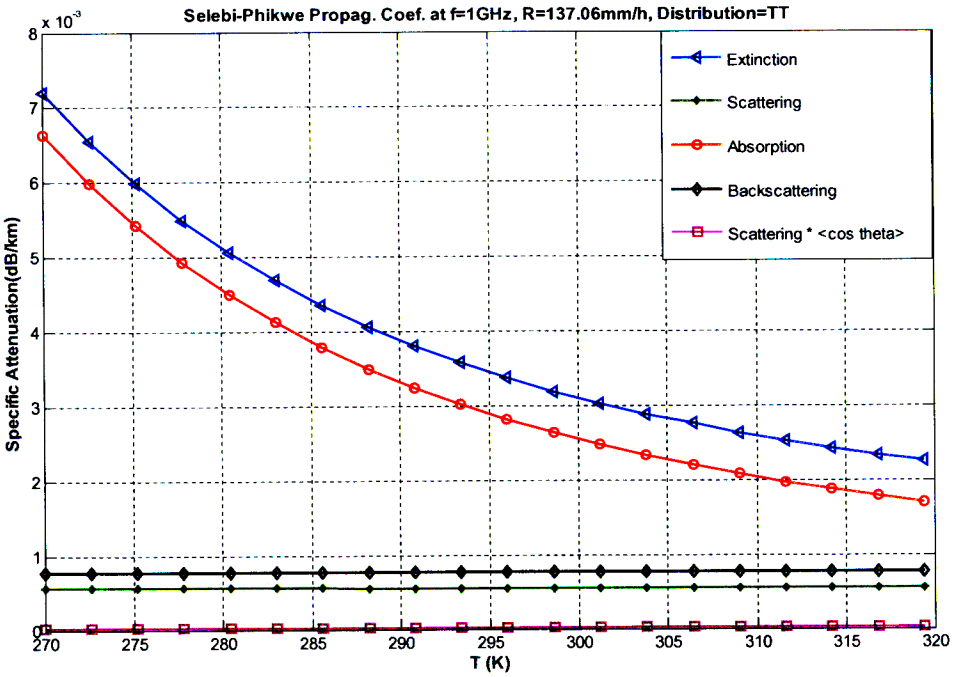

(rr)

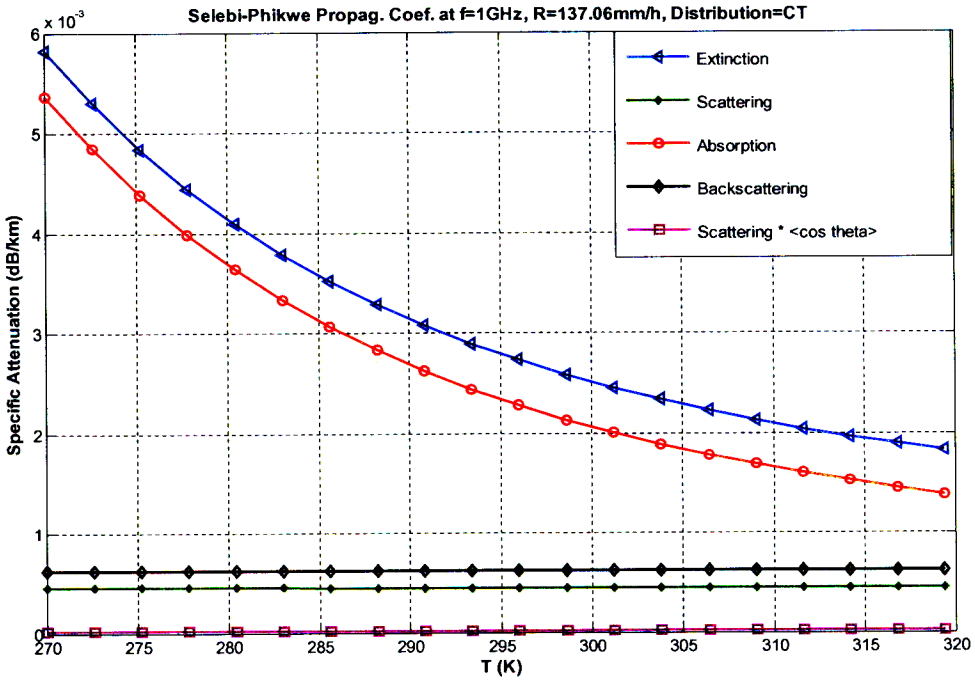

(ss)

Figure B 12 pp, qq, rr, ss, : Attenuation coefficient due to rain versus Temperature for Selebi-Phikwe using CT and TT lognormal distributions.

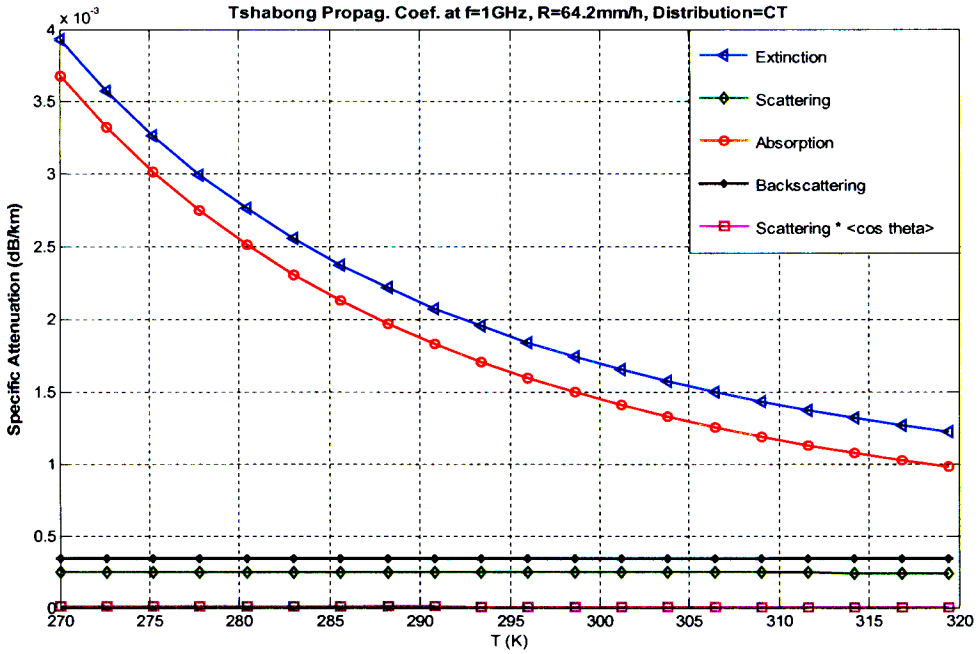
Tshabong Propag. Coef. at f=1GHz, R=64.2mm/h, Distribution=CT
x 10^-3
Specific Attenuation (dB/km)
T (K)
Extinction
Scattering
Absorption
Backscattering
Scattering * <cos theta>
0
0.5
1
1.5
2
2.5
3
3.5
4
270
275
280
285
290
295
300
305
310
315
320

(tt)

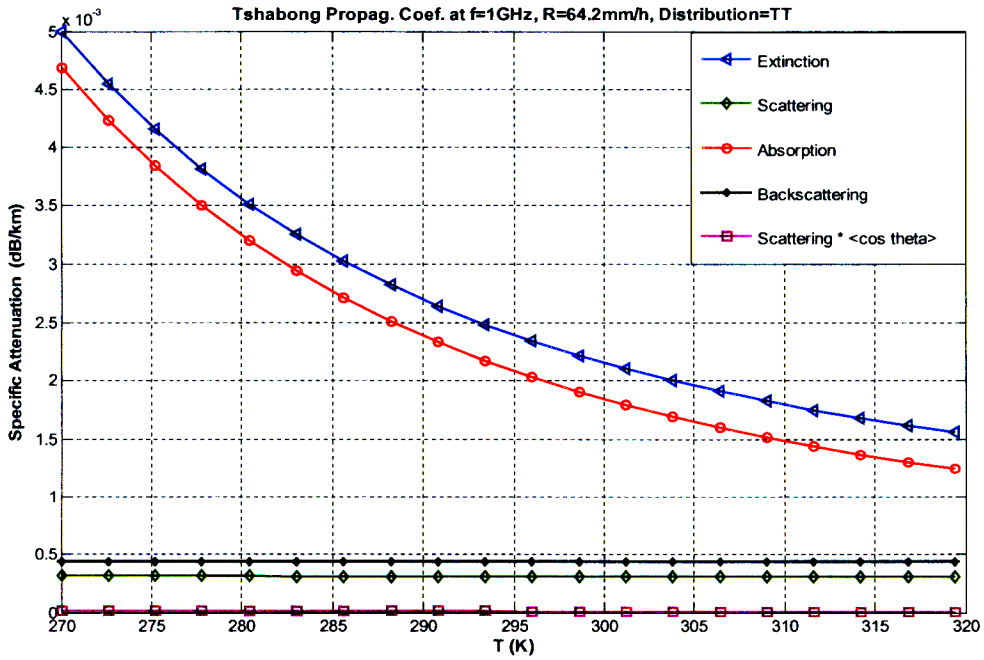
Tshabong Propag. Coef. at f=1GHz, R=64.2mm/h, Distribution=TT
x 10^-3
Specific Attenuation (dB/km)
T (K)
Extinction
Scattering
Absorption
Backscattering
Scattering * <cos theta>
0
0.5
1
1.5
2
2.5
3
3.5
4
4.5
5
270
275
280
285
290
295
300
305
310
315
320

(vv)

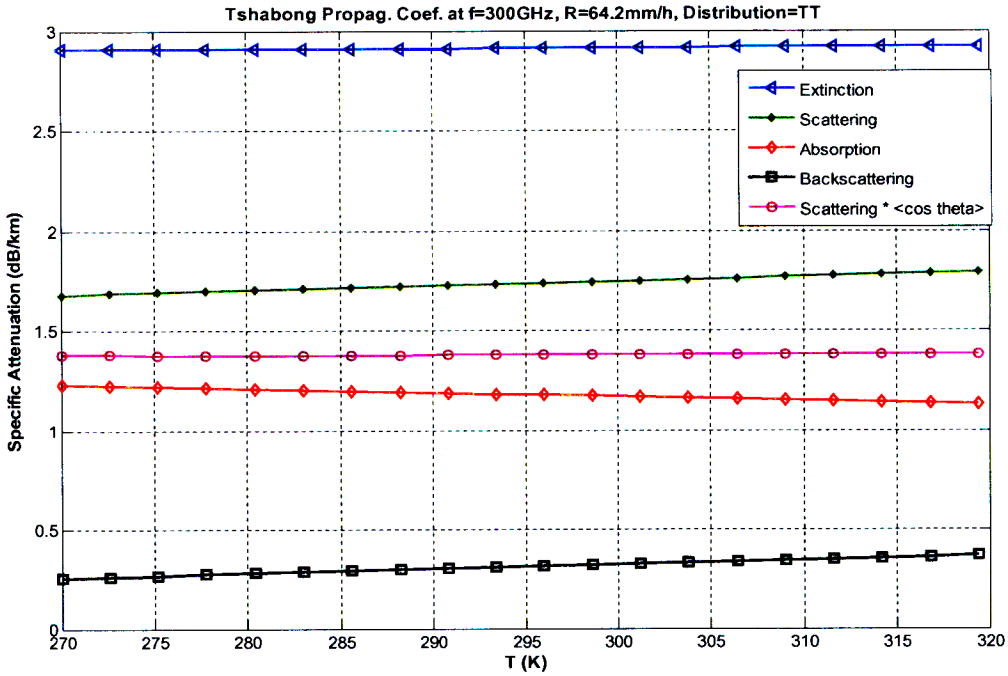

(ww)

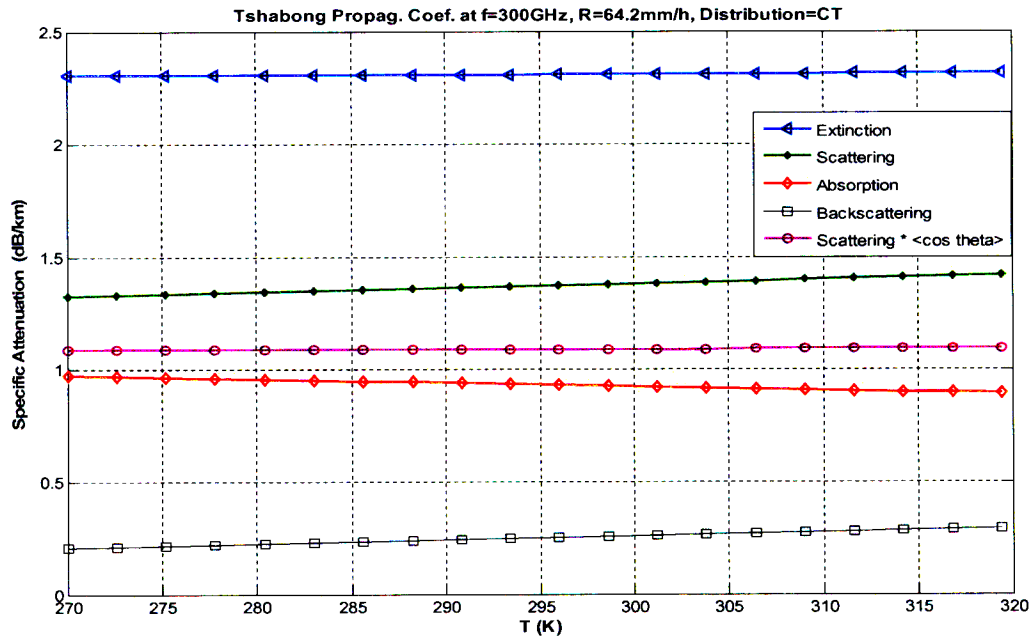

(yy)

Figure B 13 tt, vv, ww, yy: Attenuation coefficient due to rain versus Temperature for Tshabong using CT and TT lognormal distributions.

References

Ajayi, G. O and E.B.C. Ofoche (1983), Some Tropical rainfall rate characteristics at Ile-Ife for Microwave and millimeter Wave Application, *J. of Climate and Applied., Meteor.*, Vol. 23, pp 562-567.

Ajayi, G.O. and I.A. Adimula (1996), I.A, Variations in Raindrop Size Distribution and Specific Attenuation Due To Rain in Nigeria, *Ann. Telecommun.*, 51(1-2), pp. 87-93.

Ajayi, G.O., and Olsen, R.L. (1985), Modeling of Tropical Raindrop Size Distribution for Microwave and Millimeter Waves Applications, *Radio Sci.*, 20(2), pp. 193-202.

Ajayi, G.O., S. Feng, S.M. Radicella, and B.M. Reddy (Eds) (1996), *Handbook on Radio Propagation Related to Satellite Communication in Tropical and Subtropical Countries*, pp. 2-4, ICTP Press, Trieste.

Akira Ishimaru (1991), *Electromagnetic Wave Propagation, Radiation, and Scattering*, Prentice-Hall, Inc., New Jersey.

Akira Ishimaru (1978), *Wave Propagation and Scattering in Random Media,* volume 1 and 2, Academic Press, New York.

Alfred, J. and Jr. Bogush (1989), *Radar and the Atmosphere*, Artech House, Inc., MA.

Atlas, D., and Ulbrich, C. W. (1977), Path- and Area-integrated Rainfall Measurement by Microwave Attenuation in the 1-3cm band, *J. Appl. Meteorol.*, 16, pp. 1322-1331.

Balanis, C. A. (1989), *Advanced Engineering Electromagnetics,* New York: Wiley.

Beard, K. V., and Jameson, A. R., (1982), Raindrop Canting, *J. Atmos. Sci.*, 40 (10), pp. 448-454.

Best, A.C. (1950), Empirical Formulae for the Terminal Velocity of Water Falling Through the Atmosphere, *Quart. J.R. Met. Soc.,* 76, pp. 302-311.

Bohren C.F., and D.R. Huffman (1978), Absorption *and Scattering of Light by Small Particles,* John Wiley: New York, NY.

Crane, R. K., (1996), Electromagnetic Wave Propagation through Rain, *Wesley.*

Deirmendjian, D. (1969), *Electromagnetic Scattering on Spherical Polydispersions*, American Elsevier, New York, NY.

Detlefsen, J. (1989), *Radartechnik: Grundlagen, Bauelemente, Verfahren, nwendungen,* Springer - Verlag, Berlin, Heidelberg.

De Wolf, D. A., and Albert J. Zwiesler (1996), Rayleigh-Mie Approximation for Line-of-sight Propagation Through Rain at 5-90 GHz, IEEE *Trans. Ant. Prop.*44(3), March.

Eyring, H. (1941), *The Theory of rate processes*, McGraw-Hill Book Co. Inc., New York.

Fashuyi, M. O., and T. J. Afullo (2007), Rain attenuation prediction and modeling for line-of-sight links on terrestrial paths in South Africa, *Radio Sci.*, 42, RS5006, doi:10.1029/2007RS003618, October.

Fashuyi, M.O. , P.A. Owolawi and T.J. Afullo (2006), Rainfall Rate Modeling for LOS Radio Systems in South Africa, *Transactions of South African Institute of Electrical Engineers (SAIEE) Vol. 97 (1):* pp. 74 – 81.

Fang, D. J. and C. H. Chen (1982), Propagation of centimeter/millimeter wave along slant path through precipitation, *Radio sci.,* vol. 17, pp. 989-1005.

Fedi, F. (1981), Prediction of attenuation due to rainfall on terrestrial links, *Radio Science*, Vol. 16, No5, Sept-Oct, pp. 731-743.

Frohlich, H. (1949), *Theory of dielectrics*, Clarendon Press, Oxford.

Gunn and Kinzer (1949), The terminal velocity of water droplets in stagnant air, *J. Meteorol.,* 6, pp. 243-248.

Hassen, A. A. (2006), Indicators for the Signal Degradation and Optimization of Automotive Radar Sensors under Adverse Weather Conditions, PhD Dissertation, *Technischen Universität Darmstadt*, Germany.

Harrington, R. F. (1961), *Time-Harmonic Electromagnetic Fields*, New York: McGraw-Hill.

Inada, H. (1973), New Calculation of Surface Wave Contributions Associated with Mie Backscattering, *Applied Optics*, Vol. 12, No. 7, July.

Ivanovs, G. and D. Serdega (2006), Rain Intensity Influence on Microwave Line Payback Terms, *Electronic and Electrical Engineering*, ISSN 1392-1215, Nr.6(70).

ITU-R (2005), Specific attenuation model for rain for use in prediction methods, *Rec. 838-3 ITU-R P.* Int. Telecomm. Union, Geneva.

ITU-R (2007), Propagation data and prediction methods required for the design of terrestrial line-of-sight systems, *Rec. ITU-R P.530-12*, Int. Telecomm. Union, Geneva.

ITU-R P.838-1 (2000), ITU-R Recommendations on Radiowave Propagation, *Supplement to vol. 1997, P Series Part*, p.162-163, Geneva, Switzerland.

ITU-R P.837-1,2,3,4, (2001), Characteristics of Precipitation for Propagation Modelling, *International Telecommunication Union*, Geneva, Switzerland.

Joseph Nemarich, Ronald J.Wellman and James Lacombe (1988), Backscatter and attenuation by falling snow and rain at 96, 140, and 225 GHz, *IEEE Trans. Geoscience and Remote Sensing*, 26, pp. 319-329, May.

Jonathan H. Jiang and Dong L. Wu (2004), Ice and water permittivity for millimeter and sub-millimeter remote sensing applications, *Atmospheric Science Letters*, March 31, 5, pp. 146-151.

J. N. Murrell, A. D. Jenkins (1994), *Properties of Liquids and solutions,* 2nd Ed. John Wiley & Sons, Chichester, England.

Kharadly, M. M. Z. (1989), Scattering by rain and melting snow, *IEEE Trans. Antenna and Propagation*, 2, pp. 406-410.

Karasawa, Y. and T. Matsudo (1991), One-Minute Rain Rate Distributions in Japan Derived from AMEDAS One-Hour Rain Rate Data, *IEEE Transactions on Geosciences and Remote Sensing*, Vol.29,No 6, pp. 890-898,November.

Karasawa, Y. and T.Matsudo (1990), A prediction method of one-minute rain rate distributions in Japan, *Trans. IEICE Japan*, vol. J73-B-II, No.47, pp.518-527.

Kerr, D. E. (ed.), (1951), *Propagation of Short Radio Waves*, MIT Radiation Laboratories Series, vol. 13, McGraw-Hill Book Company, inc.

Liebe, H.J., G.A. Hufford and T. Manabe (1991), A model for the complex permittivity of water at frequencies below 1THz, *Internat. J. Infrared mm. Waves*, 12, pp. 659-675.

Liebe H. J., G. A. Hufford and M.G. Cotton, (1993), Propagation Modeling of Moist Air and Suspended Water/Ice Particles at Frequencies Below 1000GHz, AGARD *Conference Proc. 542, Atmospheric Propagation Effects through Natural and Man-Made Obscurants for Visible to MM-Wave Radiation*, pp.3.1-3.10.

Manabe, T., Ihara, T., and J. Awaka (1987), The relationship of raindrop-size distribution to attenuations of raindrop-size distribution to attenuations experienced at 50, 80, 140 and 240 GHz, *IEEE Trans. on Antennas and Propagation*, AP-35:1093-1096, November.

Massambani, O., C.A. Morales Rodriguez (1990), Specific Attenuation As Inferred From Drop Size Distribution Measurements in The Tropics, *Proceedings of URSI Commission*

F Open Symposium, Rutherford Appleton Laboratory, Rio de Janeiro, Brazil, 3-7 December.

Mätzler, C. (2002a), Effects of Rain on Propagation, Absorption And Scattering of Microwave Radiation Based on The Dielectric Model of Liebe, *IAP Res. Rep. No. 02-10*, University of Bern, June.

Mätzler, C. (2002b), MATLAB Functions for Mie Scattering and Absorption, Version 2, *IAP Res. Rep. No. 2002-08*, University of Bern, Switzerland, June.

Mätzler, C. (2002c), Drop-size Distributions and Mie Computations for Rain, *IAP Res. Rep. No. 2002-16*, University of Bern, Switzerland, August.

Meador W.E. and W.R. Waver (1992), Two-Stream Approximations to Radiative Transfer in Planetary Atmospheres: A Unified Description of Existing Methods and a New Improvement, *J. Atm. Sciences,* 37, 630-643.

Mishchenko, M. I., L.D. Travis and A.A. Lacis (2002), *Scattering, Absorption, and Emission of Light by Small Particles*, Cambridge University

Moupfouma, F. and J. Tiffon (1982), Raindrop Size Distribution from Microwave Scattering Measurements in Equatorial and Tropical Climates, *Electron., Lett*, 18(23), pp. 1112-1113.

Moupfouma, F. and L.Martin (1995), Modeling of Rainfall-rate Cumulative Distribution for design of satellite and terrestrial communication systems, *International Journal of Satellite Communications*, vol.13, pp.105-115.

Mulangu, C.T., P.A. Owolawi and T.J.O. Afullo (2007), Rainfall Rate Distribution for LOS Radio System in Botswana in *Proceedings of 10th Southern Africa Telecommunication, Networks and Application Conference (SATNAC), Mauritius,* ISBN No. 978-0-620-39351-5, September.

Mulangu, C.T., and T.J. Afullo (2008), Path Attenuation Computation and Modeling for Microwave Link Systems for South African Coast, Proceedings of the XXX General Assembly of the International Union of Radio Science (URSI), Symposium Chicago, USA, (Proceedings on CD Rom).

Mulangu,C.T., and T.J. Afullo (2008), Effects of Rain on Microwave Remote Sensing Systems and Ground-Based Radars Use in Durban, *Proceedings of SATNAC*, ISBN No. 978-0-620-41696-2, Eastern Cape, South Africa, pp. 53-58.

Mulangu, C. T., and T. J. O. Afullo (2009), Variability of the Propagation Coefficients Due to Rain for Microwave Links in Southern Africa, *Radio Sci.*, doi:10.1029/2008RS003912, March.

Naicker, K., and S. H. Mneney (2006), Propagation Measurements and Multipath Channel Modeling for Line-Of-Sight Links at 19.5 GHz, *SAIEE Res. J., 97(2),* pp. 162-171.

Naicker, K. (2006), *Rain Attenuation Modelling for Line-of-Sight Terrestrial Links*, MSc Dissertation, University of Kwazulu-Natal, South Africa.

Nemarich, J., Ronald J.Wellman and James Lacombe (1988), Backscatter and attenuation by falling snow and rain at 96, 140, and 225 GHz, *IEEE Trans. Geoscience and Remote Sensing*, 26:319-329, May.

Odedina, M.O. (2006), A study of Rain Attenuation on Terrestrial Paths at Millimetric Wavelengths in South Africa, MSc Dissertation, University of Kwazulu-Natal, South Africa.

Oguchi, T. (1981), Scattering by hydrometeors: A survey, *Radio Sci.,* 16 (5), pp.691-730.

Oguchi, T. (1983), Electromagnetic wave propagation and scattering in rain and other hydrometeors, *Proc. IEEE Trans. Antennas Propagat.*, AP-26 (2), pp.318-329.

Olsen, R.L., D.V. Rogers and D.B. Hodge (1978), The aR^b Relation in the Calculation of Rain Attenuation, IEEE *Trans. Antennas Propag.* Vol. AP-26(2), pp. 318-329.

Owolawi, P.A. (2006), Rain Rate and Raindrop Size Distribution Models for Line-of-sight Millimetric Systems in South Africa, MSc Dissertation, University of Kwazulu-Natal, South Africa.

Owolawi, P.A. and T.J. Afullo, (2007), Rainfall Rate and Its Worst Month Statistics for LOS in South Africa at Millimetric Band, *Radio Science, Vol. 42, November.*

Poggio, A. J. and E. K. Miller (1987), *Integral equation solutions of three-dimensional scattering problems in Computer Techniques for Electromagnetics,* ed. R. Mittra, New York: Hemisphere.

Pozar, D.M. (2005), *Microwave engineering*, John Willey.

Ray, P. S. (1972), Broadband Complex Refractive Indices of Ice and Water, *Appl. Opt.*, 11 (8), pp.1836-1844.

Rice, P. L and N. R. Holmberg (1973), Cumulative time statistics of surface-point rainfall rates, *IEEE Trans.Commun.,* COM-21, 10, pp.1131-1136.

Rogers, D.V. and R.L. Olsen (1976), Calculation of Radiowave Attenuation due to Rain at Frequencies up to 1000 GHz, *CRC. Rep. 1299*, Department of Communications, Ottawa, November.

Sadiku, M. N. O., (1992), *Numerical Techniques in Electromagnetics*, CRC Press, Inc., Florida.

Sadiku, M. N. O. (2002), *Numerical Techniques in Electromagnetics*, CRC.

Segal, B. (1986), The Influence of Raingage Integration Time on Measured Rainfall-Intensity Distribution Functions, *J. of Atmospheric and Oceanic Tech*, Vol. 3, pp.662-671.

Segelstein, D. J. (1981), The complex refractive index of water, in physics, *University of Missouri*, Kansas City.

Sekine, M., Chen, C., and Musha, T. (1979), Rain attenuation from log-normal and Weibull raindrop-size distributions, *IEEE Trans. Antennas Propagat.*, AP-35 (3), pp. 358-359.

Silver, S. (1949), *Microwave Antenna Theory and Design*, McGraw-Hill, New York.

Skolnik, M. I. (1962), *Radar Systems*, 2nd Edition McGraw-Hill, Inc., New York.

Stratton, J. A. (1941), *Electromagnetic Theory,* New York, McGraw-Hill.

Takeshi Manabe, Toshio Ihara, and Jun Awaka (1987), The relationship of raindrop-size distribution to attenuations of raindrop-size distribution to attenuations experienced at 50, 80, 140 and 240 GHz, *IEEE Trans. on Antennas and Propagation*, AP-35, pp.1093-1096, November.

Ulaby, F. T., Moore, R. K., and Fung, A. K. (1981), *Microwave Remote Sensing*, Addison-Wesley.

Uijlenhoet, R. (1998), Raindrop Size Distributions and Radar Reflectivity-rain rate Relationships for Radar Hydrology, *Hydrol. Earth. Syst. Sci.*, 5 (4), 615-627.

Van de Hulst, H. C. (1957), Light Scattering by Small Particles, *John Wiley & Sons*, New York, pp. 470.

Watson, P.A., Sathiaseelan and B. Potter (1981), Development of a Climatic Map of Rainfall Attenuation for Europe, *Post Graduate School of Electrical and Electronic Engineering, University of Bradford*, U.K, Rep. No.300, pp. 134.